LASER TIME-RESOLVED SITE SELECTION SPECTROSCOPY OF Nd^{3+} IONS IN MIXED GARNET CRYSTALS

By

MASUD ZOKAI

Bachelor of Science
University of Isfahan
Isfahan, Iran
1970

Master of Science
Pahlavi University
Shiraz, Iran
1972

Master of Science
University of Kansas
Lawrence, Kansas
1976

Submitted to the Faculty of the Graduate College
of the Oklahoma State University
in partial fulfillment of the requirements
for the Degree of
DOCTOR OF PHILOSOPHY
May, 1979

LASER TIME-RESOLVED SITE SELECTION SPECTROSCOPY

OF Nd^{3+} IONS IN MIXED GARNET CRYSTALS

Thesis Approved:

R. C. Powell
Thesis Adviser

Lu G. Rockley

W. A. Sibley

Joel J. Martin

Norman N. Durham
Dean of the Graduate College

ACKNOWLEDGMENTS

I want to express my thanks to those who helped me along the way for completion of this research. I am especially thankful to Dr. R. C. Powell, my Thesis Adviser and Committee Chairman. Thanks are also due the members of my Committee, Dr. W. A. Sibley, Dr. J. J. Martin, and Dr. M. G. Rockley for their help and advice. Special thanks are due Dr. B. Di Bartolo and Dr. G. F. Imbusch for their valuable discussions. Finally, special gratitude is expressed to my wife, Parvin. It was through her faith and support that the program of study was indicated and sustained. Deepest affection is also extended to my son, Ali for his thoughtfulness and consideration throughout this work, and I would like to thank my parents for their helpful and supportive attitude through my graduate studies.

TABLE OF CONTENTS

LIST OF TABLES

LIST OF FIGURES

Figure Page

CHAPTER I

INTRODUCTION

As laser systems have been developed over the last two decades and their technology has been applied in new areas, there is more and more need for detailed knowledge of optical materials. Investigation into basic properties of optical materials will enable development of more sophisticated and efficient optical devices, such as lasers, phosphors, frequency upconverters, and quantum counters. Since migration of electronic excitation energy in crystals with impurity ions to "traps" can result in the quenching of photon emission, it is important to characterize energy migration of this type. The techniques of site-selection (1) and time-resolved spectroscopy (2,3) offer the potential to study energy transfer in impurity doped solids much more directly than previously possible.

Past Work on Time-Resolved Spectroscopy and Site-Selection Spectroscopy of Ions in Solids

Site-Selection Spectroscopy

Single step energy transfer between two isolated impurity ions is more clearly understood than multistep migration of energy among ions of the same type. However, the multistep phenomenon is of importance in both concentration quenching and cooperative absorption processes. For

investigation in this area, the selective excitation of specific ions by lasers is quite useful.

By using a narrow band dye laser emission, we can selectively excite ions in specific crystal field sites in the mixed crystals, such as Nd^{3+} ions, thus enabling the study of the shape and time evolution of the resulting luminescence signals. This yields useful data about the inhomogeneous and homogeneous broadening of the levels and about the spectral transfer rates among the Nd ions.

The utility of the tunable dye laser in this study is because the electronic energies of impurity ions in a crystal tend to be perturbed by differences in the local environment, thus the energy of a given electronic transition may vary observably among ions which lie near different lattice imperfections or contaminants. If a dye laser beam of sufficiently narrow linewidth is tuned to the appropriate wavelength, it may thus be possible to selectively excite ions in one type of site while exciting few ions in other types of sites. In energy transfer studies, this allows one to follow the transfer of excitation from the selectively pumped type of ions to the unexcited types by following the time evaluation of a fluorescence signal after excitation, according to time-resolved spectroscopy (TRS) techniques (2,3).

The available wavelengths of dye laser pulses are such that the Nd^{3+} ions are brought to levels located at approximately 16,800 cm^{-1} above the ground level. From these levels the ions may be expected to decay non-radiatively to the $4F_{3/2}$ metastable level and then undergo radiative transitions. The shape and the time evolution of the luminescence signals associated with those transitions may then provide information about (a) the inhomogeneous and homogeneous broadening of

the levels "in time" with respect to the laser pulse and about (b) the spectral transfer rate among the Nd^{3+} ions (4,5).

Homogeneous contributions to fluorescence line widths are due to phonon relaxation and scattering processes. This comes together with an inhomogeneous contribution due to imperfections, to produce the width of the fluorescence line of impurity centers in a solid. The inhomogeneous contribution is generally greater than the former at low temperatures. The laser, being a highly monochromatic energy source, enables the selective excitation of those centers located at sites whose local field causes their absorption transition to be at the laser wavelength (6,7). This "laser-induced fluorescence line narrowing" (8,9) makes fluorescence lines appear narrower, if the laser line width is less than the inhomogeneous line width of the transition.

A case may exist where the active centers are present in such a high concentration that energy may migrate through the crystal being transferred from one center to another. This means that the emission may come from any of the active centers reached in the energy transfer, even though laser absorption may be at only selective sites. Here again, the fluorescence line will show inhomogeneous broadening. This concentration-dependent effect has been observed in a variety of materials and is useful in studying energy transfer (10).

Time-Resolved Spectroscopy

Although the majority of studies on energy transfer have examined ratios of the fluorescence intensities or lifetimes as functions of activator concentration, many investigations have shown the concentration dependence data used for establishing the interaction mechanism of

energy transfer are prone to be ambiguous. Moreover, researchers have been hindered in the use of temperature dependent studies in this area by the many complications which affect the results. For example, for exciton diffusion defect scattering, thermal scattering, and trapping all produce different types of temperature dependencies of the diffusion constant. For these reasons, time-resolved spectroscopy has developed into an important tool in studying energy transfer.

Data are gathered on the total time evolution of the fluorescence intensities coming from sensitizers (the type of atoms or molecules that absorb the excitation energy) and activators (the type of atoms or molecules that emit the energy). From this information it is possible to determine the time dependence of the energy transfer rate. In long range resonant interaction (LRRI) theory, this energy transfer rate decreases with time (for dipole-dipole interaction it goes as $t^{-\frac{1}{2}}$). This is because, in a setting of randomly distributed excited sensitizers and unexcited activators, the excited sensitizers which are close to activators transfer their energy quickly while those more distant from activators transfer their energy slowly. In exciton diffusion theory the sensitizer excited states migrate in randomly throughout the lattice so that a random distribution with respect to the activators is always maintained. In such a circumstance there is no reason for a change in probability of transferring their energy and thus the energy transfer rate is constant.

Summary of Thesis

The author investigated various garnet crystals of the formula $Y_3(Al_{1-x}Ga_x)_5O_{12}$. Our samples ranged from 100% Ga content to 100% Al

content, with the mixed intermediates having Ga percentages of 10%, 22%, 39% and 50%. All crystals were doped with Nd^{3+}, having approximately 1% Nd^{3+} substituted in yttrium sites. These samples were obtained from R. K. Watts of Texas Instruments, Inc.

This thesis is organized so that the major basic energy transfer theories and many aspects of spectroscopic research are discussed and compared in Chapter II. Included in this section is a comparison of approaches to combine theories of diffusion and long-range resonance transfer, radiationless processes in crystals. A description of the samples and experimental apparatus forms the content of Chapter III. The experimental methodology is described and background information is given on the nature and preparation of the crystals. The experimental results, presented in brief summary in the present section, are given detailed treatment in Chapters IV, V, and VI.

Spectroscopic study of the YAlG:Nd and YGaG:Nd systems forms the context for this study, and discussion of these systems is a necessary component. A complete understanding of data found concerning the energies and homogeneous broadening of the levels of neodymium ions in doped YAlG and YGaG is an essential preliminary step for analyzing and understanding the mixed Al/Ga crystals. Then the author examined the spectra of the mixed crystals and related our findings to the YAlG:Nd and YGaG:Nd systems. The results of the experimental work are interpreted in terms of the homogeneous and inhomogeneous broadening of the levels and in terms of the excitation transfer among distinct Nd sites.

Narrow band dye laser light pulses can selectively excite ions at a particular site since the energy band splits into distinct energy levels. Neodymium ions excited by these pulses rise to a band approxi-

mately 16,800 cm^{-1} above ground level, and then decay non-radiatively, dropping to the $4F_{3/2}$ level, approximately 11,450 cm^{-1} above ground level. The ions then undergo radiative transitions, emitting luminescence signals in association with these transitions that may be analyzed. The shape and time evolution of the radiation helps us understand the inhomogeneous and homogeneous broadening of the levels, as well as the spectral transfer rate among the sensitizer and activator ions in the crystal lattice.

In this study, the author focused on determining the characteristic properties of the $4F_{3/2}$ transitions to the $^4I_{9/2}$ ground state manifold. Increasing Ga concentration in the crystals is shown to produce a linear shift in the position of the crystal field levels observed. Inhomogeneous broadening of the spectral lines also results from the addition of Ga. Apparently the Ga ions are found in an approximately uniform distribution, according to evidence from line shape analysis. Narrow line laser excitation techniques produced selective pumping of Nd^{3+} ions in lattice sites with specific amounts of Ga, for a linear relation was observed between pumping wavelength and the position of the emission lines.

The author also found that spectral lines produced by Nd transitions in our mixed crystal samples had distinct structure, so some sites apparently have significantly different energies of transition than others.

Using high resolution pulsed dye laser excitation and scanning across the broad $^4G_{5/2}$, $^2G_{7/2}$ absorption band results in different relative intensities of the fluorescence lines from the $^4F_{3/2}$ level to the different components of the $^4I_{9/2}$ ground state. These spectra can be

associated with ions in different crystal field sites which have different transition rates to the various ground state Stark levels. Time-resolved spectroscopy techniques were used to monitor the time evolution of the fluorescence and the results are interpreted in terms of energy transfer between Nd ions in different types of crystal field sites. The transfer rate is found to be a constant at 14K implying that there is some spatial correlation between the Nd ions in the different types of sites. The energy transfer characteristics vary with excitation wavelength and with temperature.

Thermal activation is necessary to produce the energy migration and trapping processes. The data is explained well by the mechanisms of two-phonon assisted energy transfer. A greater energy transfer efficiency was exhibited by the mixed crystal hosts than by YAlG:Nd and YGaG:Nd.

CHAPTER II

THEORETICAL BACKGROUND

The process of energy transfer in solids involves exciting one kind of atom or ion, and then observing the transfer of excitation energy to another ion. After this transfer the latter ion then emits the energy. It is termed the activator and the atom or ion originally excited is referred to as the sensitizer. The energy transfer between ions in specific systems may result from several mechanisms and many models have been proposed to explain this phenomenon. These include the exchange interaction and such electric multipole interactions as dipole-dipole, dipole-quadripole and quadripole-quadripole. The important example of electric dipole-dipole interaction is discussed in the next section.

Energy Transfer From Sensitizer to Activator by Dipole-Dipole Resonant Interaction

Energy transfer from an excited sensitizer to an unexcited activator entails a transition from the Ψ_i state, which is the product of Ψ_s^* (the initial state for the excited sensitizer) and Ψ_a (the initial state for the ground state activator) to the Ψ_f state, which is the product of Ψ_s (the sensitizer ground state) and Ψ_a^* (the excited activator state), i.e.

$$\Psi_i> = |\Psi_s^*(\vec{r}_s, w_s^*)>|\Psi_a(\vec{r}_a, w_a)> \qquad \text{(II-1)}$$

and

$$\Psi_f> = |\Psi_s(\vec{r}_s, w_s>|\Psi_a^*(\vec{r}_a, w_a^*)>$$

where $\vec{r}_s$ and $\vec{r}_a$ represent the positions of sensitizer and activator respectively, and the wave functions represent a particular energy state denoted by w which includes both the electronic state energy and the energy of the vibrational sub-state (11). The rate for this electric dipole-dipole energy transfer may be derived from the "golden rule" of time dependent perturbation theory, with the needed Hamiltonian being bound by means of a multipole expansion for the electrostatic interaction. Hence the probability for occurrence of transition per unit time is

$$\omega_{sa} = \frac{2\pi}{\hbar} \rho_E \left| \int \Psi_i^* H_1 \Psi_f \right|^2 \qquad \text{(II-2)}$$

where ρ_E = the final density of the states

H_o = the interaction Hamiltonian.

We may define $P_s^*(W_s^*)$ and $P_a(Wa)$ as the functions showing the probabilities of the sensitizer having W_s^* as initial energy and the activator having Wa as initial energy, respectively. The normalization of the initial state energies and wave functions is given by:

$$\int_o^\infty |\Psi_s^*(w_s^*)|^2 \, d\tau = \int_o^\infty |\Psi_a(w_a)|^2 \, d\tau = 1 \qquad \text{(II-3)}$$

and

$$\int_o^\infty P_s^*(w_s^*) dw_s^* = \int_o^\infty P_a(w_a) \, dw_a = 1$$

The ranges of the sensitizer and activator energies of the final

state are W_s to $W_s+\Delta W$ and W_a^* to $W_a^* + \Delta W$, respectively. Thus the final state wave functions may be normalized by

$$\frac{1}{\Delta w} \int_w^{w+\Delta w} dw_s^* \int_o^\infty |\Psi_s(w_s)|^2 \, d\tau = 1 \qquad \text{(II-4)}$$

and

$$\frac{1}{\Delta w} \int_w^{w+\Delta w} dw_a^* \int_o^\infty |\Psi_a^*(w_a^*)|^2 \, d\tau = 1 \qquad \text{(II-5)}$$

The energy distribution functions P_s^* and P_a may absorb the density of states ρ_E if a Dirac delta is included for energy conservation. In addition the $1/\Delta w$ terms in Equation (II-4) and (II-5) be absorbed into $|\langle H_1 \rangle|^2$, the square of the matrix element, thus producing a unitless quantity. We now must sum the transfer probability over all the initial and final states, which may contribute to the transition probability. Also since only one of the degenerate states is actually filled we must divide by g_s' and g_a to account for degeneracies of the initial sensitizer and activator states.

Now the total probability is shown by:

$$\omega_{sa} = \frac{2\pi}{\hbar} \sum_i \sum_f \frac{1}{g_s' g_a} \int dw_a^* \int dw_s \int dw_a P_a(w_a) \int dw_s P_s^*(W_s^*)$$

$$x \; |\langle H_1(W_s^*, w, w_s, w_a^*) \rangle|^2 \; \delta(w_s^* + w_a - w_s - w_a^*) \qquad \text{(II-6)}$$

Defining:

$$E = W_a^* - W_a = W_s^* - W_s \qquad \text{(II-7)}$$

and using the Dirac delta function to integrate over W_s,

$$\omega_{sa} = \frac{2\pi}{\hbar} \sum_i \sum_f \frac{1}{g'_s g'_a} \int dE \int dw_a P_a(w_a) \int dw_s^* P_s^*(w_s^*) \left| \langle H_1(w_s^*, w_a; \right.$$

$$\left. x\ w_s^* - E,\ w_a + E) \rangle \right|^2 \qquad \text{(II-8)}$$

For purposes of this study the interaction Hamiltonian needed is the dipole part of the energy H of a charge distribution $\rho(\vec{r})$ resulting from an external dipole potential field $\phi(r)$:

$$H = \int \rho(\vec{r}) \phi(\vec{r}) d\tau \qquad \text{(II-9)}$$

Supposing that the activator ion has N electrons and M-N protons, then the charge distribution is:

$$\rho(r) = \sum_{i=1}^{N} (-e)\ \delta(\vec{r} - r_{ai}) + \sum_{i=N+1}^{M} e\delta(\vec{r} - \vec{r}_{ai}) = \sum_{i=1}^{M} q_i\ \delta(\vec{r} - \vec{r}_{ai}) \qquad \text{(II-10)}$$

If $\vec{R}$ gives the activator position relative to the sensitizer, the potential field may be expanded about the center of mass of $\vec{R}$:

$$\phi(\vec{r}_{ai}) = \phi(\vec{R}) + \vec{r}_{ai} \cdot \nabla\phi(\vec{R}) + \cdots\cdot$$

$$= \phi(\vec{R}) - \vec{r}_{ai} \cdot \vec{E}(\vec{R}) + \cdots\cdot \qquad \text{(II-11)}$$

Since the monopole term $\Sigma q\phi(\vec{R})$ is not applicable for the interaction Hamiltonian, only the dipole term is needed. Thus,

$$H_1 = \sum_{i=1}^{M} (-q_i)\ \vec{r}_{ai} \cdot E(\vec{R}) \qquad \text{(II-12)}$$

If the net dipole moment of the activator is written

$$\vec{P}_a = e\vec{r}_a = \sum_i q_i\ \vec{r}_{ai} \qquad \text{(II-13)}$$

Then

$$H_1 = - e\vec{r}_a \cdot \vec{E}(\vec{R}) \tag{II-14}$$

only the dipole term of the external field is considered important in electric dipole-dipole interaction, so that

$$\vec{E}(\vec{R}) = \frac{3\hat{R}(\vec{P}_s \cdot \hat{R}) - \vec{P}_s}{\kappa R^3} \tag{II-15}$$

where κ is the relative permeability. In this equation the sensitizer dipole moment definition is analogous to that of the activator dipole moment,

$$\vec{P}_s = \sum_{i=1}^{N_a} (-e)\vec{r}_{si} + \sum_{i=N_s+1}^{N_a} (+e)\vec{r}_{si} = e\vec{r}_s \tag{II-16}$$

Therefore, we write the dipole-dipole interaction Hamiltonian as

$$H_1 = - e\vec{r}_a \cdot \frac{3e\hat{R}(\vec{r}_s \cdot \hat{R}) - e\vec{r}_s}{\kappa R^3}$$

$$= \frac{e^2}{\kappa R^3} \left\{ \vec{r}_a \cdot \vec{r}_s - 3 (\vec{r}_a \cdot \hat{R})(\vec{r}_s \cdot \hat{R}) \right\} \tag{II-17}$$

Combining (II-8) and (II-17) gives

$$\omega_{sa} = \frac{2\pi}{\hbar} \sum_{I,F} \left(\frac{e^2}{\kappa^2 R^6} \right) \frac{1}{g_s g_a} \int dE \int dw_a P_a(w_a) \int dw_s^* P_s^*(w_s^*)$$

$$\times \left| \langle \vec{r}_s \rangle \cdot \langle \vec{r}_a \rangle - 3(\langle \vec{r}_s \rangle \cdot \hat{R})(\langle \vec{r}_a \rangle \cdot \hat{R}) \right|^2 \tag{II-18}$$

Next, an average is taken over all orientations of $\langle \vec{r}_s \rangle$ and $\langle \vec{r}_a \rangle$. For

this θ is defined as the angle between $\langle\vec{r}_a\rangle$ and $\vec{R}$, θ' as the angle between $\langle\vec{r}_s\rangle$ and $\vec{R}$, and θ as the aziminthan angle of $\langle\vec{r}_s\rangle$ relative to that of $\langle\vec{r}_a\rangle$. Thus,

$$\langle\vec{r}_s\rangle\cdot\langle\vec{r}_a\rangle = |\langle\vec{r}_s\rangle||\langle\vec{r}_a\rangle|(\cos\theta\cos\theta' + \sin\theta\sin\theta'\cos\theta),$$

$$\langle\vec{r}_a\rangle\cdot\hat{R} = |\langle\vec{r}_a\rangle\cos\theta,$$

$$\langle\vec{r}_s\rangle\cdot\hat{R} = |\langle\vec{r}_s\rangle\cos\theta'.$$

Now

$$\omega_{sa} = \frac{2\pi}{\hbar}\frac{e^4}{\kappa^2 R^6}\sum_{I,f}\frac{1}{g_s' g_a}\int dE\int dw_z\, P_a(w_a)\int dw_s^*\, P_s^*(w_s^*)$$

$$\times\ |\langle\vec{r}_a\rangle|^2|\langle\vec{r}_s\rangle|^2\langle|\phi|^2\rangle\ ,$$

where

$$\langle|\phi|^2\rangle_{av} = \langle|\cos\theta\cos\theta' + \sin\theta\sin\theta'\cos\phi - 3\cos\theta\cos\theta'|^2\rangle_{av}$$

$$= \langle|\sin\theta\sin\theta' - \cos\phi - 2\cos\theta\cos\theta'|^2\rangle_{av} = 2/3 \qquad \text{(II-19)}$$

We may show the specific energy states that are involved in $\langle\vec{r}_a\rangle$ and $\langle\vec{r}_s\rangle$ by rewriting them as $\langle\vec{r}_a(w_a,w_a+E)\rangle$ and $\langle\vec{r}_s(w_s^*,w_s^*-E)\rangle$ respectively, then the transition probability per unit time for dipole-dipole transfer may be shown by:

$$\omega_{sa} = \frac{4\pi\, e^4}{3\hbar\kappa^2 R^6 g_s' g_a}\sum_{I,f}\int dE\int dw_s^*\, P_s^*(w_s^*)\,|\langle\vec{r}_s(w_s^*,w_s^*-E)\rangle|^2$$

$$\times\ \{\int dw_a P_a(w_a)\,|\langle\vec{r}_a(w_a,w_a+E)\rangle|^2\} \qquad \text{(II-20)}$$

ω_{sa} may be calculated if the wave functions ψ_i and ψ_f are known. If such information is not known, as frequently happens, ω_{sa} may be related to experimentally determined parameters by using A and B parameters.

Expressing the Hamiltonian for the interaction between a collection of charges and the radiation field in terms of annihilation and creation operators for photons, the following equation is developed:

$$H_i = \frac{e}{mc}\vec{A}\cdot\vec{P} = \frac{e}{m}\sum_{k,\lambda}\left(\frac{h}{v\omega_k}\right)^{\frac{1}{2}}\left(a_k^{\lambda}\, e^{i\vec{k}\cdot\vec{r}} + a_k^{\lambda}\, e^{-\vec{k}\cdot\vec{r}}\right)(\hat{\pi}_k^{\lambda}\cdot\vec{P}) \qquad \text{(II-21)}$$

where $\hat{\pi}_k^{\lambda}$ is the polarization velor of phonon with wave vector $\vec{K}$ in branch λ. The expotentials are expanded as follows:

$$e^{\pm i\vec{k}\cdot\vec{r}}\,\vec{P} \doteq \vec{P} \pm i(\vec{k}\cdot\vec{r})\vec{P} \qquad \text{(II-22)}$$

The first term in the resultant expansion of H_i is the electric dipole term, which will be called H_1.

$$H_1 = \frac{e}{m}\sum_{k,\lambda}\left(\frac{h}{vw_k}\right)^{\frac{1}{2}}\left(a_k^{\lambda} + a_k^{\lambda t}\right)\hat{\pi}_k^{\lambda}\cdot\vec{P}$$

$$= \frac{e}{m}\sum_{k,\lambda}\left(\frac{h}{v\omega_k}\right)^{\frac{1}{2}}\left(a_k^{\lambda} + a_{\lambda}^{\lambda t}\right)\hat{\pi}_k^{\lambda}\cdot\left(\sum_i \vec{P}_i\right) \qquad \text{(II-23)}$$

P_k^{λ}, the probability of emission or absorption of one photon $\vec{K},\lambda$ (per unit time) is:

$$P_k^{\lambda} = \frac{2\pi}{\hbar}\left|M_k^{\lambda}\right|^2 g(\omega_k) \qquad \text{(II-24)}$$

where $M_k^{\lambda} = \langle\psi_f|H_i|\psi_i\rangle$, $n_{k_f}^{\lambda} = n_{k_i}^{\lambda} \pm 1$

Since $K_\lambda = \frac{2\pi}{L} \cdot n_x$, $K_y = \frac{2\pi}{L} \cdot n_y$, $K_z = \frac{2\pi}{L} \cdot n_z$ for a crystal of volume V = LxLxL, the density of states is

$$g(\vec{K})d\vec{K} = dn_x dn_y dn_z = \frac{L^3}{(2\pi)^3} dK_x dK_y dK_z = \frac{V}{8\pi^3} K^2 dK d\Omega_k$$

$$= \frac{V}{8\pi^3} \frac{\omega_k^2 d\omega_k}{r^3} d\Omega_k = g(\omega_k) d\omega_k d\Omega_k \qquad \text{(II-25)}$$

Also,

$$M_k^\lambda = \frac{e}{m}\left(\frac{h}{v\omega_k}\right)^{1/2} \begin{bmatrix} \sqrt{n_k^\lambda} \\ \sqrt{n_k^\lambda + 1} \end{bmatrix} \langle \psi_f \left| \begin{matrix} \sum_i e^{i\vec{K}\cdot\vec{r}_k} \hat{\pi}_k^\lambda \cdot \vec{P}_i \\ \sum_i e^{-i\vec{K}\cdot\vec{r}_i} \hat{\pi}_k^\lambda \cdot \vec{P}_i \end{matrix} \right| \psi_i \rangle ,$$

So,

$$P_k^\lambda d\Omega_k = \frac{\omega_k e^2}{hc^3 m^2} \begin{bmatrix} n_k \\ n_k + 1 \end{bmatrix} \left| \langle \psi_f \left| \begin{matrix} \sum_i e^{i\vec{K}\cdot\vec{r}_i} \hat{\pi}_k^\lambda \cdot \vec{P}_i \\ \sum_i e^{-i\vec{K}\cdot\vec{r}_i} \hat{\pi}_k^\lambda \cdot \vec{P}_i \end{matrix} \right| \psi_i \rangle \right|^2 \begin{matrix} \rightarrow \text{absorption} \\ \rightarrow \text{emission} \end{matrix}$$

(II-26)

It can be shown that:

$$\left| \langle \psi_f | e^{-i\vec{K}\cdot\vec{r}} \hat{\pi}_k^\lambda \cdot \vec{P} | \psi_i \rangle \right|^2 = \left| \langle \psi_i | e^{i\vec{K}\cdot\vec{r}} \hat{\pi}_k^\lambda \cdot \vec{P} | \psi_f \rangle \right|^2 \qquad \text{(II-27)}$$

This indicates $P_{emission} = P_{em}$ (spontaneous) + P_{em} (induced) with P_{em} (ind) = $P_{absorbed}$. The A coefficient is produced by summing P_{em} (spon.)

over all λ and integrating over all solid angles, so that

$$A = \frac{\omega_k e^2}{hC^3 m^2} \sum_k \int d\Omega_k \left| \langle \psi_f | \sum_i e^{i\vec{K}\cdot\vec{r}_i} \hat{\pi}_k^{\lambda} \cdot \vec{P}_i | \psi_i \rangle \right|^2 , \qquad \text{(II-28)}$$

$$A_{dipole} = \frac{\omega_k e^2}{2\pi\hbar C^3 m^2} \cdot \frac{2}{3} \cdot 4\pi \cdot \left| \langle \psi_f | \vec{P} | \psi_i \rangle \right|^2 \qquad \text{(II-29)}$$

Substituting the electric dipole term for full H_i. In this equation the 4π is from the $\int d\Omega_k$ and the $\frac{2}{3}$ is the sum of $\hat{\pi}_k^{\lambda} \cdot \vec{P}$ since this is the same as the averaging over orientations done earlier. Now,

$$\dot{F} = \frac{-i}{\hbar} [F,H] \text{ if } \frac{\partial F}{\partial t} = 0, \text{ so}$$

$$\dot{X} = \frac{-i}{\hbar} [X,H] = \frac{i}{\hbar} [H,X]$$

Therefore,

$$\vec{P} = \frac{im}{\hbar} [H,\vec{r}]$$

Thus,

$$\langle \psi_f | [H,\vec{r}] | \psi_i \rangle = \langle \psi_f | H\vec{r} - \vec{r}H | \psi_i \rangle$$

$$\frac{\hbar}{i} \langle \psi_f | \dot{\vec{r}} | \psi_i \rangle = (E_f - E_i) \langle \psi_f | \vec{r} | \psi_i \rangle$$

Now

$$E_f - E_i = \hbar\omega_k ,$$

So

$$\langle \Psi_f | \vec{P} | \Psi_i \rangle = i \frac{\not{h}}{\not{h}} \omega_k m \langle \psi_f | \vec{r} | \Psi_i \rangle$$

Thus

$$A_{dipole} = \frac{4\omega_k^3 e^2}{3\not{h}c^3} \left| \langle \Psi_f | \vec{r} | \Psi_i \rangle \right|^2 \qquad \text{(II-30)}$$

Or

$$A(E) = \frac{4e^2E^3}{3\not{h}^4c^3} \left| \langle \psi_f | \vec{r} | \psi_i \rangle \right|^2, \; E = \not{h}\omega_k \qquad \text{(II-31)}$$

Thus we show the Einstein A(E) coefficient, (the emission probability distribution over energy E), for an isolated atom, considering only electric dipole Hamiltonian as equation (II-31). In a crystal the inclusion of a probability function for the broadened energy levels modifies this quantity, and by the ratio $(\varepsilon_c/\varepsilon)$ which expresses how the crystal modifies the electric field and which must enter twice since the electric field occurs in the matrix element, which is squared. In addition, the probability includes K^2dK and K is multiplied by the index of refraction n in a crystal, so a factor of n^3 enters.

If a summation is made over all possible transitions that result in energy change E and (b) the degeneracy is divided out as before, the following equation results:

$$A(E) = \sum_i \sum_f \frac{4e^2E^3}{3\not{h}^4c^3g_i^*} (\varepsilon_c/\varepsilon)^2 n^3 \int \left| \langle r_{if}(w^*, w^*-E) \rangle \right|^2 P^*(w^*)dw^* \qquad \text{(II-32)}$$

The absorption probability distribution (the Einstein B-coefficient) is developed in a similar manner:

$$B(E) = \sum_i \sum_f \frac{2\pi e^2}{3\hbar^2 g_i} (\varepsilon_c/\varepsilon)^2 \int |\langle r_{if}(w,w+E)\rangle|^2 P(w)dw \qquad \text{(II-33)}$$

The Einstein A(E) coefficient indicates the probability for decay, so if it is integrated over E,

$$\int A(E)dE = 1/\tau \qquad \text{(II-34)}$$

where $A(E) = 1/\tau f(E)$, and τ = the radiative lifetime of the excited atom.

A normalized function f(E) may thus be defined, having an integral over E of unity. This function matches the shape of the emission spectrum. By using this part of Equation (II-20) may be evaluated in terms of experimentally determined parameters:

$$\sum_i \sum_f \int |\langle r_{if}(w^*,w^*-E)\rangle|^2 P^*(w^*)dw^* = \frac{3\hbar^4 c^3 g^*}{4n^3 c^2 E^3} (\varepsilon/\varepsilon_c) \frac{f(E)}{\tau} \qquad \text{(II-35)}$$

This derivation may only be used for very low concentrations since it ignores interactions between the emitter and other impurities.

The absorption cross section of an impurity is

$$\sigma(E) = \frac{2\pi\hbar E}{c/n} B(E)$$

where c/n = Photon velocity in a crystal.

If a normalized function F(E) is introduced which gives the shape of $\sigma(E)$, and the cross section is integrated over E, such that,

$$\int \sigma(E)dE = Q \qquad \text{(II-37)}$$

Then,

$$\sum_i \sum_f \int \left| \langle r_{if}(w, w+E) \rangle \right|^2 P(w)\,dw = \frac{3\hbar C g}{4\pi^2 e^2 n E} (\varepsilon/\varepsilon_c)^2 Q F(E) \qquad \text{(II-38)}$$

Now, making these substitutions for the sensitizer emission (II-35) and the activator absorption (II-20), the rate of dipole-dipole transfer becomes:

$$\omega_{sa} = \frac{3C^4 \hbar^4 Q_a}{4\pi K^2 n^4 R^6 \tau_s} (\varepsilon/\varepsilon_c)^4 \int \frac{f_s(E) F_a(E)}{E^4} dE \qquad \text{(II-39)}$$

Arranging the factors in customer groups results in (12,13)

$$\omega_{sa} = 1/\tau_s (R_o/R)^6 \qquad \text{(II-40)}$$

Whre R_o is the critical energy distance. This is a distance at which energy transfer between an isolated sensitizer-activator pair occurs at rate equal to the rate of deexcitation by all other means (given by the inverse of τ_s, the fluorescence lifetime).

$$R_o = \left[\frac{3C^4 h^4 Q_a}{4\pi K^2 n^4} (\varepsilon/\varepsilon_c)^4 \int \frac{f_s(E) F_a(E)}{E^4} dE \right]^{1/6} \qquad \text{(II-41)}$$

Time Dependence of Transfer to Random Sites

In a crystal in which both sensitizer and activator sites are randomly distributed, the fluorescence emission rate of the sensitizer is equal to $1/\tau'$ which is the sum of the radiative and non-radiative rates of decay, plus an energy transfer rate characteristic of its activator environment. Thus, all s-nsitizers surrounded by the same distribution of unexcited activators will decay at the same rate. Let

class C be the class of sensitizer with the same distribution of activators in their environment, and let N_s and N_c be the total number of sensitizers and the number of sensitizers in class C respectively. The number of excited sensitizers in class C may be termed N_c^*, and N_a is the number of activators. Further, let w_{sa} be the energy transfer rate to activators from sensitizers in class C, and let R, equal the distance of a sensitizer from activator. Then this energy transfer rate for electric dipole-dipole interaction is:

$$\omega_{sa} = 1/\tau \sum_{i=1}^{N_a} \left(\frac{R_o}{R_i} \right)^6 \qquad \text{(II-42)}$$

If a very short pulse of energy at t = o produces the initial sensitizer excitation, then for later times

$$\frac{dn_C^*}{dt} = 1/\tau \; n_c^* - \omega_{sa} \; n_c^* \qquad \text{(II-43)}$$

Therefore,

$$n_c^*(t) = n_c^*(O) \; e^{-(1/\tau+\omega_{sa})t} \qquad \text{(II-44)}$$

Let the probability of a sensitizer having environment C defines as P_c,

$$N_c = N_s P_c$$

In an earlier step (II-40), the orientations of sensitizer and activator dipoles have already been averaged into ω_{sa} and therefore into R_o. Thus, the probability of a sensitizer seeing environment C(P_c) may be seen as the product of probabilities of an activator

(taken over all activators) being a distance of R_i from that sensitizer.

Next, this probability of having an activator distance R_i away from the sensitizer is equal to the ratio of the volume within a thin spherical shell (Radius = R_i) of the crystal divided by the total volume (V): $4\pi R_i^2 dR_i/V$. Therefore,

$$P_c = \prod_{i=1}^{N_a} \frac{4\pi R_i^2 dR_i}{V} \tag{II-46}$$

which with Equations (II-44) and (II-45) gives

$$N_c^*(f) = KN_s\, e^{-(1/\tau+\omega_{sa})t} \prod_{i=1}^{N_a} 4\pi R_i^2 dR_i/V \tag{II-47}$$

Where K is the fraction of sensitizers originally excited. Thus, n*(t), the total number of excited sensitizers is

$$n^*(t) = KN_s \int_{N_a} \cdots \int e^{-(1/\tau+\omega_{sa})t} \prod_{i=1}^{N_a} \frac{4\pi R_i^2 dR_i}{V}$$

$$= KN_s\, e^{-t/\tau} \int \cdots \int \prod_{i=1}^{N_a} e^{-t/\tau (R_o/R_i)^6} \frac{4\pi R_i^2 dR_i}{V}$$

$$= KN_s\, e^{-t/\tau}\, (M)^{N_a} \tag{II-48}$$

Where

$$M = \int_0^{R_v} e^{-t/\tau (R_o/R)^6} \frac{4\pi R^2 dR}{V} \quad \text{and} \quad V = \frac{R\pi R_v^3}{3} \tag{II-49}$$

To evaluate M, let $y = (R_o/R)^6\, t/\tau$ and note that t is no larger than a few τ for times of interest.

Thus,

$$R^2 dR = \frac{R_o^3 t^{1/2}}{6\tau^{1/2} y^{3/2}} dy \qquad \text{(II-50)}$$

and

$$M = \int_{y=\infty}^{y_v} e^{-y} \frac{-4\pi R_o^3 t^{\frac{1}{2}}}{6\tau^{\frac{1}{2}}} \left(\frac{3}{4\pi R_v^3}\right) y^{-3/2} dy \qquad \text{(II-51)}$$

$$= \tfrac{1}{2} y_v^{\frac{1}{2}} \int_{y_v}^{\infty} e^{-y} y^{-3/2} dy \qquad \text{(II-52)}$$

where $y_v = (R_o/R_v)^6 t/\tau$. Integrating by parts,

$$M = \tfrac{1}{2} y_v^{\frac{1}{2}} \left[2e^{-y_v} y_v^{-\frac{1}{2}} - 2 \int_{y_v}^{\infty} e^{-y} y^{-\frac{1}{2}} dy\right] \qquad \text{(II-53)}$$

$$= e^{-y_v} - y_v^{\frac{1}{2}} \left[\int_o^{\infty} e^{-y} y^{-\frac{1}{2}} dy - \int_0^{y_v} e^{-y} y^{-\frac{1}{2}} dy\right], \qquad \text{(II-52)}$$

For any time of interest $y_v << 1$, since for almost any crystalline sample $R_v >> R_o$; therefore,

$$M = 1-y_v + \cdots - (\pi y_v)^{\frac{1}{2}} + y_v^{\frac{1}{2}} \int_o^{y_v} (y^{-\frac{1}{2}} - y^{\frac{1}{2}} + \cdots) dy \qquad \text{(II-53)}$$

$$\doteq 1-y_v - (\pi y_v)^{\frac{1}{2}} + 2y_v = 1+(\pi y_v)^{\frac{1}{2}} + \text{higher order terms.}$$

Thus,

$$M \doteq 1 - \frac{4\pi^{3/2} t^{1/2}}{3v\tau^{1/2}} R_o^3 \qquad \text{(II-54)}$$

Since $Y_v << 1$,

$$(M)^{N_a} \doteq \left(\frac{1-4\pi^{3/2}R_o^3}{3v} (t/\tau)^{\frac{1}{2}} \right)^{N_a} \qquad \text{(II-55)}$$

$$\doteq \exp \left[\frac{-N_a 4\pi^{3/2}R_o^3}{3v} (t/\tau)^{\frac{1}{2}} \right] \qquad \text{(II-56)}$$

Finally,

$$n^*(t) = KN_s \exp \left[- \frac{t}{\tau} - N_a 4\pi^{3/2}R_o^3/3v \ (t/\tau)^{\frac{1}{2}} \right] \qquad \text{(II-57)}$$

or

$$n^*(t) = KN_s \exp \left[- t/\tau - \omega_r t \right]$$

where ω_r defined as the total rate of transfer from the sensitizer population.

$$\omega_r = \omega_r(t) = 4\pi^{3/2} R_o^3 \, Ca/3(\tau t)^{\frac{1}{2}}$$

where $C_a = N_a/V$ is the activator concentration.

Diffusion Transfer Rate and Random Walk

In a situation where far more sensitizers than activators are present in a crystal, the proximity of an excited sensitizer to many unexcited sensitizers may make it likely that the excitation energy will migrate from sensitizer to sensitizer in multi-step sequence before finally being transferred to an activator. Since we view activator as a perfectly absorbing trap, we may describe the migration of the quanta of excitation exciton energy by either a diffusion equation or a random walk model. Both models gives the same theoretical predictions

if considered in the limit of many steps (14).

For both the diffusion transfer rate model and the random walk model, we consider the lattice sites for exciton motion to be in a uniform array. Both excitons and activator impurity ions are considered to be randomly distributed over these lattice sites. The activators are seen as functioning as spherical exciton "traps", and are assumed to have constant radii. An individual exciton may move through a crystal lattice without being affected by any traps located in that crystal so long as it does not enter the trapping sphere. Once the exciton migrates within the sphere there is unit probability that its energy will transfer to the activator.

In a lattice with the conditions delineated above, an exciton population will change at a rate described by the diffusion equation

$$\frac{\partial N(\vec{r},t)}{\partial t} = w(t) - \beta_s N(\vec{r},t) + D\nabla^2 N(\vec{r},t) \qquad \text{(II-58)}$$

With the boundary conditions

$$N(\vec{r},t) = N_o \quad \text{for} \quad t=o, \quad r>R$$
$$N(\vec{r},t) = o \quad \text{for} \quad t>o, \quad r=R \qquad \text{(II-59)}$$

In Equation (II-58), W(t) = rate of generating excited sensitizers, = decay rate for excitons, and D = the diffusion coefficient.

To solve the diffusion Equation (II-58) the following substitution is made:

$$N(\vec{r},t) = \frac{U(\vec{r},t)}{r} e^{-\beta_s t} \qquad \text{(II-60)}$$

resulting in

$$\frac{\partial U(r,t)}{\partial t} = r\, e^{\beta_s t}\, w(t) + D\, \frac{\partial^2 U(r,t)}{\partial r^2} \qquad \text{(II-61)}$$

A solution is already available for the homogeneous part (15) of Equation (II-61) within the appropriate boundary conditions as given in (II-59):

$$U(r,t) = 1 - \frac{R}{r} + \frac{2R}{r\pi^{\frac{1}{2}}} \int_o^{\frac{r-R}{2(Dt)^{\frac{1}{2}}}} e^{-x^2}\, dx \qquad \text{(II-62)}$$

The Green's function technique enables us to determine the particular solution, and the exciton concentration becomes

$$N(r,t) = \frac{e^{-\beta_s t}}{r} \int_o^t r\, e^{\beta_s y}\, w(y) \left[1 - \frac{R}{r} + \frac{2R}{2\pi^{\frac{1}{2}}} \int_o^{\frac{r-R}{2D^{\frac{1}{2}}(t-y)^{\frac{1}{2}}}} e^{-x^2}\, dx \right] dy \qquad \text{(II-63)}$$

Then we find the flux of excitons crossing into the sphere of the trap to be

$$F(t) = 4\pi R^2 \left[D\, \frac{\partial N(r,t)}{\partial r} \right]_{r=R} \qquad \text{(II-64)}$$

and we can make the substitution

$$F(t) = 4\pi\, DRe^{-\beta_s t} \int_o^t e^{\beta_s y}\, w(y) \left[1 + \frac{R}{\sqrt{\pi D(t-y)}} \right] dy \qquad \text{(II-65)}$$

in a situation where $W(t) = N_o\, \delta(t)$, we can obtain $F(t)$ by multiplying the exciton concentration ($N_o\, e^{-\beta_s t}$) times a rate constant that is a function of time:

$$F(t) = 4\pi DR\left[1 + \frac{R}{(\pi Dt)^{\frac{1}{2}}}\right] N_o e^{-\beta_s t} \qquad \text{(II-66)}$$

No trays correlation effects need to be considered in conditions where the concentration of traps in the lattice remains small. Now a product of this time-dependent rate constant and a trap concentration N_t can be substituted for the diffusion term $D\nabla^2 N(\vec{r},t)$, of Equation (II-58), resulting in

$$\frac{\partial N}{\partial t} = w(t) - \beta_s N - \omega(t)N \qquad \text{(II-67)}$$

where

$$W(t) = N_o \delta(t) \qquad \text{(II-68)}$$

and the otal trapping rate for N_t traps is

$$\omega(t) = 4\pi DRN_t\left(1 - \frac{R}{(\pi Dt)^{\frac{1}{2}}}\right) \qquad \text{(II-69)}$$

The time dependent term of (II-69) is nearly always so small with respect to the first term that for t>0.1 nsec it can be neglected and the energy transfer rate can be considered independent of time.

The rate for times of interest is thus the constant term

$$\omega = 4\pi DRN_t \qquad \text{(II-70)}$$

Therefore (II-58) becomes

$$\frac{\partial N}{\partial t} = W(t) - \beta_s N - \omega N \qquad \text{(II-71)}$$

Connection With Experiments

The motion of excitons produced randomly in the lattice by irradiation can be observed by their luminescent decay from both "host" molecules and the traps into which they must have migrated. We may connect the theory to experimental results by determining whether the equations accurately predict the fluorescent decay

We first examine the following rate equations:

$$\frac{\partial N_s(t)}{\partial t} = W(t) - \beta_s N_s(t) - \omega N_s(t) \qquad \text{(II-72)}$$

$$\frac{\partial N_s^{(o)}(t)}{\partial t} = W(t) - \beta_s N_s^{(o)}(t) \qquad \text{(II-73)}$$

These describe the time dependencies of excitons in the presence and absence of activators.

These may be solved by using the delta function excitation to obtain

$$N_s(t) = N_s^{(o)} \exp[-(\beta_s + \omega)t] \qquad \text{(II-74)}$$

$$N_s^{o}(t) = N_s^{(o)}(o) \exp(-\beta_s t) \qquad \text{(II-75)}$$

The predictions of these equations can be used to explain data obtained on total fluorescent decay times. Equations (II-74) and (II-75) predict that sensitizer fluorescence decays purely exponentially regardless of whether the sample being observed is doped or undoped.

We may use (II-74) and (II-75) to determine the sensitizer decay time ratio for doped and undoped samples when taken as a function of the activator concentration:

$$\frac{\tau_s^{(o)}}{\tau_s} = 1 + \tau_s^{(o)}\omega \qquad \text{(II-76)}$$

If (II-74) and (II-75) are then integrated overall time, a ratio of fluorescence intensities, similar to that given above, is obtained.

$$\frac{I_s^{(o)}}{I_s} = 1 + \tau_s^{(o)}\omega \qquad \text{(II-77)}$$

Results of both (II-76) and (II-77) enable evaluation of experimental data resulting from measurement of fluorescent decay. In addition, the equations may be solved to determine ω, the energy transfer rate constant.

Random Walk Model

As mentioned previously, it is assumed that lattice sites are uniformly distributed, traps are randomly spaced, and traps exhibit perfect absorbance (16). When an exciton is created at a lattice site the excitation energy is transferred to a closely neighboring ion after the elapsing of some time. If only this simple nearest-neighbor hopping is assumed, the hops may be said to occur at regular intervals "τ" where τ is a constant. The object of the energy transfer may either be a host or a trap site. The probability of luminescence from a host site after each hop may be referred to as "α" and as long as a trap is not entered this hopping process may continue, with each step having a probability $(1-\alpha)$ per time of the step. Hence, the excitation results in emission of a host fluorescence photon with a constant probability of α per time of one step. Alternatively, the energy may hop into a

trap, stopping the movement. A trap fluorescence photon is emitted later, and the probability of this luminescence per time of one step is ρ.

Utilizing these terms we may determine the probability of host fluorescence for a random step, n, of the walk in conditions where traps are present or absent.

$$\text{Traps absent:} \quad \alpha(1-\alpha)^{n-1} \tag{II-78}$$

$$\text{Traps present:} \quad \alpha(1-\alpha)^{n-1}(1-q) \tag{II-79}$$

where V_n = number of distinct sites visited on a walk before n is reached. The last factor in (II-79) is therefore the probability that none of the sites before n be traps.

According to random walk theory (16),

$$V_n \rightarrow (1-F)n \ .$$

where F is the probability that a walker returns at some point to the origin. Values for F for different lattice structures are given by Montroll (17) as

simple cubic lattice: 0.340537336

face-centered cubic lattice: 0.256318237

body-centered cubic lattice: 0.28222985

Thus, the host luminescence on step n is given by:

$$I_n^H = \frac{\alpha}{1-\alpha}\left[(1-\alpha)(1-q)^{1-F}\right]^n \ . \tag{II-81}$$

Probability for trap luminescence on the nth step is (18):

P = (Prob. of no luminescence in n, steps on host sites)

. (Prob. of no luminescence in waiting period on trap)

. ($n-n_1-1$ time interval). (Prob. of lum. in nth time interval)

. (Prob. of hitting a trap on, but not before, the n_1^{th} step).

Summed over all possible n_1's on which trapping might have occurred, the probability of trapping exactly on the n_1^{th} step is calculated using the known expressions for the probability of avoiding trapping. Thus,

$$P_{\text{trap at } n_1} = P_{\substack{\text{trap before} \\ \text{or at } n_1}} - P_{\text{trap before } n_1}$$

$$= \left[1-P_{\substack{\text{no trap before} \\ \text{or at } n_1}}\right] - \left[1-P_{\substack{\text{no trap} \\ \text{before } n_1}}\right]$$

$$= [1-(1-q)^{(1-F)n_1}] - [1-(1-q)^{(1-F)(n_1-1)}] \quad \text{(II-82)}$$

But expansion of $(1-q)^{1-F}$ for small q is

$$(1-q)^{1-F} = 1-(1-F)q \quad \text{(II-83)}$$

Therefore,

$$P_{\text{trap at } n_1} = -(1-q)^{(1-F)n_1} + (1-q)^{(1-F)n_1}[1-(F-1)q]$$

$$= (1-F)q(1-q)^{(1-F)n_1} \quad \text{(II-84)}$$

The total luminescence probability from the trap on the n^{th} time interval is:

$$I_n^T = \sum_{n_1=1}^{n} (1-\alpha)^{n_1-1} (1-\beta)^{n-n_1-1} \beta(1-F)q(1-q)^{(1-F)n_1}$$

$$= \frac{\beta(1-F)q(1-\beta)^n}{(1-\alpha)\ (1-\beta)} \sum_{n_1=1}^{n} \left[\frac{(1-\alpha)(1-q)^{1-F}}{(1-\beta)} \right]^{n_1} \qquad \text{(II-85)}$$

Now

$$\sum_{n_1=1}^{n} x^{n_1} = x \cdot \frac{1-x^n}{1-x} \qquad \text{(II-86)}$$

Therefore,

$$I_n^T = \frac{\beta(1-F)q(1-\beta)^n}{(1-\alpha)\ (1-\rho)} \cdot \frac{(1-\alpha)(1-q)^{1-F}}{(1-\rho)} \cdot \frac{1-\left[\frac{(1-\alpha)(1-q)^{1-F}}{(1-\beta)}\right]^n}{1-\left[\frac{(1-\alpha)(1-q)^{1-F}}{(1-\beta)}\right]}$$

$$= \frac{\beta(1-F)q(1-q)^{1-F}}{(1-\rho)\left[1-\rho-(1-\alpha)(1-q)^{1-F}\right]} \left\{ (1-\beta)^n - \left[(1-\alpha)(1-q)^{1-F}\right] \right\}$$

$$= \frac{\beta(1-F)q(1-q)^{1-F}}{(1-\beta)\left[\alpha-\beta+(1-\alpha)(1-F)q\right]} \left\{ (1-\beta)^n - \left[(1-\alpha)(1-q)^{1-F}\right]^n \right\} \qquad \text{(II-87)}$$

using the above small q approximation.

The define a, b, and c such that $(1-\alpha) \doteq e^{-a}$, $(1-\beta) = e^{-b}$, and $(1-q) = e^{-c}$, and note that for sufficiently small α, ρ, and q (16), $\alpha \doteq a$, $\beta \doteq b$, $q \doteq c$. Then

$$I_n^T = \frac{b(1-F)C(1-q)^{1-F}}{(1-\beta)\left[a-b+(1-a)(1-F)C\right.} \left\{ e^{-bn} - \left[e^{-an} e^{-(1-f)Cn} \right] \right\}$$

$$= \frac{b}{\frac{a-b}{(1-F)C} + (1-a)} \cdot \frac{(1-q)^{1-F}}{(1-\beta)} \left\{ e^{-bn} - e^{-\left[a+(1-F)C\right]n} \right\} \qquad \text{(II-88)}$$

Expressing time as $t = n\tau$, we have, if $(1-\beta)$ cancels with $(1-q)^{1-F}$ as in Rosenstock's paper (18).

$$I^{T}_{(t)} = \frac{b}{\frac{a-b}{(1-F)C} + (1-a)} \left[e^{-bt/\tau} - e^{-[a+(1-F)C]t/\tau}\right] \qquad \text{(II-89)}$$

and

$$I^{H}_{(t)} = \frac{a}{1-a} e^{-[a+(1-F)C]t/\tau} \qquad \text{(II-90)}$$

The decay time of host fluorescence in the presence of traps is determined from (II-90) as

$$\tau_H^{-1} = \frac{a+(1-F)C}{\tau} \qquad \text{(II-91)}$$

The same host fluorescence in the absence of trap is

$$\tau_H^{(o)-1} = a/\tau \qquad \text{(II-92)}$$

Since

$$\tau_H^{-1} = \tau_H^{(o)-1} + \omega \qquad \text{(II-93)}$$

The energy transfer rate is found as:

$$\omega = \frac{(1-F)C}{\tau} \qquad \text{(II-94)}$$

where τ^{-1} = probability of hopping onto a new site

$(1-F)$ = probability of not returning to origin

c = probability of new site being a trap.

Equations (II-91) and (II-92) may be used to calculate the ratio of host fluorescence decay time in the doped and undoped sample.

$$\frac{\tau_H^{(o)}}{\tau_H} = 1 + \tau_H^{o}\omega \qquad \text{(II-95)}$$

Then, integrating Equation (II-90) and Equation (II-91) over time, host and trap fluorescence intensities can be evaluated.

$$I_H = \int_o^\infty I_H(t)dt = \frac{a}{(1-a)} \cdot \frac{\tau}{[a+(1-F)C]} \qquad \text{(II-96)}$$

$$I_T = \int_o^\infty I_T(t)dt = \frac{b}{1+\left[\frac{a-b}{(1-F)C}\right]} \left[\frac{\tau}{a+(1-F)C} - \frac{\tau}{b} \right] \qquad \text{(II-97)}$$

The ratio of intensity for fluorescence in doped and undoped sample is:

$$\frac{I_H^{(o)}}{I_H} = 1 + \tau_H^{(o)}\omega \qquad \text{(II-98)}$$

By making comparisons between (II-95) and (II-98) and (II-76) and (II-77) it is determined that the random walk model produces the same basic theoretical predictions as the diffusion equation, at least (a) within the limit of many steps used in obtaining (II-89) and (II-90) and (b) where we assume excitons can only hop into nearest neighboring sites.

Effects of Diffusion on Energy Transfer

The assumption of a "trapping radius" is not expected to be always accurate, and it is probable that some direct energy transfer

from sensitizers to activators occurs. The effect of separation on transfer rate was indicated in Equation (II-40): a rapid but smooth variation of transfer rate as distance increases.

The model of "diffusion-limited relaxation" (19) may be more accurate than the "trapping radius" model unless diffusion into the trapping vicinity takes place very quickly. Yokota and Tanimoto (20) developed a model that takes into account both diffusion and electric dipole-dipole interaction in the sensitizer-activator relationship. The following description gives a detailed account of Yokota and Tanimoto's work.

Excited sensitizers are distributed according to the function of $n_s(R,t)$. When influenced by the diffusion of sensitizers and dipole-dipole transfer to activator ions,

$$\frac{\partial n_s}{\partial t} = \frac{1}{\tau} n_s - \sum_i \frac{\alpha}{r_i^6} n_s + D\nabla^2 n_s \qquad \text{(II-99)}$$

where D = diffusion constant

τ = sensitizer lifetime, and

r_i = the distance between a given sensitizer-activator pair

Here we use the term alpha from Equation (II-40), in which

$$\alpha = R_o^6/\tau_s$$

Where donors and activators are assumed to be in uniform and random distribution, respectively, a summation is made over all sensitizers and an average taken over all activator positions.

$$N_s(t) = N_s(o)\, e^{-t/\tau} \left\langle e^{-t(-D\nabla^2 + \sum_i \alpha/r_i^6)} \right\rangle_{av} \qquad \text{(II-100)}$$

where the total number of excited sensitizers is represented by N_s and the averaging over activators by $\langle\ \rangle_{av}$.

Next we assume that the activators have a low concentration so that each is unaffected by others and we represent the total number of activators by the term N_a. Now the sensitizer decay term due to energy transfer to one activator may be taken to the N_a power. If we convert the sum over all sensitizer-activator separations to an integral over the crystal volume, a step possible because of the assumed uniform distribution for sensitizers, we get the average transfer rate to a single activator. Thus,

$$N_s(t) = N_s(o)\, e^{-t/\tau} \left\{ \frac{1}{v} \int_o^{R_v} 4\pi r^2\, e^{-t(-D\nabla_r^2 + \alpha/r^6)}\, dr \right\}^{N_a} \qquad \text{(II-101)}$$

where $V = 4\pi R_{v/3}^3$. Due to the angular independence of the Equation (II-40), no angular dependence appears in this expression. An expansion may then be performed, for both ∇_r^2 and r^{-6} are Hermitian.

$$\exp\left(tD\nabla_r^2 - \frac{\alpha t}{r^6}\right) = \exp\left(-\frac{\alpha t}{r^6}\right) \left\{ 1 + \sum_{n=1}^{\infty} (-1)^n \right.$$

$$\left. \times \int_o^t dt_1 \cdots \int_o^{t_{n-1}} dt_n\, U(t_1) \cdots U(t) \right\}$$

where

$$U(t) = e^{t\alpha/r^6} (-D\nabla_r^2)\, e^{-\alpha t/r^6} \qquad \text{(II-102)}$$

only a few terms of the sum need to be retained if we assume D to be

rather small, and we can write

$$N_s(t) = N_s(o)\, e^{-t/\tau} \left[\frac{4\pi}{v} \int_o^{R_v} dr\, r^2\, e^{-t\alpha/r^6} \left\{1+\int_o^t dt_1\, e^{\alpha t_1/r^6}\right.\right.$$

$$\times D\nabla_r^2\, e^{-\alpha t_1/r^6} + \int_o^t dt_1 \int_o^{t_1} dt_2 \left(e^{t_1\alpha/r^6}\right.$$

$$\left.\times \left(e^{t_2\alpha/r^6} D\nabla_r^2\, e^{-\alpha t_2/r^6}\right)\right.$$

$$+ \int_o^t dt_1 \int_o^{t_1} dt_2 \int_o^{t_2} dt_3 \left(e^{\alpha t_1/r^6} D\nabla_r^2\, e^{-\alpha t_1/r^6}\right)$$

$$\times \left(e^{\alpha t_2/r^6} D\nabla_r^2\, e^{-\alpha t_2/r^6}\right)$$

$$\left.\left.\cdot \left(e^{\alpha t_3/r^6} D\nabla_r^2\, e^{-\alpha t_3/r^6}\right) + \ldots\ldots\right\}\right]^{N_a}$$

$$= N_s(o)\, e^{-t/\tau} \left[I_o + I_1 + I_2 + I_3 + \cdots\right]^{N_a} \qquad \text{(II-103)}$$

An evaluation of these terms (where I_n is the term dependent on D^n), through T_3, will now be shown. I_o was previously considered by Eisenthal and Siegal (21).

$$I_o = \frac{4\pi}{v} \int_o^{R_v} e^{-\alpha t/r^6}\, r^2 dr = -\frac{2\pi(\alpha t)^{\frac{1}{2}}}{3V} \int_\infty^{x_v} e^{-x}\, x^{-3/2}\, dx \qquad \text{(II-104)}$$

where

$$x = \alpha t/r^6 \text{ and } X_v = \alpha t/R_v^6 = tR_o^6/\tau R_v^6 .$$

The X_v term may be assumed much less than 1 since for all terms we are interested in t is less than several. If we now integrate by parts,

we have

$$I_o = \frac{2\pi(\alpha t)^{\frac{1}{2}}}{3V} \{2e^{x_v} x_v^{-\frac{1}{2}} - 2\int_{x_v}^{\infty} e^{-x} x^{-\frac{1}{2}} dx\}$$

$$= \frac{4\pi(\alpha t)^{\frac{1}{2}}}{3V} \{e^{-x_v} x_v^{-\frac{1}{2}} + \int_o^{x_v} e^{-x} x^{-\frac{1}{2}} dx - \int_o^{\infty} e^{-x} x^{-\frac{1}{2}} dx\}$$

$$= \frac{4\pi(\alpha t)^{\frac{1}{2}}}{3V} \{x_v^{-\frac{1}{2}} - x_v^{\frac{1}{2}} + \cdots + \int_o^{x_v} (x^{-\frac{1}{2}} - x^{\frac{1}{2}} + \cdots)dx - \Gamma(\tfrac{1}{2})\}$$

$$\doteq \frac{4\pi(\alpha t)^{\frac{1}{2}}}{3V} \{x_v^{-\frac{1}{2}} - \Gamma(\tfrac{1}{2}) + \text{higher order terms}\} . \qquad \text{(II-105)}$$

We now find the I_o term (noting that $\Gamma(\frac{1}{2}) = \pi^{\frac{1}{2}}$ and $V = \frac{4\pi}{3} R_v^3$) as

$$I_o \doteq 1 - \frac{4\pi^{3/2}(\alpha t)^{\frac{1}{2}}}{3V} \qquad \text{(II-106)}$$

We should perform the time integration for evaluating the term linear in D:

$$\int_o^t dt_1 e^{\alpha t_1/r^6} D\nabla_r^2 e^{-\alpha t_1/r^6} = \int_o^t dt_1 e^{\alpha t_1/r^6} D[\frac{1}{r^2}\frac{\partial}{\partial r}$$

$$x \{r^2 \frac{\partial}{\partial r} e^{-\alpha t_1/r^6}\}]$$

$$= \int_o^t dt_1 e^{\alpha t_1/r^6} D[\frac{1}{r^2}\frac{\partial}{\partial r}(\frac{\partial \alpha t_1}{r^5} e - \frac{\alpha t_1}{r^6})]$$

$$= \int_o^t dt_1 e^{\alpha t_1/r^6} D(-\frac{30\alpha t_1}{r^8} + \frac{36\alpha^2 t_i^2}{r^{14}}) e^{-\alpha t_1/r^6}$$

$$= D\left(\frac{12\alpha^2 t^3}{r^{14}} - \frac{15\alpha t^2}{r^8}\right) \qquad \text{(II-107)}$$

Now assume $X = \alpha\, tr^{-6}$ as before, and $X_v << 1$ for times of interest, we have:

$$I_1 = \frac{4\pi D}{V} \int_o^{R_v} \left(\frac{12\alpha^2 t^3}{r^{12}} - \frac{15\alpha t^2}{r^6}\right) e^{-\alpha t/r^6}\, dr$$

where

$$\begin{cases} r = (\alpha t)^{1/6}\, x^{-1/6} \\ dr = \left(\frac{\alpha t}{6}\right)^{1/6} x^{-7/6}\, dx \end{cases}$$

$$= \frac{4\pi D}{V} \int_\infty^{X_v} (12tx - 15tx) e^{-x} \left[-1/6 x^{-7/6} (\alpha t)^{1/6} dx\right]$$

$$= \frac{4\pi D}{V} \int_{X_v}^{\infty} (2tx^{5/6} - 5/2tx^{-1/6}) (\alpha t)^{1/6}\, e^{-x} dx \qquad \text{(II-108)}$$

where $\int_o^\infty x^{n-1}\, e^{-x}\, dx = \Gamma(n)$, and by the fact that $X_v << 1$, so expand X_v, therefore,

$$I_1 = \frac{4\pi D}{V}(\alpha t)^{1/6}\, t\left[2\Gamma\left(\frac{11}{6}\right) - 2 \int_o^{x_v} (x^{5/6} - x^{1/6} + \cdots) dx - 5/2\Gamma(5/6)\right.$$

$$\left. + 5/2 \int_o^{x_v} (x^{-1/6} - x^{5/6} + \cdots) dx\right]$$

$$= \frac{4\pi D \alpha^{1/6} t^{7/6}}{V} \left[10/6\Gamma(5/6) - 5/2\Gamma(5/6) + \text{terms of order } X_v^{5/6} \right.$$

$$\left. \text{and higher}\right]$$

$$\doteq \frac{4\pi D \alpha^{1/6} t^{7/6}}{V} \left[5/6\Gamma(5/6)\right] \qquad \text{(II-109)}$$

In a similar manner we perform time integration for the quadratic term in D, making use of Equation (II-107),

$$\int_o^t dt_1 \int_o^{t_1} dt_2 \left(e^{\alpha t_1/r^6} D\nabla_r^2 e^{-\alpha t_1/r^6}\right)\left(e^{\alpha t_2/r^6} D\nabla_r^2 e^{-\alpha t_2/r^6}\right)$$

$$= D^2 \int_o^t dt_1 \int_o^{t_1} dt_2 \left(e^{\alpha t_1/r^6} \nabla_r^2 e^{-\alpha t_1/r^6}\right)\left(\frac{36\alpha^2 t_2^2}{r^{14}} - \frac{30\alpha t_2}{r^8}\right)$$

$$= D^2 \int_o^t dt_1 \int_o^{t_1} dt_2\, e^{\alpha t_1/r^6}\, 1/r^2\, d/dr\left[-\frac{36.14\alpha^2 t_2^2}{r^{13}} + \frac{8.30\alpha t_2}{r^7}\right.$$

$$\left. + \frac{6.36\alpha^3 t_1 t_2^2}{r^{19}} - \frac{30.6\alpha^2 t_1 t_2}{r^{13}}\right] e^{-\alpha t_1/r^6}$$

$$= D^2 \int_o^t dt_1 \int_o^{t_1} dt_2\, e^{\alpha t_1/r^6}\, 1/r^2 \left\{\left[\frac{36.14.13\alpha^2 t_2^2}{r^{14}} - \frac{8.30.7\alpha t_2}{r^8}\right.\right.$$

$$\left. - \frac{6.36.19\alpha^3 t_1 t_2^2}{r^{20}} + \frac{30.6.13\alpha^2 t_1 t_2}{r^{14}}\right]$$

$$\times e^{-\alpha t_1/r^6} + \left[\frac{36.14.6\alpha^3 t_1 t_2^2}{r^{20}} + \frac{8.30.6\alpha^2 t_1 t_2}{r^{14}} + \frac{6.36.6\alpha^4 t_1 t_2^2}{r^{26}}\right.$$

$$\left. \left. - \frac{30.6.6\alpha^3 t_1^2 t_2}{r^{20}}\right] e^{-\alpha t_1/r^6} \right\}$$

$$= D^2 \int_o^t dt_1 \left[\frac{36.14.13\alpha^2 t_1^3}{3r^{16}} - \frac{8.30.7\alpha t_1^2}{2r^{10}} - \left[\frac{(6.36.19)-(36.14.6)}{3r^{22}}\right]\alpha^3 t_1^4\right.$$

$$\left. - \frac{30.6.6\alpha^3 t_1^4}{2r^{22}} + \frac{(30.6.13+8.30.6)\alpha^2 t_1^3}{2r^{16}} + \frac{6.36.6\alpha^4 t_1^5}{3r^{28}}\right]$$

$$= D^2(72\alpha^4 t^6/r^{28} - 81.36\alpha^3 t^5/5r^{22} + 97.21\alpha^2 t^4/2r^{16} - 7.40\alpha t^3/r^{10}) \qquad \text{(II-110)}$$

Making the substitution as before,

$$I_2 = \frac{4\pi D^2}{6V}(\alpha t)^{-1/6} t^2 \int_{X_v}^{\infty} dx\, e^{-x}\left[72x^{19/6} - \frac{81.36x^{13/6}}{5} + \frac{97.21x^{7/6}}{2} - 7.40x^{1/6}\right]$$

$$= \frac{4\pi D}{6V}\alpha^{-1/6} t^{11/6}\left[72\Gamma(25/6) - 81.36/5\Gamma(14/6) - 97.21/2\Gamma(13/6) - 7.40\Gamma(7/6) + \int_o^{X_v} dx\ (\text{terms of order } x^{1/6})\right]$$

$$\doteq \frac{89\pi D^2}{15V}\alpha^{-1/6} t^{11/6}\left[\Gamma(13/6)\right] \qquad \text{(II-111)}$$

Now we will calculate the cubic term, making time integration as follows, using Equation (II-110)

$$I_3 = \int_o^t dt_1 \int_o^{t_1} dt_2 \int_o^{t_2} dt_3\ (e^{\alpha t_1/r^6} D\nabla_r^2 e^{-\alpha t_1/r^6})$$

$$\times\ (e^{\alpha t_2/r^6} D\nabla_r^2 e^{-\alpha t_2/r^6}) \cdot (e^{\alpha t_3/r^6} D\nabla_r^2 e^{-\alpha t_3/r^6})$$

$$I_3 = D^3 \int_o^t dt_1 \int_o^{t_1} dt_2 \int_o^{t_2} dt_3 (e^{\alpha t_1/r^6} \nabla_r^2 e^{-\alpha t_1/r})\left(\frac{36.36}{r^{28}} t_2^2 t_3^2 \alpha^4 - \frac{6.33.36}{r^{16}} t_2 t_3^2 \alpha^3 - \frac{30.36\alpha^3 t_2^2 t_3}{r^{22}} + \frac{6.21.30}{r^{16}} t_2 t_3 \alpha^3\right.$$

$$+ \frac{13.14.36}{r^{16}} \alpha^2 t_3^2 - \frac{7.8.30\alpha t_3}{r^{10}})$$

$$= D^3 \int_o^t dt_1 \int_o^{t_1} dt_2 \int^{t_2} dt_3 \left[\frac{36.36.36}{r^{42}} \alpha^6 t_1^2 t_2^2 t_3^2\right.$$

$$- \frac{6.36.36.61}{r^{36}} \alpha^5 t_1 t_2^2 t_3^3 - \frac{6.33.36.36}{r^{36}} \alpha^5 t_1^2 t_2 t_3^2$$

$$- \frac{30.36.36}{r^{36}} \alpha^5 t_1^2 t_2^2 t_3 + \frac{27.28.36.36}{r^{30}} \alpha^4 t_2^2 t_3^2 + \frac{33.36.36.44}{r^{30}} \alpha^4 t_1 t_2 t_3^2$$

$$+ \frac{6.30.36.49}{r^{30}} \alpha^4 t_1 t_2^2 t_3 + \frac{6.21.30.36}{r^{30}} t_1^2 t_2 t_3 \alpha^4 + \frac{13.14.36.36}{r^{30}} \alpha^4 t_2^2 t_3^2$$

$$- \frac{6.21.22.33.36}{r^{24}} \alpha^3 t_2 t_3^2 - \frac{21.22.30.36}{r^{24}} \alpha^3 t_2^2 t_3$$

$$- \frac{21.30.36.37}{r^{25}} \alpha^3 t_1 t_2 t_3 - \frac{6.13.14.36.37}{r^{24}} \alpha^3 t_1 t_3^2$$

$$- \frac{7.8.30.36}{r^{24}} \alpha^3 t_1^2 t_3 + \frac{16.21.30.40}{r^{18}} \alpha^2 t_2 t_3$$

$$\left. + \frac{13.14.15.16.36}{r^{18}} t_1^2 \alpha^2 + \frac{8.25.30.42}{r^{18}} t_1 t_3 \alpha^2 - \frac{30.56.40}{r^{15}} t_3 \alpha\right]$$

$$= D^3 \left[\frac{288\alpha^6}{r^{42}} t^9 - \frac{29.592\alpha^5}{5r^{36}} t^8 + \frac{187.542\alpha^4}{5r^{30}} t^7 - \frac{842.709\alpha^3}{10r^{24}} t^6\right.$$

$$\left. + \frac{57.288\alpha^2}{r^{18}} t^5 - \frac{6.300\alpha}{r^{12}} t^4\right] \qquad \text{(II-112)}$$

Now I_3 is calculated by means of the same technique

$$I_3 = \frac{4\pi D^3}{6V} (\alpha t)^{-\frac{1}{2}} t^3 \int_{X_v}^{\infty} dx\, e^{-x}\left[288x^{11/12} - \frac{29.592}{5} x^{0/2}\right.$$

$$\left. + \frac{187.542}{5} x^{7/2} - \frac{842.709}{10} x^{5/2} + 57.288x^{3/2} - 6.300x^{\frac{1}{2}}\right]$$

$$= \frac{4\pi D\alpha^{-\frac{1}{2}}}{6V} t^{5/2} \left[288\Gamma\left(\frac{13}{2}\right) - \frac{29592}{5} \Gamma\left(\frac{11}{2}\right) + \frac{187.542}{5} \Gamma\left(\frac{9}{2}\right)\right.$$

$$\left. - \frac{842.709}{10} \Gamma\left(\frac{7}{2}\right) + 572.288\, \Gamma\left(\frac{5}{2}\right) - 6.300\, \Gamma\left(\frac{3}{2}\right) + \int_o^{x_v} dx \text{ (terms of order } x^{\frac{1}{2}})\right]$$

$$\doteq \frac{4}{6V} D^3\alpha^{-\frac{1}{2}} t^{5/2} \left[-\frac{693}{8} \Gamma\left(\frac{3}{2}\right)\right]$$

$$I_3 = -\frac{4\pi^{3/2}}{V} D^3\alpha^{-\frac{1}{2}} t^{5/2} \left[\frac{693}{96}\right] \qquad \text{(II-113)}$$

Now the time dependent excited sensitizer population, using these calculations and Equation (II-103), may be expressed as

$$N_s(t) \doteq N_s(o)e^{-t/\tau} \{1 - \frac{4\pi^{3/2}}{3V} \alpha^{\frac{1}{2}}t^{\frac{1}{2}} \left[1 + \frac{5}{2} \pi^{-\frac{1}{2}} \Gamma\left(\frac{5}{6}\right)\right.$$

$$\left. \cdot D\alpha^{-1/3}t^{2/3} - \frac{89}{20} \pi^{-\frac{1}{2}}\Gamma\left(\frac{13}{6}\right)D^2\alpha^{-2/3}t^{4/3} + \frac{693}{32} D^3\alpha^{-1}t^2\right]\}^{N_a}$$

Then by making the substitution of $n_a = \frac{N_a}{V}$, and the fact that $\alpha^{\frac{1}{2}}/V$ is proportional to $(R_o^3/R_v^3) << 1$,

$$N_s(t) \doteq N_s(o)\ \exp\{-\frac{t}{\tau} - \frac{4\pi^{3/2}}{3} n_a \alpha t t^{\frac{1}{2}} [1 + \frac{5}{2}\pi^{-\frac{1}{2}}\Gamma(\frac{5}{6})D\alpha^{-1/3}t^{2/3}$$

$$- \frac{89}{20}\pi^{-\frac{1}{2}}\Gamma(\frac{13}{6})D^2\alpha^{-2/3}t^{4/3} + \frac{693}{32}D^3\alpha^{-1}t^2]\} \qquad \text{(II-114)}$$

It should be noted that when D = o, we will get the number of excited sensitizers, which we described in single step rate of Equation (II-56). Also note that the term linear in D in Equation (18) of Reference (20) has a misprint, showing the wrong exponent for π.

Long term behavior of (II-14) is not clear. Although diffusion to trapping ans single-step energy transfer rate during the period shortly after excitation occurs, causing a complicated time dependence, long-term behavior would more closely resemble a simple diffusion model with a pure exponential decay. The reason for this is that sensitizers that were originally in close proximity to activators would have a high probability of transferring their energy as time passes. So as time increases these will become depleted and no longer make a contribution to the transfer rate. Then the diffusion of excitation quanta, excitons, into the vicinity of activators will limit the transfer rate, producing the trend toward pure exponential decay. Because of this situation, we may use the (1,2) pade' approximant to re-express Equation (II-114). If the three pade' approximant coefficients are fit to the coefficients of D, D^2 and D^3, a long-term dependence that is physically reasonable can be determined by raising the expression to the appropriate power. We may note that the above equation's exponent takes the form of an expansion in powers of $X = D\alpha^{-1/3}t^{2/3}$, and thus write the time dependent excited sensitizer population as

$$N_s(t) \doteq N_s(o)\ \exp\left[-\frac{t}{\tau} - \frac{4\pi^{3/2}}{3} n_a\, \alpha^{\frac{1}{2}} t^{\frac{1}{2}} \left(\frac{1+a_1x+a_2x}{1+b_1x}\right)^{3/2}\right] \qquad \text{(II-115)}$$

The reason for choosing 3/4 as the exponent is that as X becomes large, the energy transfer contribution to the decay is dependent on time to an extent controlled by $t^{\frac{1}{2}}\ X^{3/4}$, proportional to t.

A Maclaurin expansion of the pade' approximant enables us to determine the a_1, a_2, and b_1 coefficients in (II-115):

$$\left[\frac{1+a_1x+a_2x}{1+b_1x}\right]^{3/4} = 1 + 3/4x \left| \left(\frac{1+a_1x+a_2x^2}{1+b_1x}\right)^{-\frac{1}{2}} \left(\frac{a_1+2a_2x}{1+b_1x} - b_1 \frac{1+a_1x+a_2x^2}{(1+b_1x)^2}\right)\right|_{x=0}$$

$$+ \frac{x^2}{2} \left| \left[\left(\frac{3}{4}\right)\left(\frac{-1}{4}\right)\left(\frac{1+a_1x+a_2x^2}{1+b_1x}\right)^{-5/4} \left(\frac{a_1+2a_2x}{1+b_2x} - b_1 \frac{1+a_1x+a_2x^2}{1+b_1x}\right) \cdot \left(\frac{a_1+2a_2x}{1+b_1x} - b_1\right.\right.\right.$$

$$\left.\left.\left. x \frac{1+a_1x+a_2x^2}{(1+b_1x)^2}\right) + 3/4 \left(\frac{1+a_1x+a_2x^2}{1+b_1x}\right)^{-\frac{1}{4}} \cdot \left(\frac{2a_2}{1+b_1x} - b_1 \frac{a_1+2a_2x}{(1+b_1x)^2} - b_1\right.\right.\right.$$

$$\left.\left.\left. x \frac{(a_1+2a_2x}{(1+b_1x)^2} + 2b_1^2\ (1+b_1x)\ \left(\frac{1+a_1x+a_2x}{(1+b_1x)^3}\right)\right]\right|_{x=0}$$

$$+ \frac{x^3}{3} \left| \left(\frac{-3}{16}\right)\left(\frac{-5}{4}\right)\left(\frac{1+a_1x+a_2x^2}{1+b_1x}\right)^{-9/4} \left(\frac{a_1+2a_2x}{1+b_1x}\right) - b_1 \frac{1+a_1x+a_2x^2}{(1+b_1x)^2}\right.$$

$$\left. \cdot \left(\frac{a_1+2a_2x}{1+b_2x} - b_1 \frac{1+a_1x+a_2x^2}{1+b_1x}\right)\left(\frac{a_1+2a_2x}{1+b_1x} - b \frac{1+a_1x+a_2x^2}{(1+b_1x)^2}\right) + \left(\frac{-3}{16}\right)\right.$$

$$\left. x \left(\frac{1+a_1x+a_2x^2}{1+b_1x}\right) - 5/4 \left(\frac{a_1+2a_2x}{1+b_1x} - b_1 \frac{1+a_1x+a_2x^2}{(1+b_1x)^2}\right) \cdot \left\{\left[\frac{2a_2}{1+b_1x} - b_1\right.\right.\right.$$

$$x\,\frac{a_1+2a_2x}{(1+b_1x)^2} - b_1\left(\frac{a_1+2a_2x}{1+b_1x} - b\,\frac{1+a_1x+a_2x^2}{(1+b_1x)^2}\right)\Big] + \Big[\frac{2a_2}{1+b_1x} - b_1\,\frac{a_1+2a_2x}{(1+b_1x)^2}$$

$$- b_1\left(\frac{a_1+2a_2x}{(1+b_1x)^2} - 2b_1\,\frac{1+a_1x+a_2x^2}{(1+b_1x)^3}\right)\Big]\Big\}\Big|_{x=o} + \cdots\cdot$$

$$= 1 + 3/4\,(a_1-b_1)x - 3/8\,\Big[\frac{(a_1-b_1)^2}{4} - 2a_2 + 2b_1\,(a_1-b_1)\Big]x^2$$

$$+ 1/8\,\Big[\frac{5}{16}\,(a_1-b_1)^3 - 3/2\,a_2(a_1-b_1) + 3/2\,b_1(a_1-b_1)^2 - 6a_2b_1 + 6b_1^2$$

$$\cdot\,(a_1-b_1)\Big]x^3 + \cdots\cdot \qquad \text{(II-116)}$$

It is only necessary to retain terms up to X^3 for this calculation. If we equate the coefficients of each power of X to the corresponding coefficients in (II-115) and then solve the resulting equations, the following values are obtained, closely agreeing with work of Yokota and Tanimota:

$$\begin{aligned} a_1 &= 10.87 \\ a_2 &= 15.51 \\ b &= 8.745 \end{aligned} \qquad \text{(II-117)}$$

These values will be used in the final expression

$$N_s(t) \doteq N_s(o)\; e^{-t/\tau}\; \exp\Big[-\frac{4}{3}\,\pi^{3/2} n_a \alpha^{1/2} t^{1/2}\,\Big(\frac{1+10.87x+15.51x^2}{1+8.745x}\Big)^{3/4}\Big] \qquad \text{(II-118)}$$

assuring agreement with previous work. Here

$$X = D\,\alpha^{-1/3} t^{2/3}\,.$$

The diffusion model type of decay, purely exponential in nature, that results when time from excitation becomes great and the sensitizer to activator transfer rate coefficient, α, is small is expressed below for $X >> 1$:

$$\underset{x\to\infty}{N_s}(t) \doteq N_s(o)\ e^{-t/\tau}\ \exp\left[-\frac{4}{3}\pi^{3/2}\ n_a\ \alpha^{\frac{1}{2}}t^{\frac{1}{2}}\ \left(\frac{15.5}{8.745}\ x\right)^{3/4}\right]$$

$$= N_s(o)\ e^{-t/\tau}\ \exp\left[-\frac{4}{3}\pi^{3/2}\ n_a\ \alpha^{\frac{1}{2}}t^{\frac{1}{2}}\ (1.536D^{3/4}\alpha^{-\frac{1}{4}}t^{\frac{1}{2}})\right]$$

$$= N_s(o)\ e^{-t/\tau}\ \exp\left[0.907\,(4\pi n\alpha^{\frac{1}{4}}D^{3/4})\,t\right] \qquad \text{(II-119)}$$

Here the trapping radius R has been replaced by the quantity $0.907\ (\alpha/D)^{\frac{1}{4}}$, as can be seen if Equation (II-119) is compared with the long time limit of Equation (II-69). If a different method is used to estimate the numerical coefficient of this rate, it may vary: 0.676 is the coefficient most commonly found in the literature, a number derived by Yokota and Tanimoto (20) complicated scattering length method. If we substitute this value, we have, the long time transfer rate:

$$\omega = 4\pi n_a D(0.676\ \alpha^{\frac{1}{4}}\ D^{-\frac{1}{4}}) \qquad \text{(II-120)}$$

and will make use of this result in the present study.

Hopping Mechanisms of Energy Transfer

The "hopping mechanisms" of energy transfer sees the rate excitation transfer from site to site in a lattice varying in a random fashion. More specifically, the ω_{sa} value (the determinant of whether or not

energy transfer to an activator will occur) has a step wise pattern of variance.

When the excitation is on sensitizer number one, during a short interval of time $(0,t_1)$, we can represent the probability of transfer to activator as

$$t_1 P_1 = t_1 \sum_i \omega_{sa}(\vec{R}_1 - \vec{R}_i) \qquad \text{(II-121)}$$

where $\vec{R}_1$ is the position of sensitizer i. A jump to sensitizer #2 occurs at $t = t_2$ and at $t = t_3$ it hops to sensitizer 3. Probability of transfer during the second time interval

$$(t_1, t_2) \text{ is: } (t_2 - t_1)P_2 \; ; \qquad \text{(II-122)}$$

and this type of representation continues for successive time intervals.

If the mean value of this time interval is τ_o, according to stochastic theory $\phi(t)$, $[\phi(t) = \int \rho(\vec{R},t)d^3\vec{R}$ is given by the solution of the Equation (II-22)

$$\phi(t) = \bar{\rho}(t)\, e^{-t/\tau_o} + \tau_o^{-1} \int_o^t \phi(t')\bar{\rho}\,(t-t')\, e^{-(t-t')/\tau_o}\, dt'$$

$$= \bar{\rho}(t) e^{-t/\tau_o} + \tau_o^{-1} \int_o^t \phi(t-t')\, \bar{\rho}(t') e^{-t'/\tau_o}\, dt'$$

where $\bar{\rho}(t)$ is the statistical average of $\rho(t)$ over the various possible sensitizer environments, if ρ_j is taken as the probability that sensitizer j at a position R_j becomes excited at time t. Thus $\phi(t)$ value depends on its previous value at time (t-t'), and can be calculated by numerical methods. For large t, exponential decay of the function $\phi(t)$ occurs at a rate determined by migration. However, if t is small enough to negate the influence of migration, $\phi(t)$ does not exhibit this

exponential decay, in this limit it approaches $\bar{\rho}(t)$.

Let us consider a crystal containing two impurity ions labeled A and B separated by the distance R. For a dipole-dipole mechanism of A and B interaction we will now attempt to characterize $\phi(t)$. The $\phi(t)$ decay for large t occurs at the exponential rate $\tau^{-1} + \omega_m$. The ω_m is given by:

$$\omega_m(\text{diff}) = 4\pi DC_B R_s, \quad R_s = (0.676)(\alpha_{AB}/D)^{\frac{1}{4}} \tag{II-124}$$

When $\phi(t)$ is the solution of the following equations:

$$\frac{\partial \rho(R,t)}{\partial t} = -\tau^{-1} + D\nabla^2 - \sum_{i=1}^{N_B} \omega_{AB}(\vec{R} - \vec{R}_i)\, \rho(\vec{R},k) \tag{II-125}$$

$$\phi(t) = \int \rho(\vec{R},T)\, d^3\vec{R}$$

To understand ω_m it is useful to create the image of a sphere surrounding the diffusing exciton whose radius has the same measure as the scattering length R_s. The rate of B ions entrance into this sphere is ω_m. It is a dipole-dipole A-A interaction, $\omega_{AA} = (\alpha_{AA}/R^6)$, causes this diffusion, then we can take the diffusion coefficient from the theory of exciton diffusion (23) and get:

$$D = \tfrac{1}{2}\left(\frac{4\pi}{3}\right)^{4/3} C_A^{4/3} \alpha_{AA} \tag{II-126}$$

Experiments on two systems (19,24) have confirmed that D is proportional to α_{AA}, when investigators varies the sensitizer concentration C_A, D increased more quickly with increasing $C_A^{3/4}$ (25,26). Measured values of D for rare earth ions fall into the range of 10^{-14} cm^2/sec to 10^{-9} cm^2/sec, hence being smaller than D values for excitons in molecu-

lar crystals by several orders of magnitude. Substitution of (II-126) in (II-125) gives

$$\omega_m(\text{diff}) = 21\, C_B\, C_A\, (\alpha_{AA}^3\, \alpha_{AB})^{1/4} \qquad \text{(II-127)}$$

When Equation (II-123) is used to obtain $\phi(t)$, ω_m can be calculated from

$$M^{(\text{hop})} = (2\pi 2/3)\, C_B\, (\alpha_{AB}/\tau_o)^{1/2} \qquad \text{(II-128)}$$

If we use the definition $\alpha_{AB} = \tau_o^{-1} R_o^6$ to obtain another critical separation R_c, we can write Equation (II-128) as

$$\omega_M(\text{hop}) = \frac{\pi}{2} \left(\frac{C_B}{\tau_o}\right) \left(\frac{4\pi R_C^3}{3}\right) \qquad \text{(II-129)}$$

The number of B ions in a sphere with radius R_c is $C_B(\frac{4\pi}{3} R_o^3)$. Since, as mentioned before, ω_m represents the rate of B ions, coming into the sphere of, interaction surrounding the hopping exciton, and thus R_c is analogous to R_s. If a dipole-dipole mechanism characterized the A-A ion interactions, the time τ_o (assumed to be much smaller than τ) is approximated as

$$\tau_o = \int_o^\infty t\bar{\rho}(t)dt / \int_o^\infty \rho(t)dt = (27/8\pi^3)(\alpha_{AA} C_A^2)^{-1} \qquad \text{(II-130)}$$

τ_o may be less than 10^{-9} sec (27) (for very high rare earth sensitizer concentration). This may be substituted into Equation (II-129) to get

$$\omega_M(\text{hop}) = 20\, C_B\, C_A\, (\alpha_{AA}\, \alpha_{AB})^{1/2} \qquad \text{(II-131)}$$

It should be noticed that although both Equations (II-127) and (II-131)

predict ω_m to be proportional to C_B and C_A, they differ with regard to the dependence on the interaction constants α_{AA} and α_{AB}. On the following page (Table I) summarized, and compaired the results of diffusion process and hopping mechanism. One noteworthy of the hopping mechanism is that the hopping distance is fixed due to an assumption of uniform separation between hoppers, in reality this obviously is not fixed, especially when the hopping occurs from a sensitizer to an activator that are randomly distributed. This limits the accuracy of the calculation. However, in the diffusion model the assumption is made that exciton transfer occurs like a wave or flow hence this is not exact either. Since neither procedure promises more accuracy the diffusion method is often preferred since it is easier, so it depends on the type of process whether one uses the one or the other.

ω_m(diff.) and ω_M(hop.) differ in the dependence on the interaction constants α_{AA} and α_{AB}, and for the case in which $\alpha_{AB} = \alpha_{AA}$ we will get the same result.

TABLE I

SUMMARIZED, AND COMPARED THE RESULTS OF DIFFUSION PROCESS AND HOPPING MECHANISM

Diffusion Process	Hopping Mechanism
$\omega_m(\text{diff.}) = 4\pi C_B R_S$ (I)	$\omega_M(\text{hop.}) = (2\pi^2/3) C_B (\alpha_{AB}/\tau_o)^{\frac{1}{2}}$ (III)
where $R_S = (0.676)(\alpha_{AB}/D)^{\frac{1}{4}}$	$= (\frac{\pi}{2}) C_B/\tau_o (4\pi R_c^3/3)$
If the diffusion is due to a dipole-dipole A-A interaction, $\omega_{AA} = \alpha_{AA}/R^6$	Where we define $\alpha_{AB} = \tau_o^{-1} R_c^6$.
Then $D = \frac{1}{2}(\frac{4\pi}{3})^{4/3} C_A \alpha_{AA}$ (II)	If the A ions interact with each other via the dipole-dipole mechanism, the time
Substitution of (II) in (I) gives:	$\tau_o = (27/8\pi^3)(\alpha_{AA} C_A^2)^{-1}$ (IV)
	Substitution of (IV) in (III) gives:
$\omega_m(\text{diff.}) = (21) C_B C_A (\alpha_{AA}^3 \alpha_{AB})^{\frac{1}{4}}$	$\omega_M(\text{hop.}) = (20) C_B C_A (\alpha_{AA} \alpha_{AB})^{\frac{1}{2}}$

CHAPTER III

DESCRIPTION OF EXPERIMENTAL APPARATUS AND SAMPLES

For the work on energy migration in $Y_3(Al_{1-x}Ga_x)_5O_{12}:Nd^{3+}$ mixed crystal, we had four different samples supplied by Texas Instruments containing 10%, 22%, 39% and 50% by weight Gallium and having approximately 1% of the Yttrium ions replaced by neodymium ions.

The $Y_3(Al_{0.5}Ga_{0.5})_5O_{12}:Nd^{3+}$ crystal was found from mass spectroscopy analysis ration of Nd to Y ions of 8.5×10^{-3} to one.

The atomic structure around an yttrium site is depicted in Figure 1. Eight oxygen atoms are arrayed nearest to the central yttrium as if forming the corners of a distorted cube. Four of the ten aluminum atoms, in relation to which the yttrium is tetrahedrally coordinated, in turn have six oxygen atoms octahedrally coordinated around them. The remaining six aluminum atoms in the lattice site are tetrahedrally coordinated by four proximal oxygen atoms (5).

Techniques and Apparatus

The experimental apparatus used for obtaining time-resolved spectra and lifetimes is shown in Figure 2. The duration of the pulse is about 8 nanoseconds and about 350 KW peak power at 3371^{o}A typically used at a repetition rate of 30HA. Also a tunable dye laser was used for site selection. The dye laser, a system science and softward DL-8, was pumped by the NRG nitrogen laser.

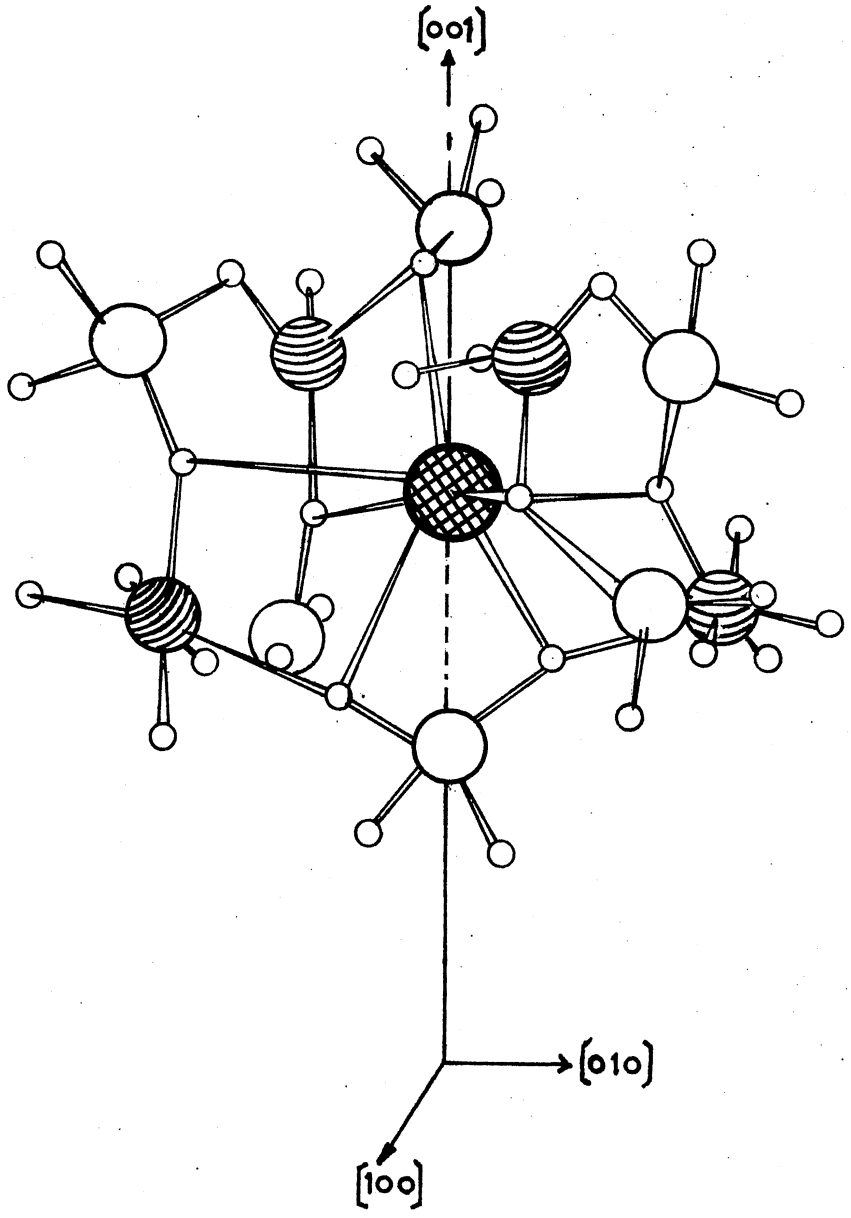

Figure 1. Basic Structure of a Site in the Garnet Crystal Surrounding an Yttrium Atom, the Checked Ball in the Center. All the other large balls are aluminums, the striped aluminums being coordinated by six oxygens (small circles) and the others by four oxygens (5)

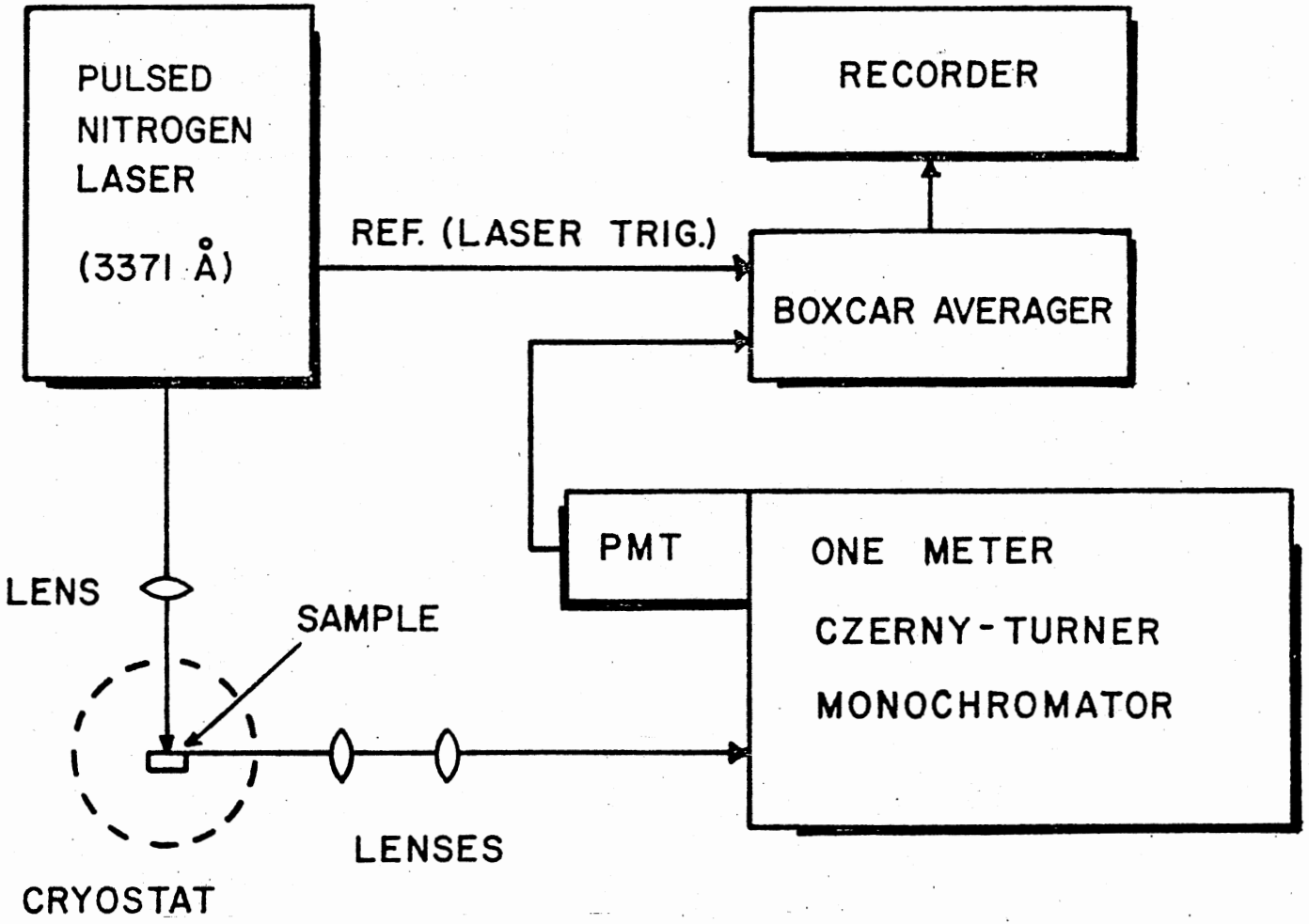

Figure 2. Time Resolved Spectroscopy Apparatus

The appropriate dye cell is inserted into an optical cavity formed by a diffraction grating and a partially transmitting mirror.

The output of the nitrogen laser is then focused within the dye by a cylindrical lens. Specific wavelengths are selected by tuning the dye laser cavity with the diffraction grating. The output line of this laser for a given dye can be tuned within an average of about 300 ^{o}A and by using different dyes it covers a range from 3559 ^{o}A to 6818 ^{o}A. The dye used in this work was a solution of rhodamine 6-G in ethanol. The laser was tuned in this study so that the linewidth of the output beam was between 0.04 and 0.05 nm.

The light from the laser system was focused on the sample which was mounted on the cold finger of an air products and chemicals model CS-2-2 displex cryogenic refrigerator. This is a closed cycle helium refrigerator with the capability of continuously varying the sample temperature from room to about 12 ^{o}K.

Thermal contact between the sample and the cold finger was aided by application of a small amount of air products cry-con conducting grease, carefully positioned behind the mounting chips holding the sample to avoid excitation of the grease by the excitation source and any resulting fluorescence. The temperature of the sample was measured by a chromel vs. gold-0.07 atomic percent iron thermocouple.

The sample fluorescence was focused onto the entrance slit of a Spex one meter Czerny-Turner monochromator. For the sample containing 50% Gallium studies the monochromator was equipped with a grating blazed at one micron, giving the monochromator a dispersion of 0.8 nm per mm. For the spectra of Nd in the host containing 22% and 39% Gallium a grating blazed at 500 nm was used, and giving a dispersion

of 0.4 nm per mm. The slit width was varied depending upon the particular circumstances of the spectra. The light was detected by a thermoelectrically cooled RCA C31034 phototube.

The output of phototube was processed by a Princeton Applied Research Corporation Model 162 Boxcar Averager that had two Model 164 processor modules to form a gated signal recovery system. A variable resistor placed in parallel with the input impedence of the Boxcar allowed adjustment of the time constant of the input circuit such that an undistorted signal could be received. The averager is triggered directly from the nitrogen laser.

The Boxcar accepts the input signal only during a selected time aperture that can be continuously adjusted from 5 ns to 50 ns after a triggering signal, and can be set fixed of scanned along a delay range from 5% to 100% of the range.

Corning color filters were used on the entrance slits of the one meter monochromator. For energy transfer study filter number 2-59 and 2-64 were used to eliminate scattered laser light while passing the fluorescence signal efficiently.

Time-Resolved Spectroscopy Measurements

Time-resolved spectroscopy is a technique which allows us to follow the time evolution of a fluorescence signal after excitation (2,3). In this case we keep the boxcar aperture fixed at a specific time after the laser pulse and we scan the spectrometer. Then the boxcar finds the average of the fluorescence signal at the specific time after the laser pulse for the given small interval of time of the aperture. In this way we could get the fluorescence spectrum at a specific time after

pulse which was a strip chart recorder.

Life Time Measurements

For measurement of lifetimes the spectrometer was set on the desired fluorescence wavelength and the boxcar aperture was scanned over a properly selected range. We can record the averaged shape in time of the fluorescence signal and thus the lifetime can be measured. A variable load resistor was again employed to minimize the response time of the system.

Other Equipment

Room temperature absorption measurements were taken on a Cary 14 spectrophotometer.

Temperature dependent absorption spectra for pure YAIG and pure YGG crystals were obtained using a 1,000 W tangstan halogen lamp as the light source. The light from the lamp was passed through the sample which was mounted on the cold finger of the cryogenic refrigerator.

The light passing through the sample was then passed through a chopper and into the one-meter monochromator. A current sensitive preamplifier and PAR lock-in amplifier were used to analyze the output signal from the photomultiplier tube.

The apparatus for temperature dependent absorption spectra is shown in Figure 3.

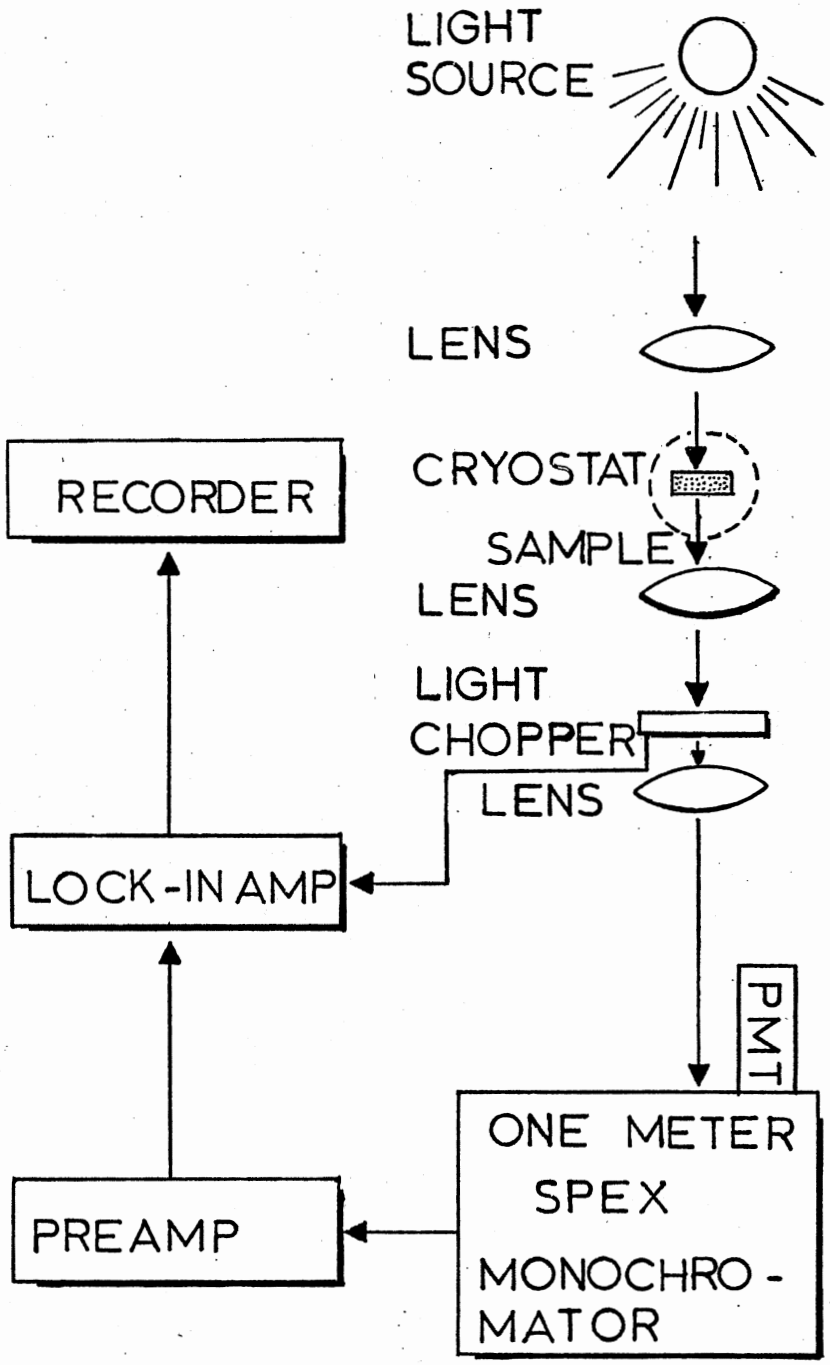

Figure 3. Block Diagram of the Apparatus Used for Obtaining Temperature Dependent Absorption Spectra

CHAPTER IV

SITE-SELECTION SPECTROSCOPY OF $Y_3(Al_{1-x}Ga_x)_5O_{12}:Nd^{3+}$

A recently developed tool for investigating energy transfer is the narrow band tunable dye laser. When such lasers are used as excitation sources, they are capable of exciting very closely spaced energy levels, such as those found for ions of some given type that are located in environments with different molecular configurations and hence different electronic characteristics. The characteristic of these lasers that enables such application is that their line widths can be varied over a very broad range and the user can select a desired line width and "tune" the laser so that other line widths are eliminated.

If a host crystal has a high concentration of active ions, ion-ion interaction may be possible so that energy migrates among those ions. Since the crystal field sites around various ions will inevitably be different, the energy migration will result in random emissions from the different sites. If the detection system has sufficient resolving power, a series of fluorescence lines may be observed in accordance with the energy level separation of these emissions. These lines will originate from ions in different crystal field sites and are often closely spaced.

Glass hosts will always feature many different types of sites, so broad band excitation will produce a very large (~100 cm^{-1}) fluores-

cence line 28. In conditions where the active ions are not sufficiently concentrated to permit ion-ion interactions or energy migration, laser excitation will result in the emission of a significantly narrower fluorescence line, with only broadening of a homogeneous type produced by electron phonon interactions. The inhomogeneous broadening will not appear. This "laser induced fluorescence line narrowing" has applications.

However, crystal hosts feature a much smaller number of field sites, producing less pronounced effects from the laser induced fluorescence line narrowing. Even when broad band excitation is attempted, there are not enough sites to produce more than a rather narrow fluorescence line. However, individual transitions may be observed as mentioned before, provided that the emissions from the different types of sites in the crystal have enough energy separation to be resolved by the detection system. Information from such site selection spectroscopy is extremely useful for interpreting energy transfer data; the investigator can use the tunable dye laser to excite ions in different regions within a Gaussian absorption line of interest and procure fluorescence emission data that indicates selective excitation of different sites associated with this absorption.

Spectra of Mixed Crystals

Watts and Holton (5) carried out a detailed examination of $Y_3(Al_{1-x}Ga_x)_5O_{12}:Nd^{3+}$. They described the nature of the variations in the crystal fields from Nd site to Nd site that produce the splitting at low temperatures. The differences in the way Va is substituted for the Al ions surrounding the Nd are important because although there is

little difference in the effective charges of the Ga and Al, the Ga is much larger than Al. The result is that as different numbers of Ga are substituted for Al atoms in the shell around the Nd site, there will be different strain fields at the Nd site due to interactions with this shell.

They pointed out that a Gaussian inhomogeneous line shape at low temperatures, which would be expected if Ga was randomly distributed in Al sites, is not found. They compared the spectra at 2 K near 1.07 μm for transitions from the $^4F_{3/2}$ level when x = 0 (pure Al), x = 0.07, and x = 0.11. Each line spits into two components of unequal intensity, with intensities more similar for x = .11 that for x = .07. This intensity distribution is clearly not Gaussian. This finding is taken to mean that Ga is nonrandomly distributed about Nd with at least two different preferred types of clustering. These differential pumping effects can also be observed at 77 K but not at room temperatures.

The conclusion of Watts and Holton is that the use of mixed crystals as a host material for Nd results in a 3.3 improvement in energy/pulse capability for Q-switched laser operation at 1.06 μm, but that a still greater improvement would have been achieved if the "detailed nature of the crystalline fields (had) been slightly different". They comment that perhaps other crystalline hosts will be found that can be "mixed" to produce even better results.

These investigators (5) also reported variations in fluorescence wave lengths versus pumping wavelengths and resolved the transitions shown by ions with varying crystal field environments. In this study the author attempts to further characterize the $Y_3(Al_{1-x}Ga_x)_5O_{12}:Nd^{3+}$ garnet system with regard to the spectroscopic properties of the neo-

dymium, but the author focuses on the $^4F_{3/2}$ - $^4I_{9/2}$ transitions, which have important bearing on various energy transfer properties that will be discussed.

Since a thorough knowledge of the energies and homogeneous broadening of the levels of Nd^{3+} in YAl G and YGaG is necessary as a preliminary step in the analysis of mixed Al/Ga crystals, the work to be reported here first deals with the spectroscopy of the YAlG:Nd and YGaG:Nd which reported by another (29). The researcher expects that the Nd sites in the mixed crystals can have energy levels within the spread values between the YAlG:Nd and YGaG:Nd crystals energies of a particular level. Some of the energy levels will have a statistically greater probability of occurring than others. For example, in the 50% Ga sample sites whose energies are midway between the YAlG:Nd and YGaG:Nd levels are more likely to be found. And in 10% Ga sample, sites whose energies are nearer to the YGaG:Nd level are more likely to be found. The levels of the mixed crystals will, then, have a large inhomogeneous broadening in addition to any homogeneous broadening which may occur. Figure 4 shows the 17°K absorption spectrum of $Y_3(Al_{0.5}Ga_{0.5})_5O_{12}:Nd^{3+}$ sample of Nd concentration 1.19 x 10^{20} cm^{-3} for the region 5750 to 5690Å. And Figure 5 shows the 17°K absorption spectrum of YAlG:Nd, and YGaG:Nd samples of Nd concentrations 1.17 x 10^{20} cm^{-3} and 3.23 x 10^{19} cm^{-3}. The structures agree with that typically observed in these materials, with the transitions of interest being the $^4I_{9/2}$ to $^4F_{3/2}$ group near 8800Å. This spectrum observed by using the techniques and equipment described in Chapter III. The observed sharp lines near 5900Å being the $^4I_{9/2}$ to $^2G_{7/2}$ and $^4G_{5/2}$ line group transitions offer the possibility of selective excitation of ions in different sites.

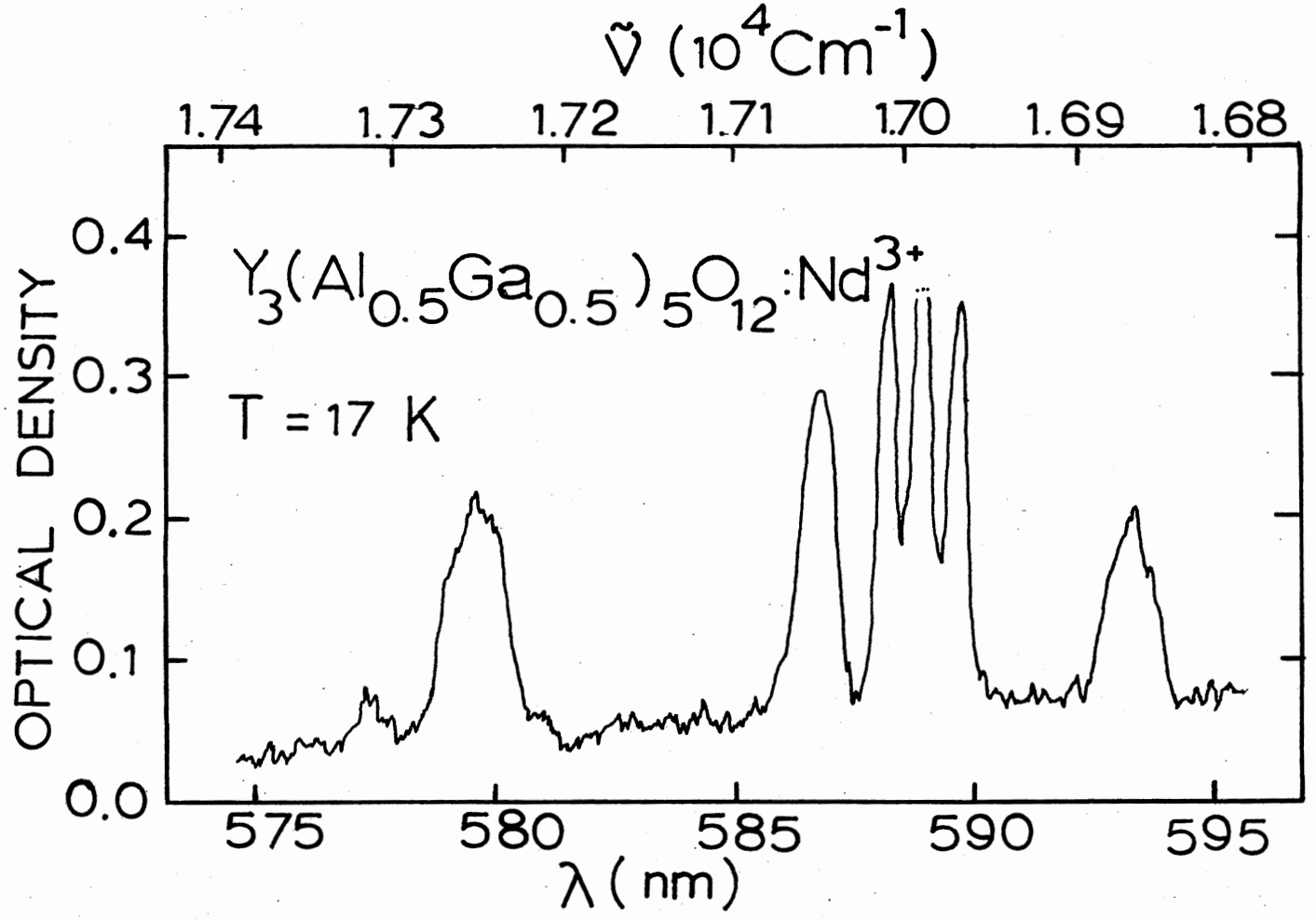

Figure 4. Absorption Spectrum of $Y_3(Al_{0.5}Ga_{0.5})_5O_{12}:Nd^{3+}$ at 17°K

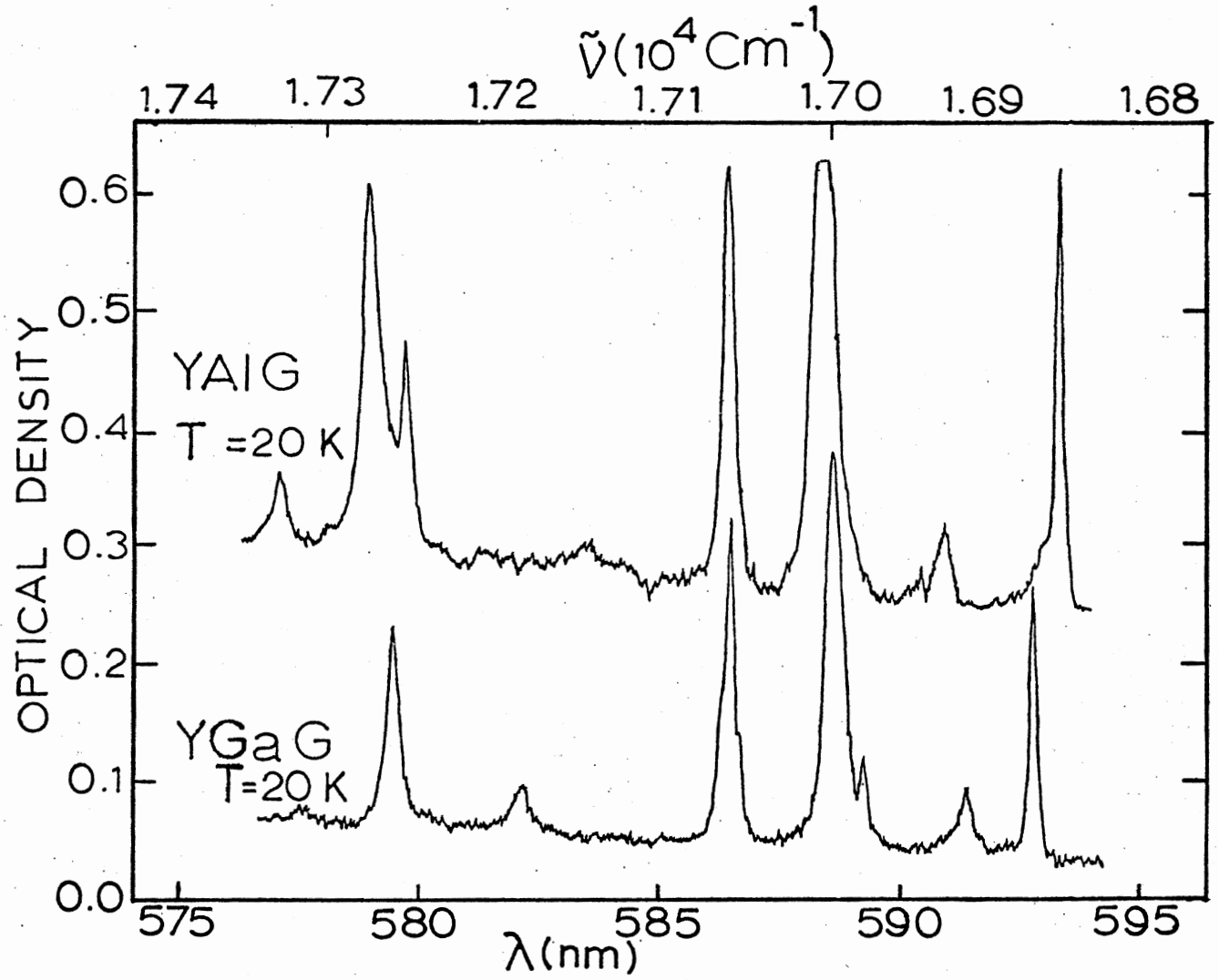

Figure 5. Absorption Spectrum of YAlG:Nd and YGaG:Nd at 17°K

The excitation pulse was 10 μsec in duration and less than half an angstrom in halfwidth.

Dependence on Excitation Wavelength and Temperature

An example of the energy levels produced by $Y_3(Al_{0.5}Ga_{0.5})_5O_{12}:Nd^{3+}$ crystal consistent with results of earlier work, is shown in Figure 6. A comparison of fluorescent spectra at 14 K Nd^{3+} ions in five garnet crystals spanning the range from pure Ga to pure Al (100% Ga, 50% Ga and 50% Al, 78% Al and 22% Ga, 90% Al and 10% Ga, and 100% Al) may be seen in Figure 7. These spectra were obtained in the region of the $^4F_{3/2} - {}^4I_{9/2}$ transitions.

Some important aspects of these spectra should be mentioned. One interesting observation is that each individual transition shifts its position uniformly as a function of the concentration of Ga, but the extent of the position shift as well as the direction is not the same for different transitions. This phenomena is elaborated in more detail in Figure 8. A consistency may be seen between these linear variations and the linear variations found in garnet lattices parameter (5) going from 12.005 angstroms in $Y_3Al_5O_{12}$ to 12.265 angstroms in $Y_3Ga_5O_{12}$ (30, 31); however, the characteristics of different shifts for different transitions cannot as yet be explained in complete detail.

Another aspect of the spectra in Figure 7 which deserves attention is the fact that the inhomogeneous broadening of the transitions increase as the proportion of Gallium (x) increases up to 0.5. The pure garnet hosts produce transition line widths which are much smaller than in any of the mixed hosts. To be specific, for the a-2 transition

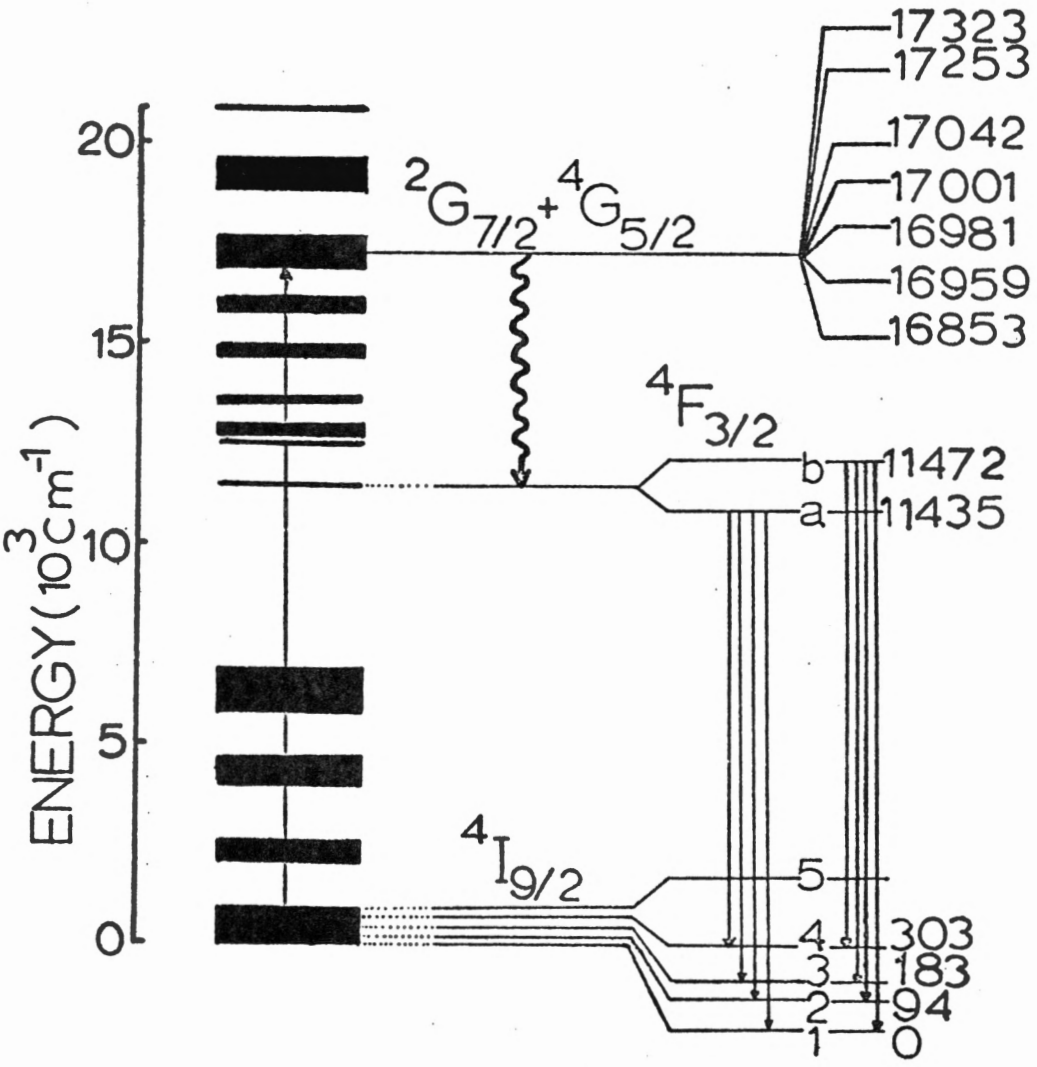

Figure 6. Energy Levels of Nd^{3+} Ions in $Y_3(Al_{0.5}Ga_{0.5})_5O_{12}$ Crystals

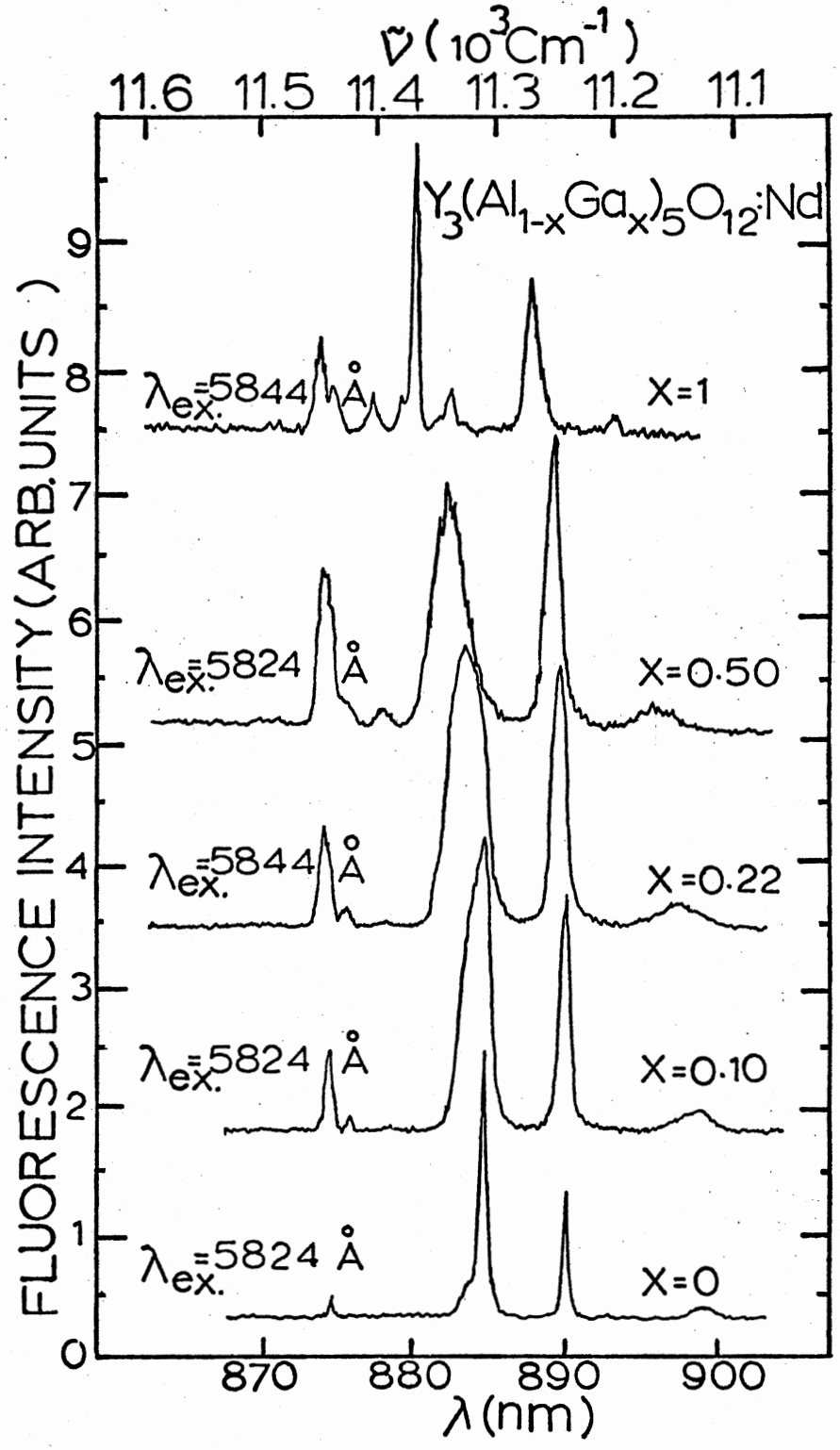

Figure 7. Fluorescence Spectra of the $^4F_{3/2}$ - $^4I_{9/2}$ Transitions at 14°K for Different Host Composition

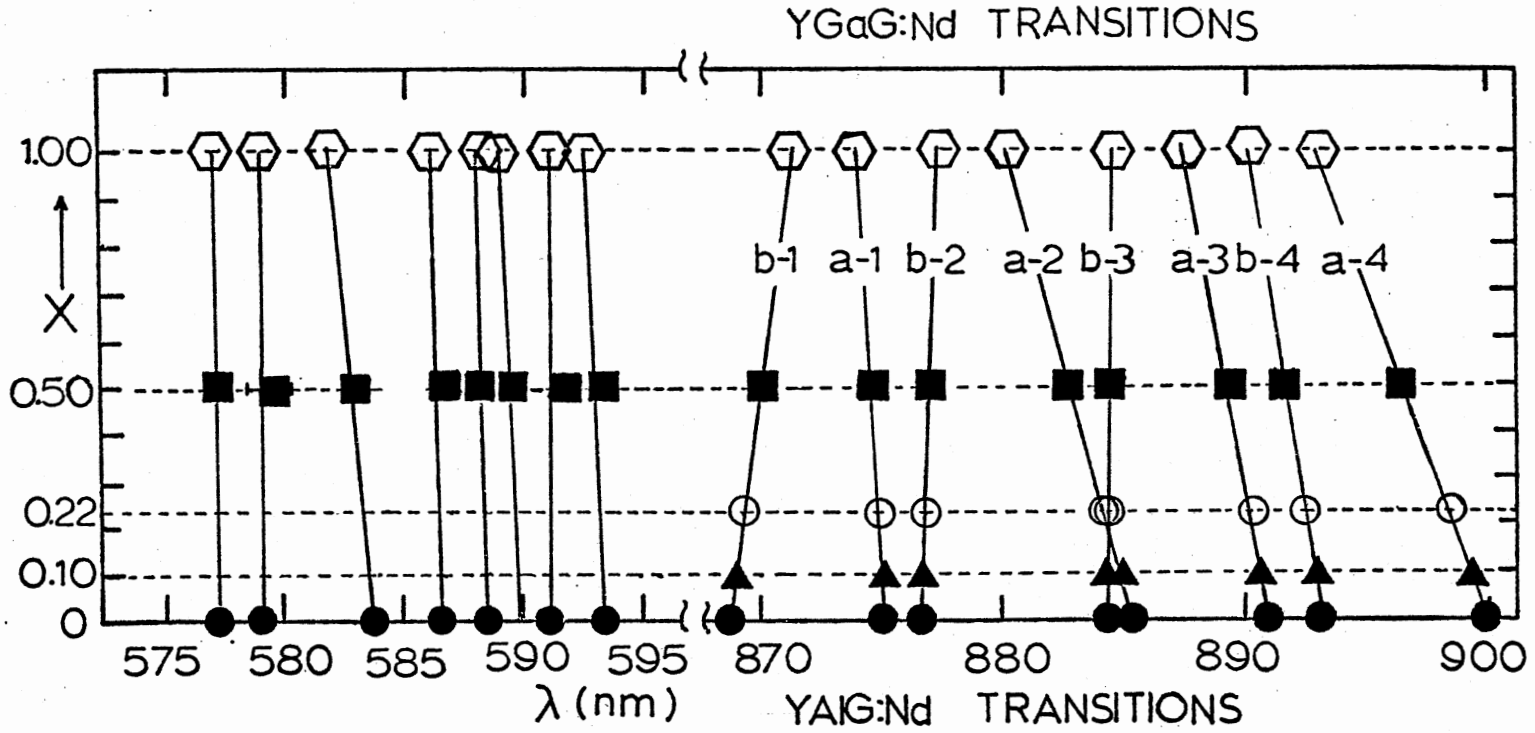

Figure 8. Fluorescence Peak Positions as a Function of Host Compositions

$\nabla\tilde{\nu}$ inhomogeneous varies from about 6.39 cm^{-1} in the $Y_3Al_5O_{12}$ crystal to about 28.9 cm^{-1} in $Y_3(Al_{0.5}Ga_{0.5})_5O_{12}$. The explanation for this consistent inhomogeneous broadening is that the neodymium ions in the doped mixed crystals are distributed randomly and hence are placed in a variety of lattice sites where the crystal fields have different microscopic strains due to somewhat different compositions. We notice that in the 50% sample, for example, the width of a_2 is not large enough to spread all the way from the a_2 position in YalG:Nd to the a_2 position in YGaG:Nd.

The transition energies for the inequivalent sites will vary enough to broaden the spectral line. The fact that peak positions shift linearly with the composition parameter x provides a clue which enables construction of a simple statistical model to account for the inhomogeneous broadening. An example will help explain how such a model may be valuable. The a-2 in the crystal with $Y_3(Al_{0.5}Ga_{0.5})_5O_{12}$. Composition is shown in Figure 10 at low temperature. We can attempt to make a statistical calculation of the number of sites in the 50% sample. And if we adopt a simple model for variation in position with % Ga, then we can calculate a line profile for the 50% sample. The model adopted is as follows--assumed that about each Nd site there are ten gallium of aluminum ions (see Figure 1 in Chapter III) and as gallium is substituted for one aluminum ion, the level of the Nd shift 1/10 of the way from $Y_3Al_5O_{12}$ to $Y_3Ga_5O_{12}$ host crystals. If we consider all the possible Ga/Al arrangements at the crystal site, 11 equally spaced transition energy line positions will be found to determine the probability of a given Ga/Al arrangement and hence a given line position, the number of ways in which this arrangement could be produced must be

determined.

The prediction from this model was plotted and found to fit nicely with the observations. This is shown in Figures 9 and 10. A slight deviation in Figure 10 may be seen on the wings on either side, but this can be explained by our assumption of no intrinsic width for the ion transitions in specific individual sites, all in all the results lend support to the assumption of random distribution of gallium ions around the site of a Nd^{3+} ion.

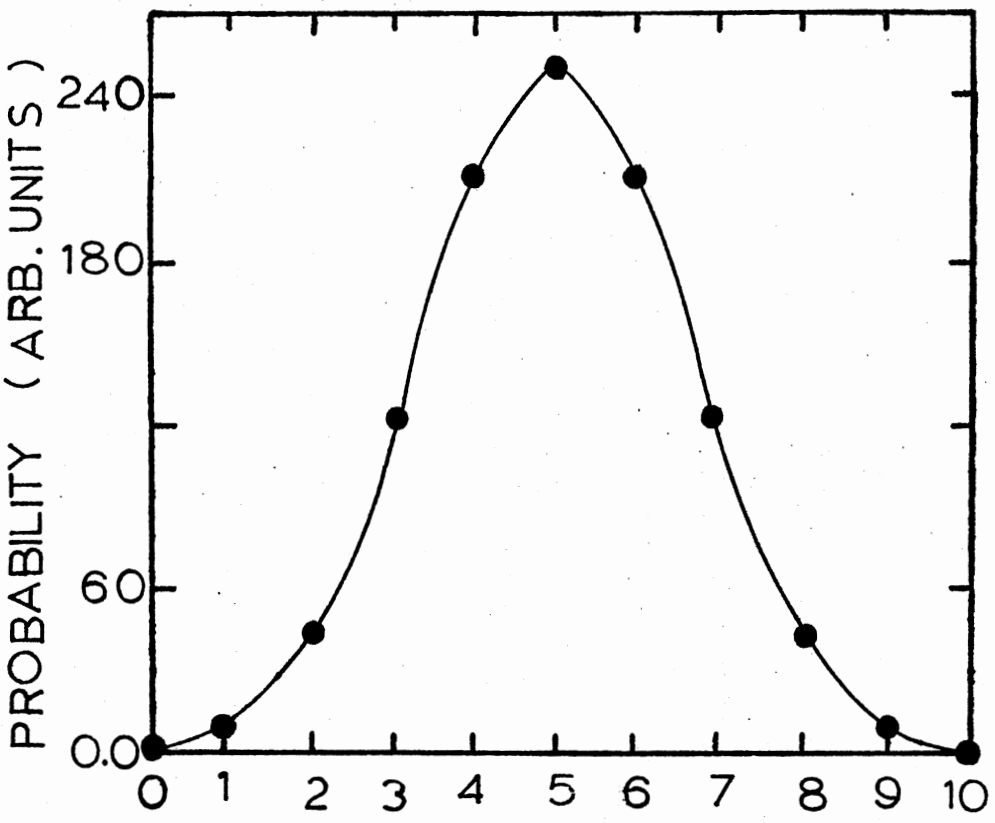

Figure 9. Statistical Line Shape Expected for 50:50 Sample

$$\text{Probability} = P_n(N) = \frac{N!}{n!(N-n)!} p^n q^{N-n} \quad \text{where } q = 1-p$$

All Al sites : 1

One Ga site : 10

Two Ga sites : $\frac{10 \times 9}{1 \times 2} = 45$

Three Ga sites : $\frac{10 \times 9 \times 8}{1 \times 2 \times 3} = 120$

Four Ga sites : $\frac{10 \times 9 \times 8 \times 7}{1 \times 2 \times 3 \times 4} = 210$

Five Ga sites : $\frac{10 \times 9 \times 8 \times 7 \times 6}{1 \times 2 \times 3 \times 4 \times 5} = 252$

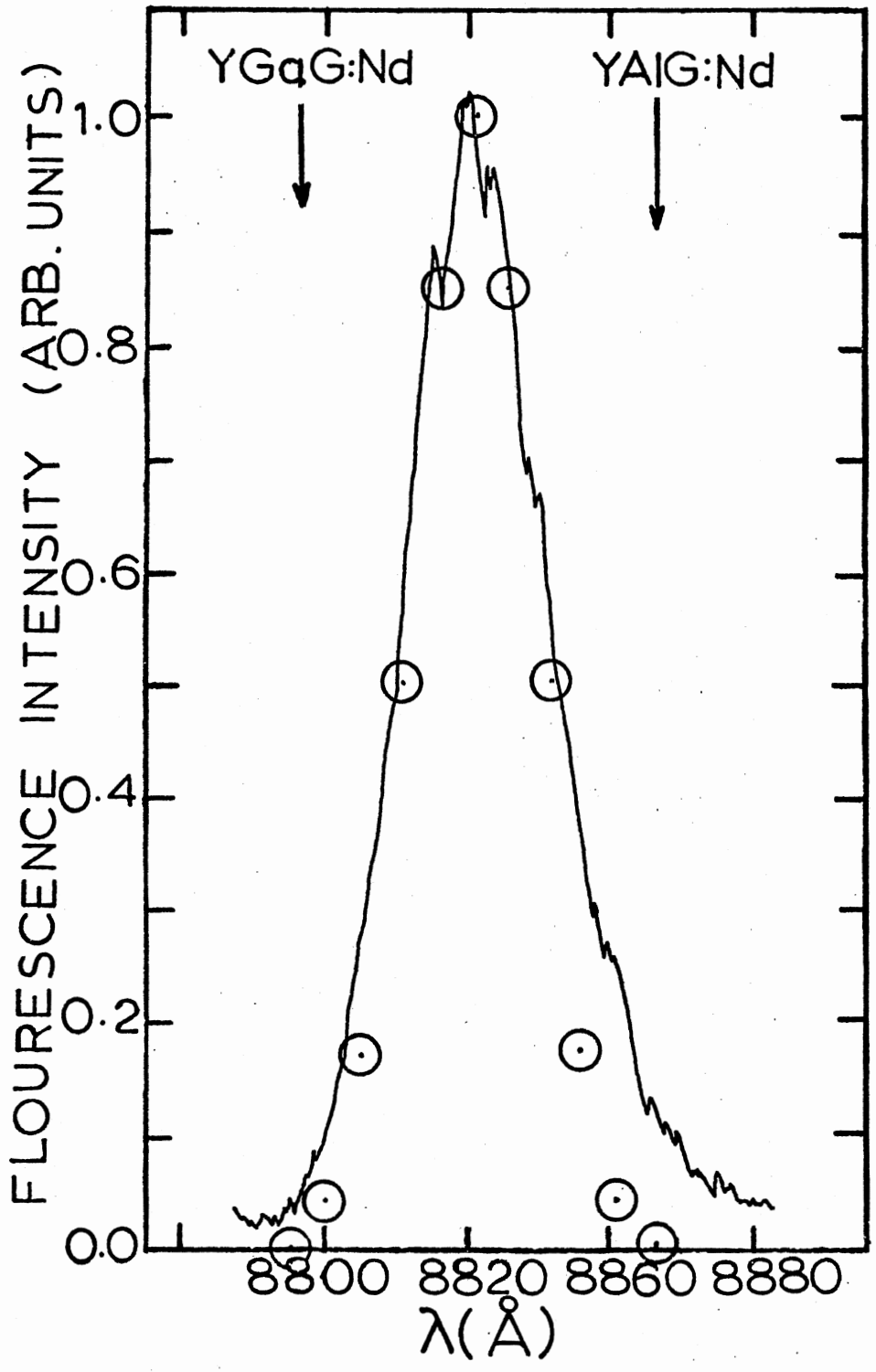

Figure 10. Lineshape of the a-2 Transition at 14°K for the x = 0.5 host (see text for explanation of theoretical points)

The various spectra of Figure 7 exhibit a third noteworthy characteristic. A significant degree of structure can be resolved in the spectral lines, especially in samples with high concentrations of gallium. This structure is produced by the Nd^{3+} ions in crystal field sites with different compositions.

The technique of narrow line laser excitation enables selective excitation of Nd ions in specific types of crystal sites. The result of narrow line laser excitation of the $Y_3(Al_{0.5}Ga_{0.5})_5O_{12}:nd^{3+}$ sample is shown in Figure 11.

The laser exci-ation wavelength is scanned from shorter (λ_{ex} = 5920Å) to longer (λ_{ex} = 5943.4Å) wavelengths and the consequent peak positions and relative intensities undergo significant changes. Figure 12 shows that spectral changes with pumping wavelength are approximately linear. The a-2 line position is shown as shifting to lower wavelengths as the laser is shifted to higher wave lengths.

The fluorescence lifetimes, although essentially independent of temperature, also vary as a function of pumping wavelength in the 200 μsec to 250 μsec range. 200 μsec and 250 μsec are the fluorescence lifetime of Nd^{3+} ions in aluminum garnet and pure gallium garnet hosts, respectively. There is general shift to higher wavelengths as we go from low temperature to room temperature. Roughly 6Å is the general shift, but all lines do not shift by exactly the same amount. From the intensities of the room temperature spectra we can get approximate values for the relative intensities of the various transitions in each crystal. In Figure 8 is the comparison of the two spectra--the line positions are plotted for YAlG:Nd and for YGaG:Nd--and then straight lines are drawn connecting similar transitions. This shows us which

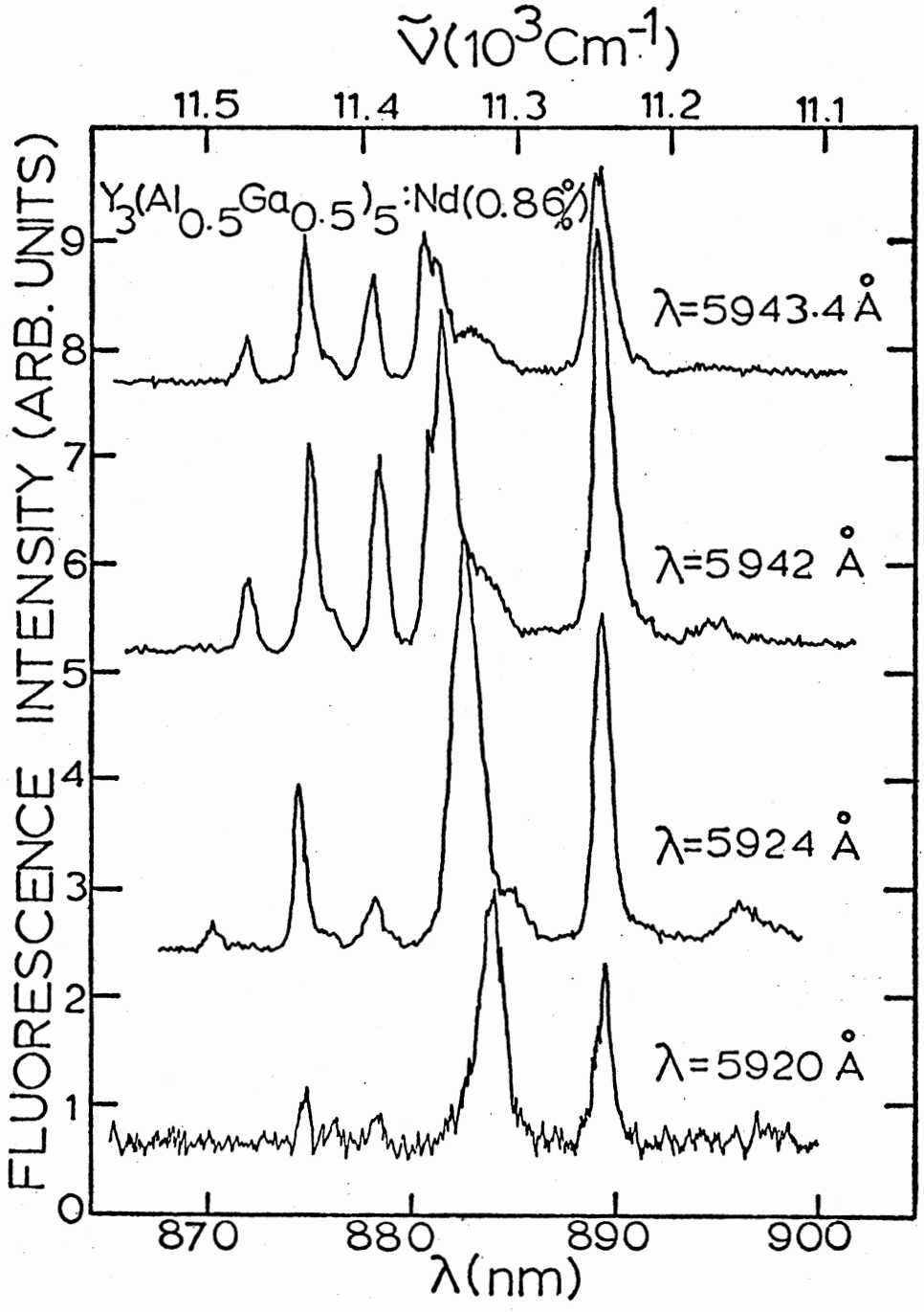

Figure 11. Fluorescence Spectra for the $Y_3(Al_{0.5}Ga_{0.5})_5O_{12}$:$Nd^{3+}$ Sample at 14°K for Different Laser Excitation Wavelengths

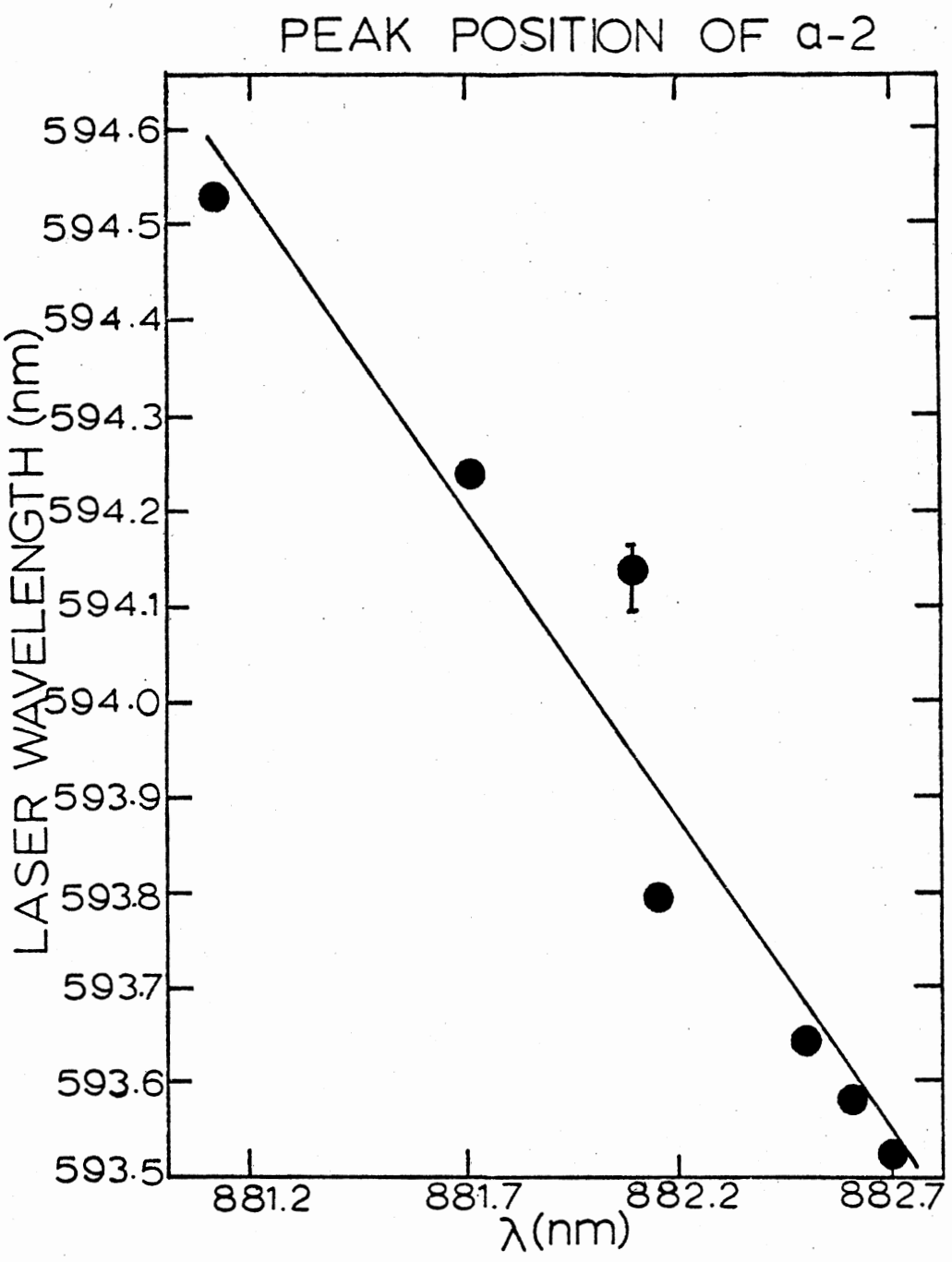

Figure 12. Peak Position of the a-2 Transition as a Function of Excitation Wavelength for the $Y_3(Al_{0.5}Ga_{0.5})_5O_{12}:Nd^{3+}$ Sample at $14^{o}K$

lines shift most. The wave lengths are corrected for spectrometer reading error. If we wish to work at low temperatures, then the researchers will have to work with a transitions. a_1 moves very little in going from YAlG:Nd to YGaG:Nd, so it will not be too suitable. a_1 seems to exhibit trapping effects at low temperatures which is another drawback to this line. a_2 moves by a much larger amount in going from YAlG:Nd to YGaG:Nd, it is also a line which is strongly detected by our system. a_4 also moves by a large amount, but it is a weaker line because of our photomultiplier response. Hence a_2 and a_3 would seem to be the suitable lines, which are called D and E lines respectively, in time dependence fluorescence spectra in the next chapter.

CHAPTER V

TIME RESOLVED SPECTROSCOPY

In this chapter, an investigation to be reported, has been made of energy transfer among trivalent neodymium ions in $Y_3(Al_{1+x}Ga_x)_5O_{12}:Nd^{+3}$, a potential laser material. The tunable dye laser described in Chapter IV was used to excite Nd ions in various crystal field sites, and time-resolved fluorescence spectra were analyzed to detect and characterize energy transfer among ions in different sites.

Four samples were used for this investigation that were obtained from Texas Instruments, and the author reported the study of energy transfer in mixed crystal YAlGaG:Nd containing 22%, 39% and 5% by weight gallium having approximately 1% Nd.

The work to be reported here deals with the investigation of the transfer processes in $Y_3Al_5O_{12}:Nd$ and $Y_3Ga_5O_{12}:Nd$, which as reported by another student in this laboratory (29).

The magnitude of the transfer rate has been estimated, using the theoretical results of Chapter II, and some conclusions have been drawn as to the possible transfer mechanisms. Also the temperature dependence of the transfer processes in 50% sample will be discussed, and estimates of ion-ion transfer rates will be made to determine approximate diffusion parameters.

Low Temperature Energy Transfer Studies

Following a tunable laser pulse, the time evolution of fluorescence spectra for various excitation wavelengths was monitored at different time intervals to obtain data that would help characterize energy transfer. An example of such time-resolved spectroscopy for $Y_3(Al_{0.5}Ga_{0.5})_5O_{12}:Nd^{3+}$ for an excitation of 5942.4Å at 14°K at short and long times after the laser pulse may be seen in Figure 13. As time increases the clearest changes in the spectrum occur in the lines marked D and E where the high energy structure decreases, while the main lines increase in intensity. These changes can be attributed to energy transfer from ions in sites with one transition energy to ions in nonequivalent sites with different transition energies. This energy transfer can be characterized quantitatively by measuring the relative integrated intensities of the lines originating from ions in different crystal field sites. Figure 14 shows the time evolution of these integrated fluorescence intensity ratios, where for the D-lines the high energy transition represents the sensitizer ions and the low energy transition the activator ions. The D-line ratios shows an increase between about 30 and 150 μsec after the pulse and then tend to level off toward a constant value. The for E-lines the low energy structure is the sensitizer and the high energy line the activator, but the time evolution is still similar in shape to the others. The solid lines represent a theoretical fit to the data which will be discussed later. The resulting fitting parameters are given in Table II.

A similar study of energy transfer among neodymium ions in 50% Ga sample has been performed for different excitation wave length of 5932.3Å at 14°K. Although the details of the spectrum were somewhat

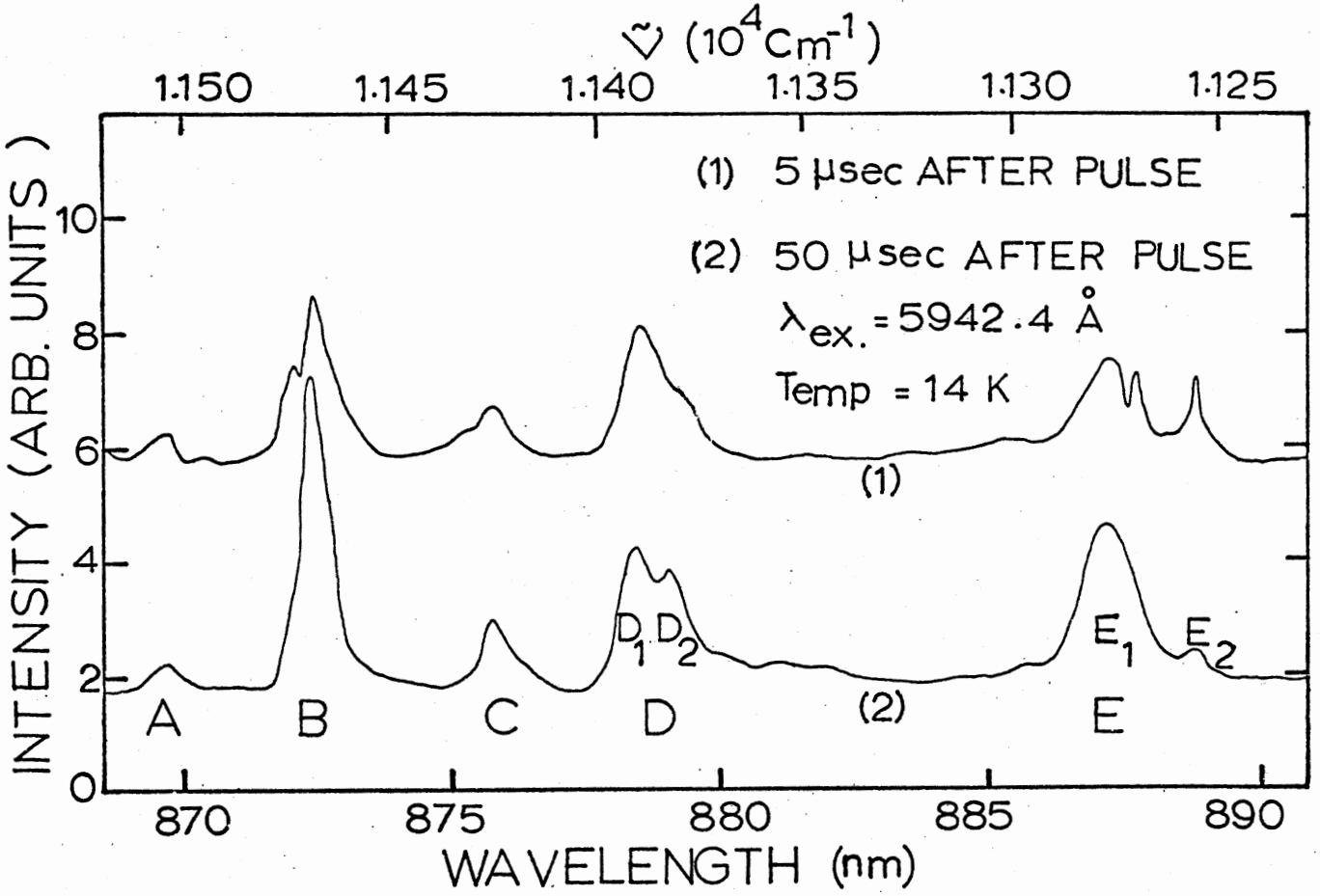

Figure 13. Fluorescence Spectra at Two Times After the Laser Pulse for the $Y_3(Al_{0.5}Ga_{0.5})_5O_{12}:Nd^{3+}$ Sample at 14 K

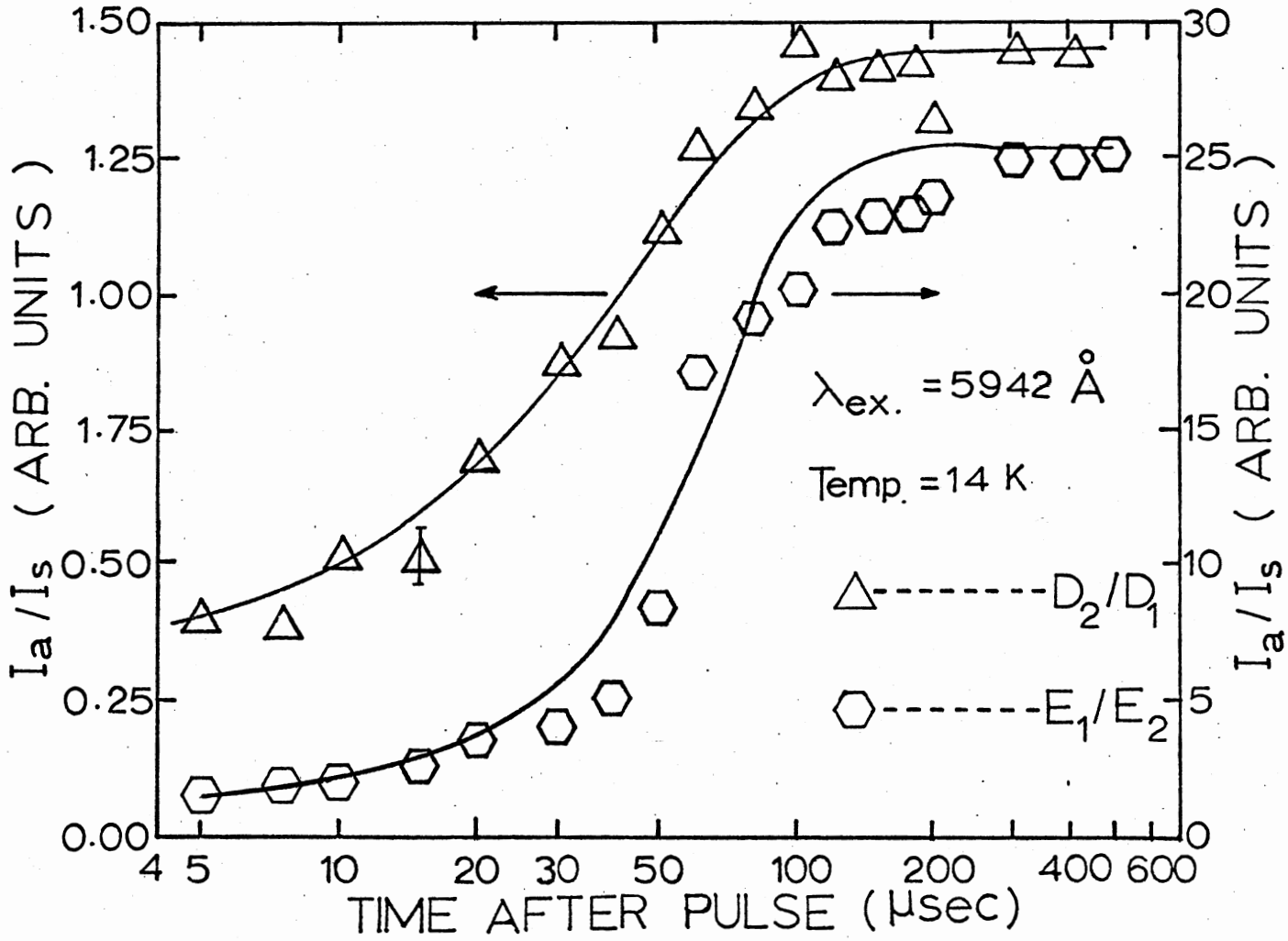

Figure 14. Time Dependence of the Integrated Fluorescence Intensity Ratios of Lines From Nd Ions in Different Crystal Field Sites in $Y_3(Al_{0.5}Ga_{0.5})_5O_{12}$ at 14°K

TABLE II

FLUORESCENCE INTENSITY RATIOS OF $Y_3(Al_{0.5}Ga_{0.5})_5O_{12}:Nd^{3+}$ AT ($14^{\circ}K$) AT DIFFERENT TIMES AFTER LASER PULSE (ARB. UNITS)

Time After Pulse (μsec)	D_1-Line	D_2-Line	D_2/D_1	E_1-Line	E_2-Line	E_1/E_2
5	18.65	7.40	0.39	16.59	10	1.66
7.5	24.20	9.05	0.37	22.29	12.19	1.83
10	25.78	12.92	0.50	30	15.76	1.90
15	33.31	16.77	0.50	33.62	13.96	2.40
20	22.40	15.20	0.68	34.80	10.23	3.41
30	21.75	18.80	0.87	30	7.9	3.79
40	21.55	19.90	0.92	34.65	7	4.95
50	18.10	20.35	1.12	32.37	3.96	8.19
60	18.31	23.17	1.26	41.54	2.49	16.95
80	18.5	24.92	1.34	42.56	2.27	18.86
100	19.35	28.40	1.46	42.72	2.15	19.86
120	17.9	25	1.39	36.35	1.63	22.22
150	19.94	28.30	1.41	43.42	2.35	22.67
180	18.64	26.46	1.42	39.03	1.75	22.72
200	19.96	26.56	1.32	41.10	1.65	24.46
300	17.80	25.93	1.45	38.70	1.55	24.96
400	22.86	32.93	1.44	47.45	1.92	24.70
500	20.60	32.20	1.56	52.06	2.08	25

different for this excitation wavelength, it was again figured out that there was some of the structure visible at short times after the laser pulse evolves into dominant lines at longer times. Again the lines marked D and E were chosen for quantitative analysis, and the D-line ratios showed an increase between about 30 and 300 μsec and then tended to level off similar to the results for the lower energy excitation wavelength, which the E-line ratios increase sharply about 20 μsec.

Composition Dependence of Energy Transfer

The same procedure has been used to investigate the energy transfer among neodymium ions in the host containing 22% and 39% gallium. Figure 15 shows fluorescence spectra measured at 5 and 500 μsec and then tend toward a constant value. Again the solid line represents theoretical fit to the data. The resulting fitting parameters are given in Table III. Finally Figure 17 shows the fluorescence spectrum for an excitation of 5892Å at 16°K at 5 and 400 μsec times after pulse, for $Y_3(Al_{0.61}Ga_{0.39})_5O_{12}$:Nd. The ratios of the integrated fluorescence intensity levels of two sets of lines have been plotted as a function of time and are shown in Figure 18, where the triangles are the measured values of E-line ratios and the circles are the D-line ratios. These particular results are relatively representative of those found at other pumping wavelengths and other samples with different types of host crystals. For both the sets of fluorescence lines a significant increase in these ratios occurs at short times, but the ratios tend to have constant values at long times. The solid lines represent the fits to the data using Equation V-3, and in Table IV the resulting fitting parameters are given.

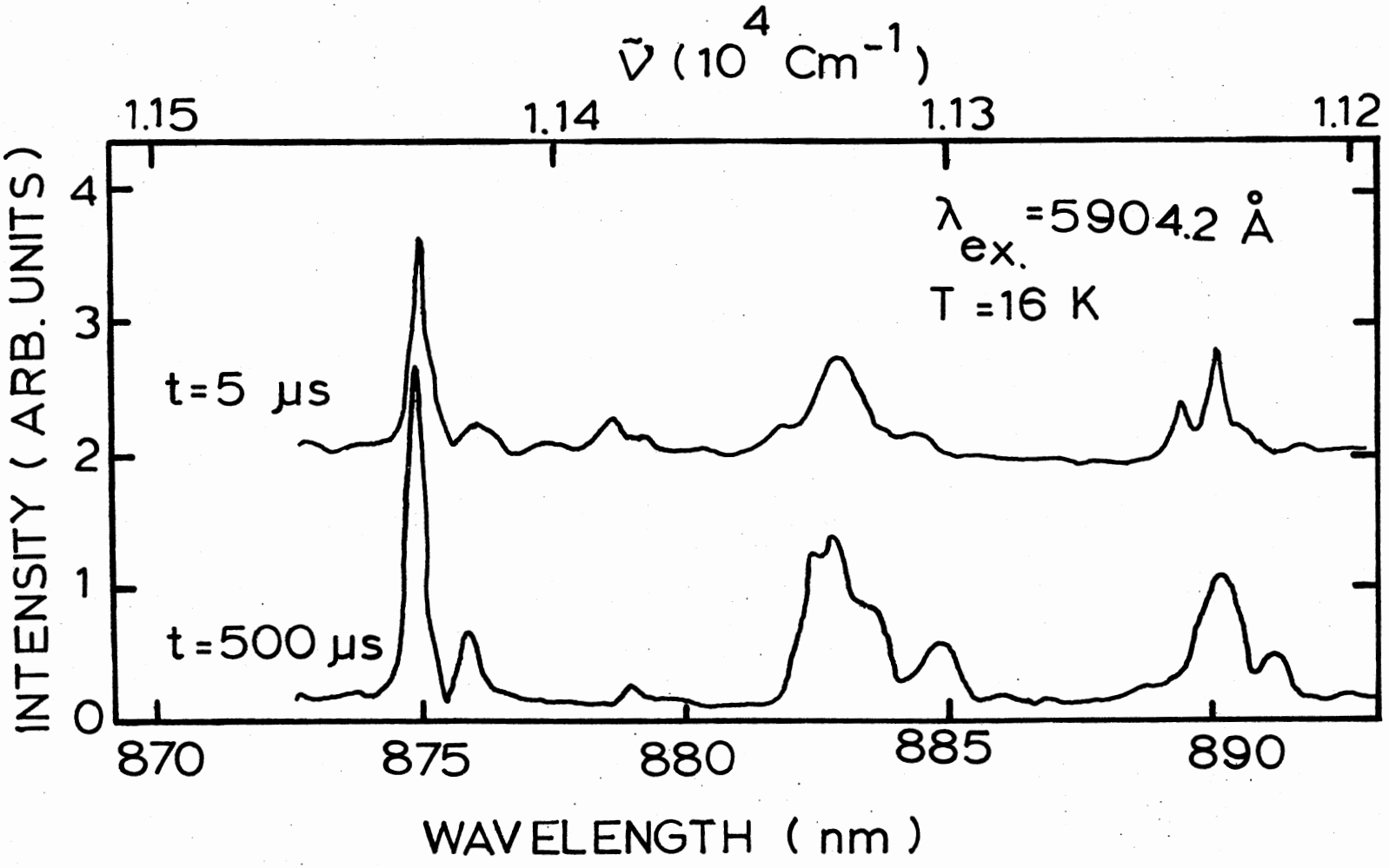

Figure 15. Fluorescence Spectra at Two Times After the Laser Pulse for the $Y_3(Al_{0.5}Ga_{0.5})_5O_{12}:Nd^{3+}$ Sample at 16°K

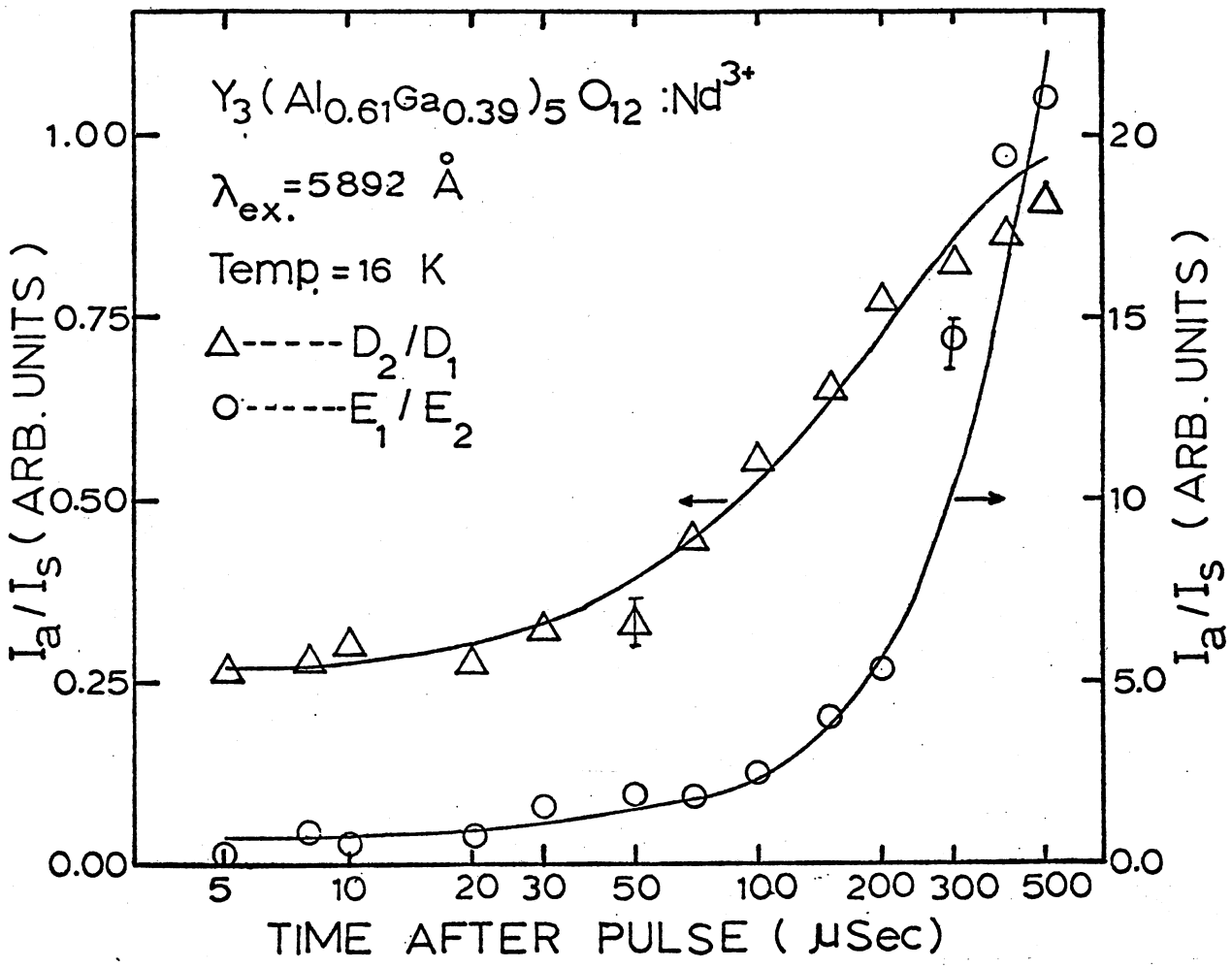

Figure 16. Time Evolution of Integrated Fluorescence Intensity Ratios of Lines From Nd Ions in Different Crystal Field Sites in $Y_3(Al_{0.78}Ga_{0.22})_5O_{12}:Nd^{3+}$ at 16°K

TABLE III

FLUORESCENCE INTENSITY RATIOS OF $Y_3(Al_{0.78}Ga_{0.22})_5O_{12}:Nd^{3+}$ AT LOW TEMPERATURE ($16^{\circ}K$) AT DIFFERENT TIMES AFTER LASER PULSE (ARB. UNITS)

Time After Pulse	D_1-Line	D_2-Line	D_2/D_1
5	47	13.55	0.28
8	44	11.55	0.26
10	29.55	8.08	0.27
20	34	8	0.27
35	36.08	15.68	0.43
50	33.77	13.60	0.40
70	36.30	22	0.60
100	28.97	17.94	0.62
150	34	29.16	0.85
200	25.12	19.60	0.78
300	28.85	30.43	1.05
400	21.58	22	1.01
500	23.92	25.97	1.08

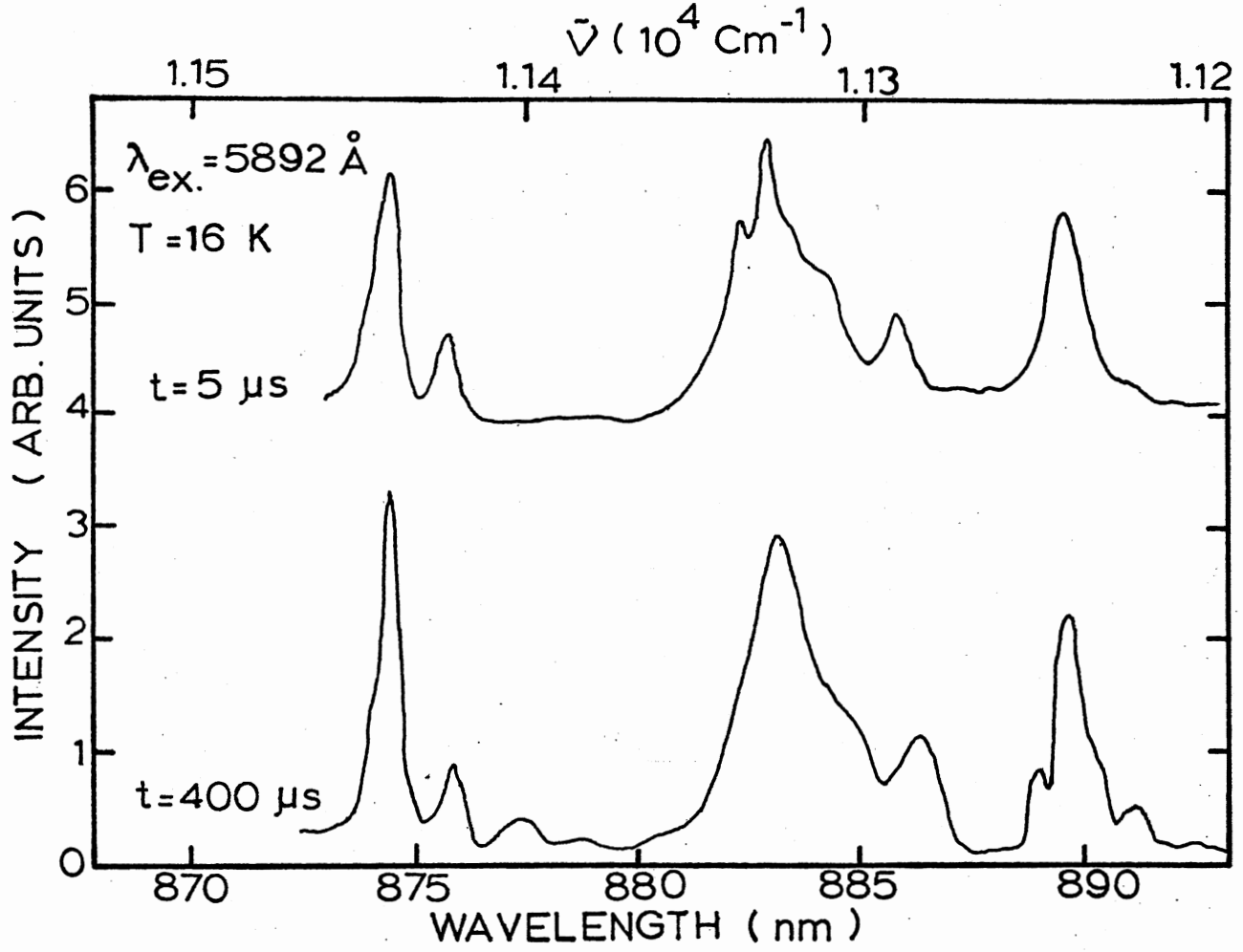

Figure 17. Fluorescence Spectra for an Excitation of 5892A at 16°K at Two Times After the Laser Pulse for the $Y_3(Al_{0.61}Ga_{0.39})_5O_{12}:Nd^{3+}$ Sample

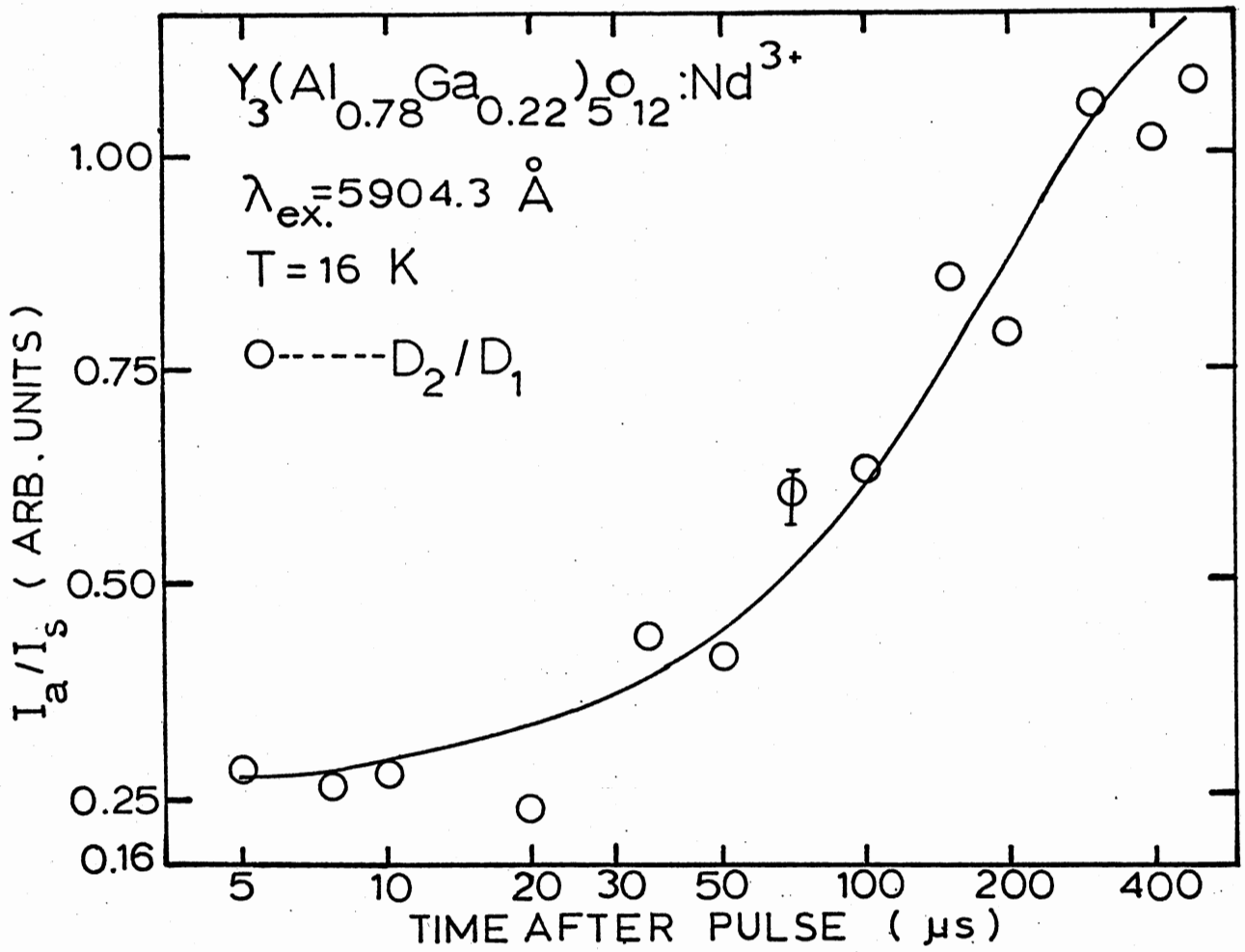

Figure 18. Time Dependence of the Integrated Fluorescence Intensity Ratios of Lines From Nd Ions in Different Crystal Field Sites in $Y_3(Al_{0.61}Ga_{0.39})_5O_{12}:Nd^{3+}$ at 16°K

TABLE IV

FLUORESCENCE INTENSITY RATIOS OF $Y_3(Al_{0.61}Ga_{0.39})_5O_{12}:Nd^{3+}$ AT $16^{o}K$ AT DIFFERENT TIMES AFTER LASER PULSE (ARB. UNITS)

Time After Pulse	D_1-Line	D_2-Line	D_2/D_1	E_1-Line	E_2-Line	E_1/E_2
5	111.2	158.67	0.53	7.7	42	0.183
8	60	33.56	0.56	11.45	13.70	0.83
10	68.40	41.30	0.60	15.35	23.41	0.65
20	64.96	36.04	0.55	8.78	12.75	0.68
30	71.90	45.75	0.64	22.51	13.76	1.63
50	78.51	52.21	0.66	26.66	14.58	1.82
70	76.73	68.94	0.90	32.89	17.65	1.86
100	61.58	67.99	1.10	33	13.81	2.39
150	64.70	84.70	1.30	47.26	11.73	4
200	54.3	84.56	1.55	49.13	9.1	5.39
300	60.14	99.56	1.65	53.85	3.74	14.39
400	50.7	87.7	1.73	48.81	2.51	19.44
500	45.83	83.23	1.81	59.9	2.84	21

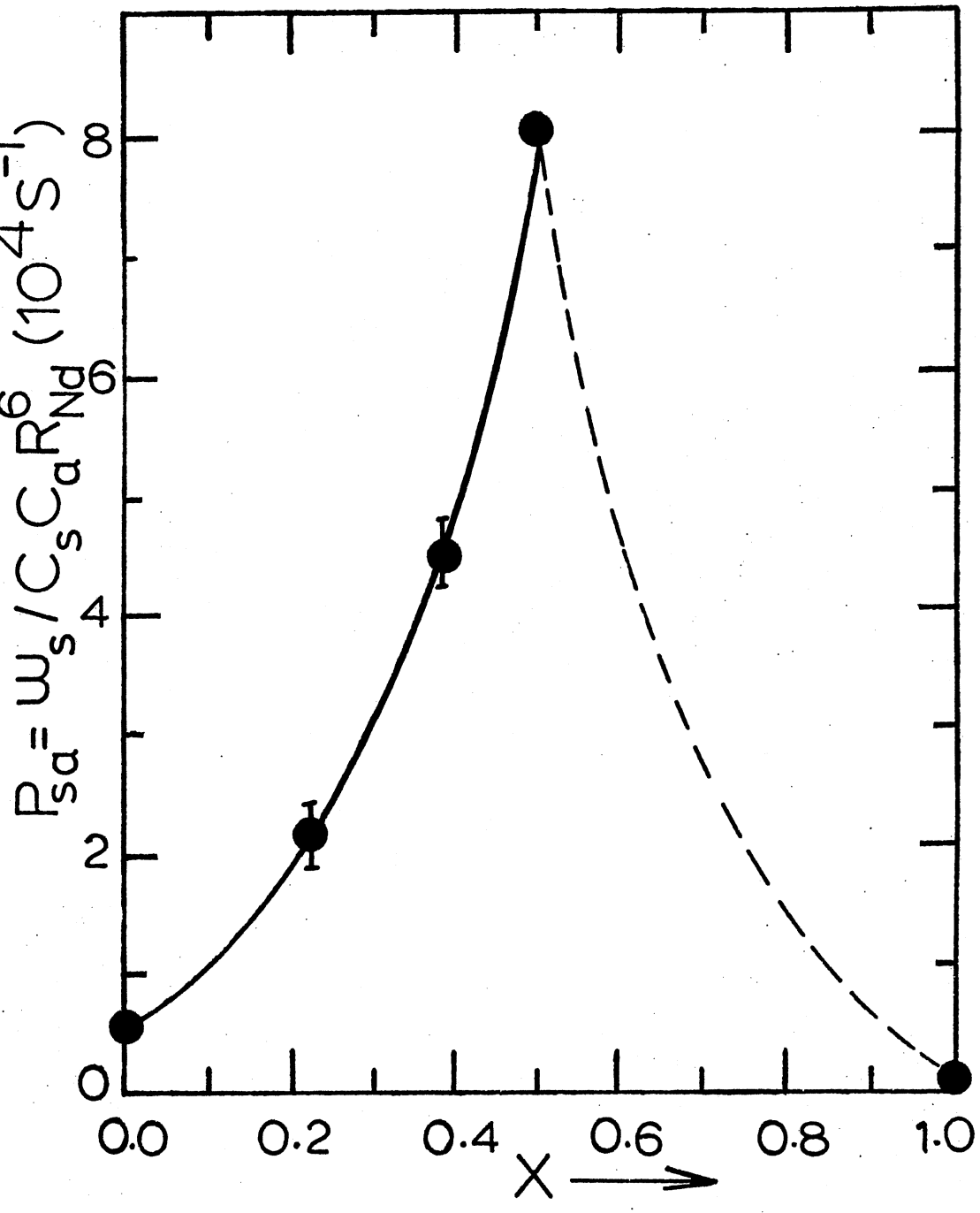

Figure 19. Variation of the Energy Transfer Strength at 14°K as a Function of Host Composition

TABLE V

ENERGY TRANSFER PARAMETERS

Spectral Parameters	Estimated Parameters	Fitting Parameters	Model Parameters
	A: $Y_3(Al_{0.5}Ga_{0.5})_5O_{12}:Nd^{3+}$ Sample		
$C_s = 6.36 \times 10^{19}$ cm^{-3}	$J^2_{a1} = 3.6 \times 10^{-8}$ cm^{-2}	ω_s(14 K) $= 2 \times 10^4$ sec^{-1}	$D_o = 1.45 \times 10^{-9}$ cm^2 sec^{-1}
$C_a = 5.43 \times 10^{19}$ cm^{-3}	$J^2_{a2} = 5.1 \times 10^{-8}$ cm^{-2}	ω_s(133 K) $= 5 \times 10^4$ sec^{-1}	$D = 5.27 \times 10^{-10}$ cm^2 sec^{-1}*
$\Delta\tilde{\nu}^{inhomo}_{ss} = 8.27$ cm^{-1}		ω_a(14 K) $= 1.4 \times 10^4$ sec^{-1}	$\ell = 8.9 \times 10^{-7}$ cm*
$\Delta E_{sa} = 8.53$ cm^{-1}		ω_a(133 K) $= 1.0 \times 10^4$ sec^{-1}	$t_{step} = 1.3 \times 10^{-5}$ sec
$\Delta E_{12} = 94$ cm^{-1}		$\vartheta = 95$ cm^{-1}	
$\Gamma = 4$ cm^{-1}		$\Delta E_{ss} = 1.6$ cm^{-1}	$n_{step} = 16.4$
$\tau^o_s = 2.14 \times 10^{-4}$ sec^{-1}			

TABLE V (Continued)

Parameters	Composition			
	x = 0.00**	0.22	0.39	1.00**
		B: Other Host Compositions		
$C_s (cm^{-3})$	1.1×10^{20}	1.02×10^{20}	8.8×10^{19}	2.7×10^{19}
$C_a (cm^{-3})$	8.4×10^{18}	1.7×10^{19}	3.1×10^{19}	5.4×10^{18}
$\Delta\tilde{\nu}_{ss}^{inhomo}$ (cm^{-1})	~1.5	5.4	6.8	~1.5
$J_1^2 (cm^{-2})$	8.3×10^{-11}	7.4×10^{-10}*	2×10^{-9}	3.6×10^{-11}
$J_2^2 (cm^{-2})$	1.66×10^{-9}	1.58×10^{-9}*	2.63×10^{-9}	4.1×10^{-11}
$\omega_s (sec^{-1})$	3.9×10^{2}	3.58×10^{3}	5×10^{3}	1.4×10^{2}
$\omega_a (sec^{-1})$	2.5×10^{3}	3.5×10^{3}	2.7×10^{3}	0
$\Delta E_{ss} (cm^{-1})$	0.29	1	1.3	0.35
$\delta (cm^{-1})$	140	111.3	108.3	83

*Values at T = 133°K.

**Values from Ref. 29.

TABLE VI

ENERGY TRANSFER PARAMETER WITH THE HOST COMPOSITION PARAMETER X

X	C_s	C_a	$\omega_{sa}(s^{-1})$	$P_{sa}(s^{-1})$
0.00*	1.1×10^{20}	8.4×10^{19}	3.9×10^{2}	0.58×10^{4}
0.22	3.08×10^{19}	8.3×10^{19}	3.85×10^{3}	2.13×10^{4}
0.39	3.8×10^{19}	5.12×10^{19}	5×10^{3}	4.49×10^{4}
0.50	6.45×10^{19}	5.43×10^{19}	2×10^{4}	8.00×10^{4}
1.00*	2.7×10^{19}	5.4×10^{18}	1.4×10^{2}	0.1×10^{4}

*Values from Ref. 21.

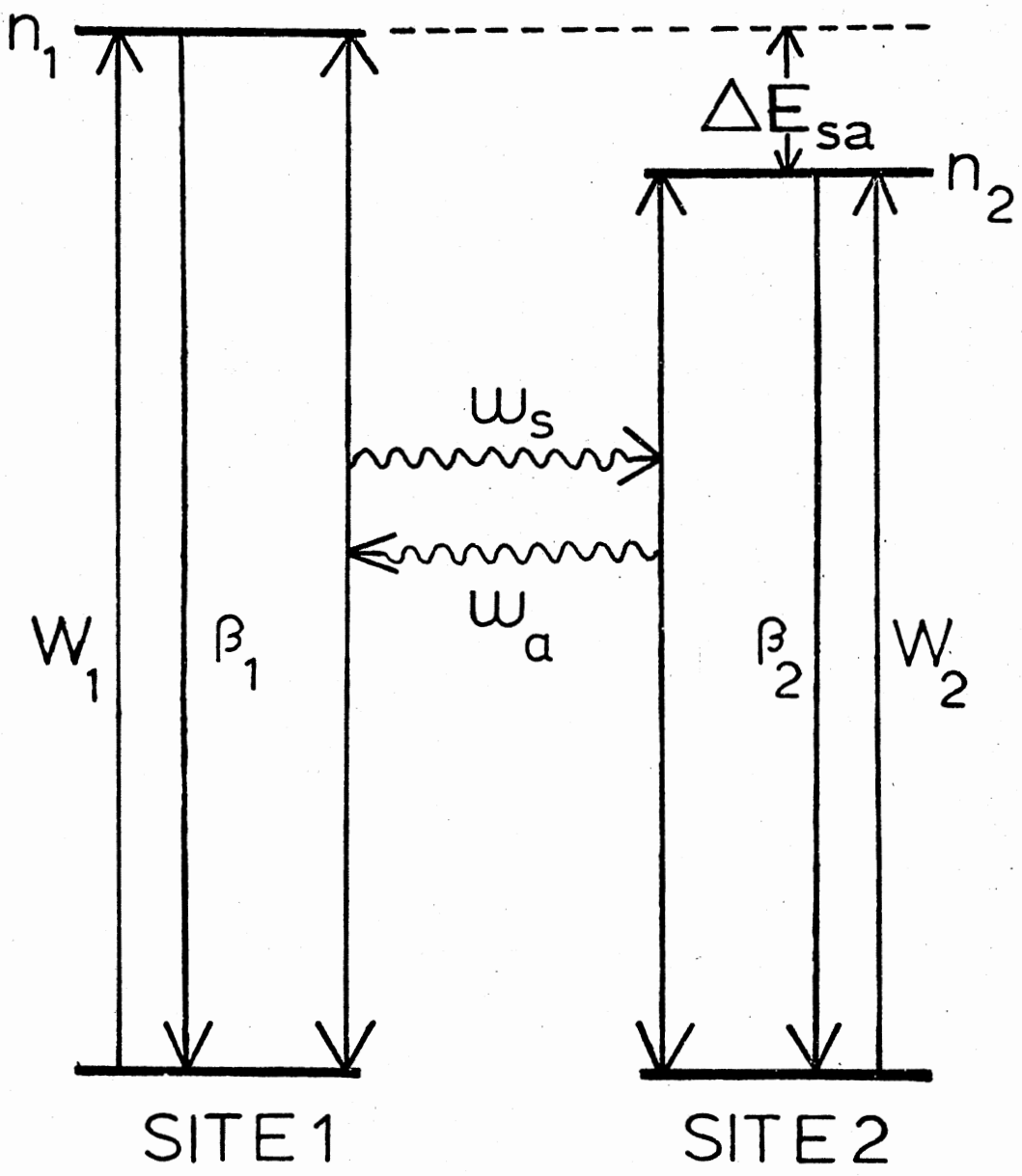

Figure 20. Model Used for Explaining Energy Transfer Between Nd^{3+} Ions in Different Crystal Field Sites (see text for explanation of symbols)

The variation of the transfer strength with the host composition parameter x is shown in Figure 19. The transfer strengths shown here are the observed transfer rates with the factors for sensitizer and activator concentrations and the average Nd^{3+} ion separation divided out. The energy transfer parameters are listed in Tables V and VI.

The results show that as x increases up to the X = 0.5 sample, the transfer strength increases, but then is smaller again for the X = 1.0 host. The inhomogeneous broadening of the sensitizer transition and the transition matrix elements, which will be discussed, are the two main parameters which could effect the transfer strength.

Interpretation of Results

An interpretation of the time-resolved spectroscopy results obtained involves the energy transfer between Nd^{3+} ions in different types of sites within the garnets. A simple two-site model can be developed using the parameters illustrated in Figure 20. Here we assume two distinct types of sites for the sensitizer and activator ions whose transition energies are separated by an amount ∇E_{sa}. The pumping rates are W_s and W_a and the fluorescence decay rates are β_s and β_a. The energy transfer and back transfer rates are ω_s and ω_a, respectively.

The populations of the excited states are n_s and n_a. The rate equations for these populations of the excited states of the ions in the two types of sites are

$$dn_s/dt = W_s - \beta_s n_s - \omega_s n_s + \omega_a n_a \qquad (V\text{-}1)$$

$$dn_a/dt = W_a - \beta_a n_a + \omega_s n_s - \omega_a n_a \qquad (V\text{-}2)$$

These can be solved assuming a delta function excitation pulse, and the resulting expressions for the time evolutions of the excited state populations are directly proportional to the observed fluorescence intensities. The expressions used for the energy transfer rates depend on the physical mechanism responsible for the transfer process. The energy transfer and back transfer rates between the sensitizer and activator sites can be treated as adjustable parameters to aid in fitting the experimental data. Various possible ways of expressing the energy transfer rates were examined in order to determine the best fit for my data. It was found that the good fits to the data, shown as a solid line in the previous figures, could be obtained only if the energy transfer rates were assumed to be constant with time. In this case the solutions to equations (V-1) and (V-2) give

$$\frac{I_a}{I_s} = K \frac{n_s(0)\omega_s}{n_a(0)\omega_a} \frac{\{[n_a(0)/n_s(0)](\beta/\omega_s)+1-\exp(-\beta t)\}}{1+\{[n_s(0)/n_a(0)](\beta/\omega_a)-1\}\exp(-\beta t)} \qquad \text{(V-3)}$$

where $\beta = \beta_s+\omega_s-\beta_a-\omega_a$, and $n_s(0)$ and $n_a(0)$ are the initial excited populations resulting from the pumping. The proportionality factor used here, K, includes the ratios of radiative decay times, oscillator strengths and branching ratios for the specific transitions exhibited by the ions from different crystal matrix environments. Table V contains a list of the fitting parameters. The best fits to the experimental results using this equation are indicated by solid lines in Figures 14, 16 and 18.

Temperature Dependence of Energy Transfer

A time dependence of the fluorescence spectrum for an excitation

of 5942.6Å, (which is the same as the excitation wavelength used at low temperature), at 133°K at 7.5 μsec and 400 μsec times after pulse, for $Y_3(Al_{0.5}Ga_{0.5})_5O_{12}:Nd^{3+}$ is shown in Figure 21. The time evolution of integrated fluorescence intensity ratios for this excitation wavelength is shown in Figure 22, which indicates the E-line ratios. The shape of the curve is generally the same as the low temperature data, but the increase occurs at shorter times after the laser pulse. Table VII lists the measured intensities of E_1/E_2 lines at high temperatures.

The time dependence of the emissions, becomes stronger as the temperature increases. Figure 23 illustrates one example of the asymptotic values of the intensity ratios at long times after the laser pulse, taken as a function of temperature. These values may be observed as relatively constant at low temperatures and as increasing exponentially at high temperatures.

The data in Table VIII indicate the integrated fluorescence intensity ratios of lines from Nd^{3+} ions in different crystal field sites at 50 μsec after the laser pulse in $Y_3(Al_{0.5}Ga_{0.5})_5O_{12}$, which is plotted on a logarithmic scale versus T^{-1} in Figure 23.

Using the techniques and equipment described in Chapter III, the author measured the fluorescence lifetimes of all the samples of $Y_3(Al_{1-x})Ga_x)_5O_{12}:Nd$ which the author had, at low temperature as shown in Table VIII. Also the fluorescence lifetimes of $Y_3(Al_{0.5}Ga_{0.5})_5O_{12}:Nd$ at two different excitation wavelength from low to high temperatures is shown in Table IX. The fluorescence lifetimes are essentially independent of temperature. The lifetimes vary as a function of pumping wavelength in the range from 200 μsec which are the fluorescence lifetimes of Nd^{3+} ions in $Y_3Al_5O_{12}$ and $Y_3Ga_5O_{12}$ hosts, respectively.

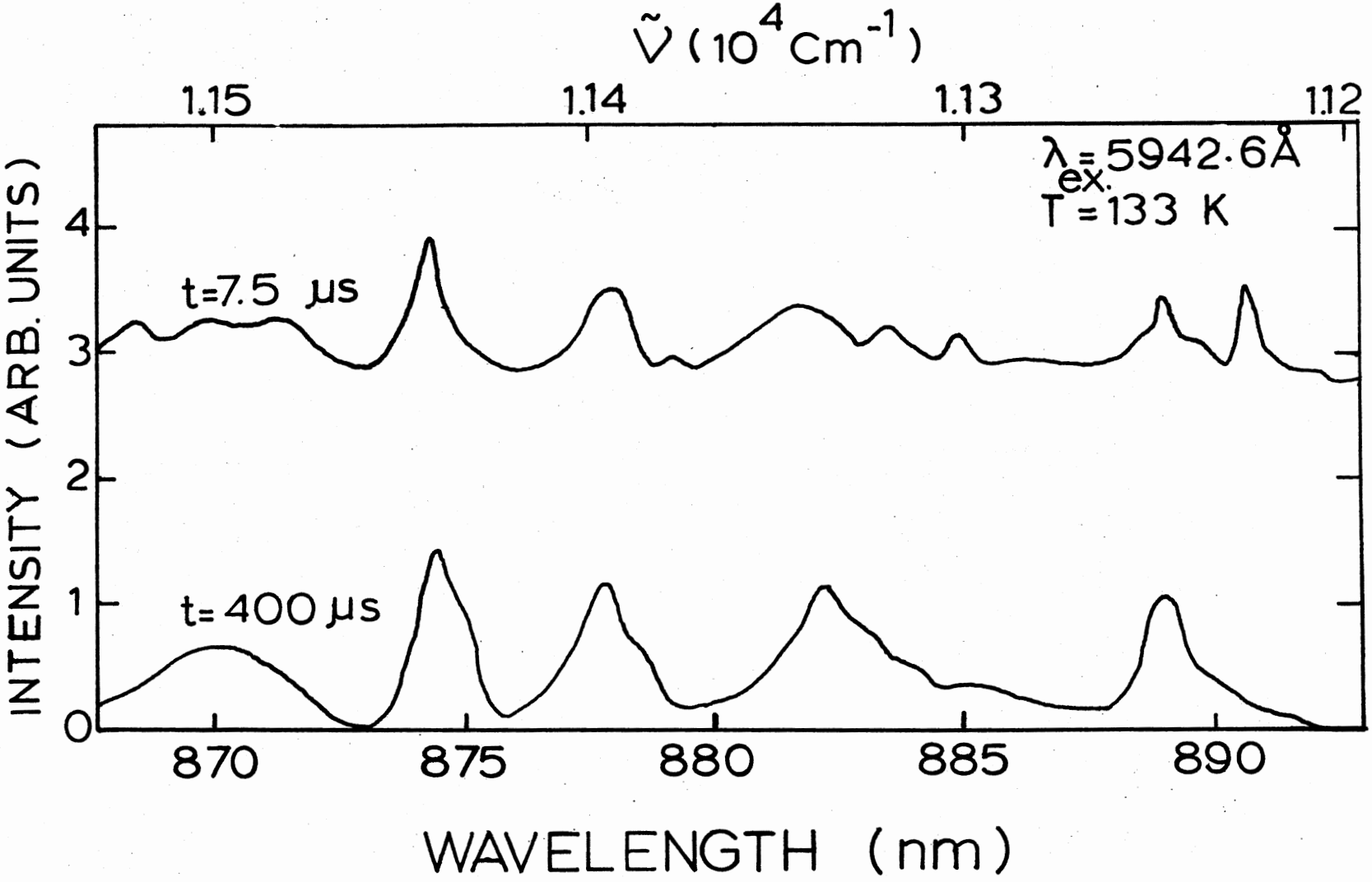

Figure 21. Fluorescence Spectra at Two Times After the Laser Pulse for the $Y_3(Al_{0.5}Ga_{0.5})_0O_{12}:Nd^{3+}$ Sample at 133°K

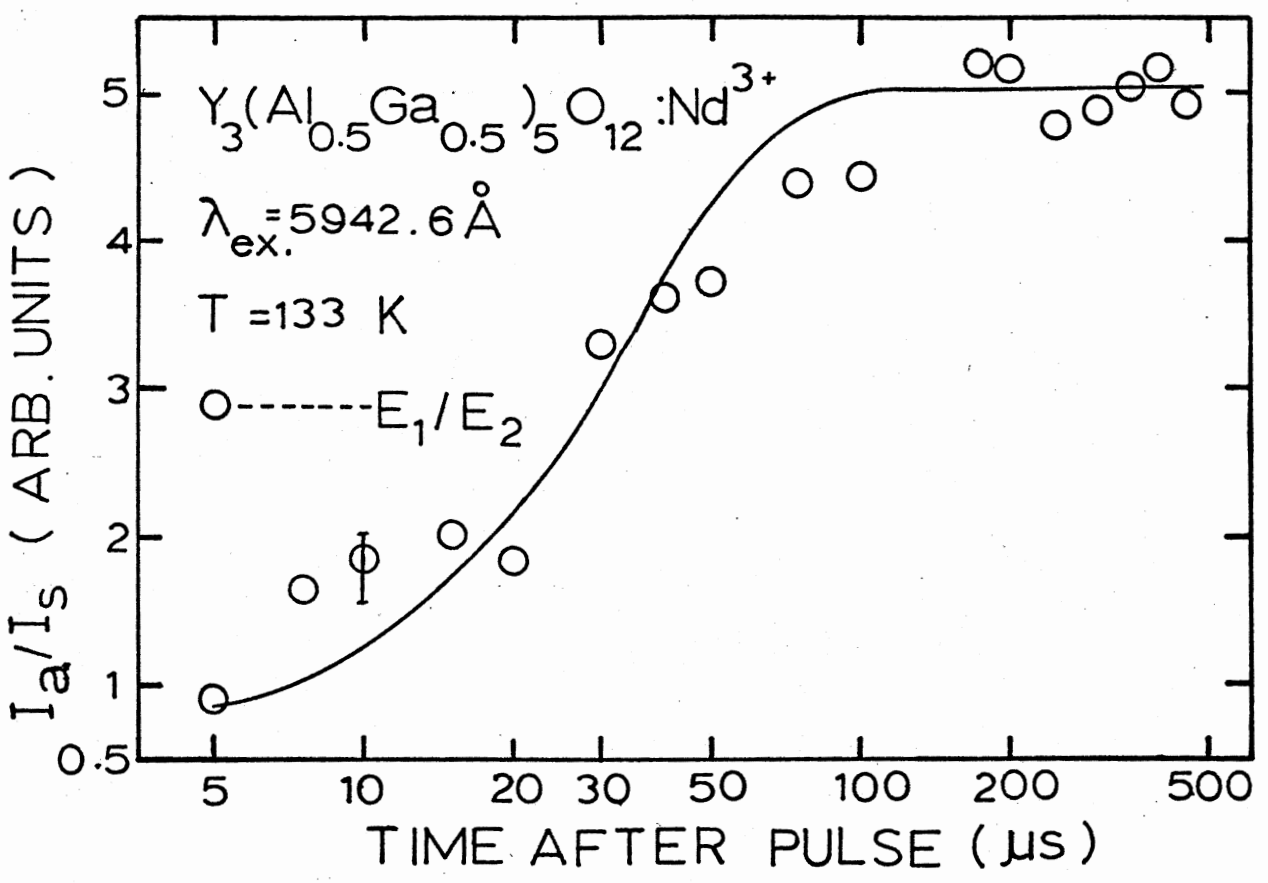

Figure 22. Time Dependence of the Integrated Fluorescence Intensity Ratios of Lines From Nd^{3+} Ions in Different Crystal Field Sites in $Y_3(Al_{0.5}Ga_{0.5})_5O_{12}$ at 133 K

TABLE VII

FLUORESCENCE INTENSITY RATIOS OF $Y_3(Al_{0.5}Ga_{0.5})_5O_{12}:Nd^{3+}$ AT HIGH TEMPERATURE (133°K)

Time After Pulse (μsec)	E_1-Line	E_2-Line	E_1/E_2
5	9.91	10.89	0.91
7.5	17.66	10.45	1.68
10	16.2	7.63	1.87
15	23.25	11.4	2.03
20	30.1	16.4	1.83
30	53.82	16.34	3.29
40	42	14.68	3.62
50	19	5.1	3.72
75	30.68	7	4.38
100	26.55	6	4.42
175	42.50	8.2	5.18
200	47.74	9.26	5.15
250	38.8	8	4.75
300	29.55	6.08	4.86
350	35.10	7.11	5
400	33.32	6.45	5.16
450	30.96	6.3	4.9

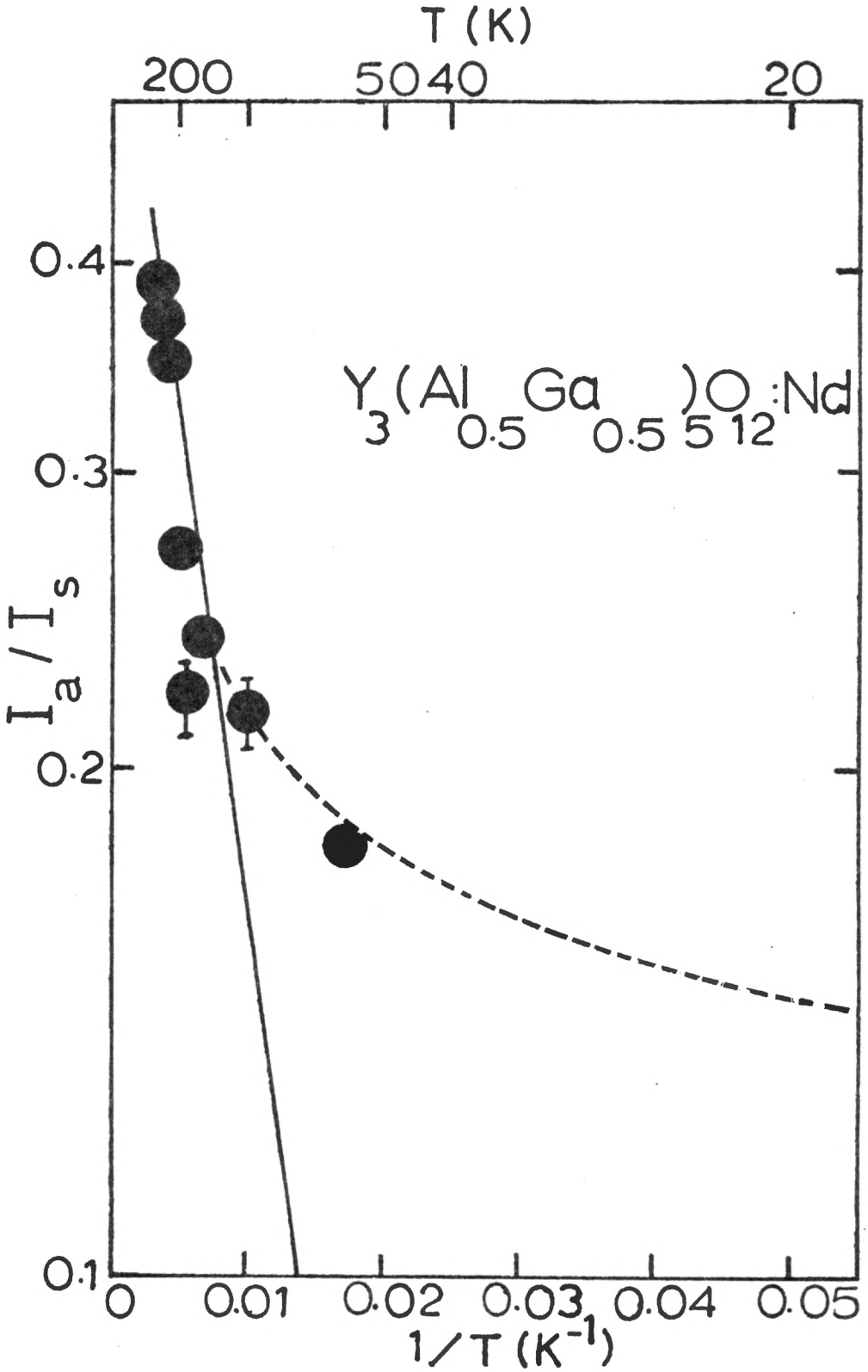

Figure 23. Temperature Dependence of the Fluorescence Intensity Ratios of Lines From Nd^{3+} Ions in Different Crystal Field Sites in $Y_3(Al_{0.5}Ga_{0.5})_5O_{12}$

TABLE VIII

INTEGRATED FLUORESCENCE INTENSITY RATIOS OF LINES FROM Nd^{3+} IONS IN DIFFERENT CRYSTAL FIELD SITES AT 50 μsec AFTER THE LASER PULSE IN $Y_3(Al_{0.5}Ga_{0.5})_5O_{12}$ AT DIFFERENT TEMPERATURES

Temperatures (K)	E_1-Line*	E_2-Line*	E_2/E_1	$1/T \times 10^{+2}$ (K^{-1})
13	31.6	4.77	0.15	7.692
58	22	4	0.18	1.724
100	32.51	7.27	0.22	1
149	36.42	8.67	0.24	0.671
170	37	8.3	0.22	0.588
200	35.88	9.74	0.27	0.500
240	24.63	8.7	0.35	0.416
270	28.4	10.56	0.37	0.370
300	28	10.93	0.39	0.333

*Arbitrary Units

TABLE IX

FLUORESCENCE LIFETIMES OF $Y_3(Al_{1-x}Ga_x)_5O_{12}$:Nd CRYSTALS WITH X-VALUES OF 0, 0.10, 0.22, 0.39, AND 50 AT LOW TEMPERATURE

x	λ_{ex} (A^o)	Lifetime (μsec)	T(K^o)
0.00	5884	200*	14
0.10	5903	239	16
0.22	5904	193	16
0.39	5892	259	16
0.50	5942	214	14
1.00	5886	250*	14

*From Ref. (21).

TABLE X

FLUORESCENCE LIFETIMES OF $Y_3(Al_{0.5}Ga_{0.5})_5O_{12}:Nd^{3+}$ AT TWO DIFFERENT EXCITATION WAVELENGTHS AT DIFFERENT TEMPERATURES

λ_{ex} = 5948.4		λ_{ex} = 5932.3	
Temperature (K)	Lifetime*	Temperature (K)	Lifetime*
13	214	14	265
29	212.5	37	248
43	200	41	250
77	190	73	228
103	175	105	240
141	250	134	238
182	212.5	151	237
207	240	183	24
242	238	212	237
280	240	240	240
		271	236
Rm. Temp.	245	Rm. Temp.	262

*Lifetimes are given in μs.

Interpretation of Results and Discussion

An expression for the temperature dependence of the intensity ratios observed at long times following the laser excitation pulse is

$$I_a/I_s = K[n_s(O)/n_a(O)]\ \omega_s/\omega_a = \omega_o \exp(-\Delta E/KT) \qquad (V-4)$$

The asymptotic experimental values of the intensity ratios (Figure 23) are fit with an activation energy of 95 cm^{-1}. If we compare the low and high temperature values of the time-resolved energy transfer fitting parameters (listed in Table V),

$$\omega_s(14^oK) = 2 \times 10^4\ sec^{-1} \text{ and } \omega_a(14^oK) = 1.4 \times 10^4\ sec^{-1}$$

where $\omega_s(133^oK) = 5 \times 10^4\ sec^{-1}$ and $\omega_a(133^oK) = 1.0 \times 10^4\ sec^{-1}$, it is clear that ω_a is basically temperature independent, while ω_s may be considered responsible for the increase in the intensity ratios as the temperature is raised.

Now that the author has made this analysis of the data, the author should by necessity seek to understand it in terms of a theory of energy transfer. An appropriate theory must treat the transfer rate as both independent of time and subject to exponential increase with temperature. An important fact of this data is that the thermal activation energy has a much greater magnitude than the energy of mismatch between the transition of ions in the different types of sites. In fact, the value for thermal activation energy is relatively similar to that of the crystal field splitting of the lowest two levels of the ground state manifold. Such a finding would not be too unexpected if the a-2 transition was significantly stronger than the a-1 transition, but does

not occur in the present situation. However, such results are consistent with those from earlier work on $Y_3Al_5O_{12}:Nd^{3+}$ and $Y_3Ga_5O_{12}:Nd^{3+}$ systems (32). The interpretation made in this recent study on Nd^{3+} ions in unmixed garnet hosts made use of an exciton migration model (33,34, 35) in which both the hopping and trapping mechanisms are assisted by two-phonon interaction processes.

A similar extent of temperature dependence is developed in the phonon-assisted energy transfer rate mechanism of Orbach et al. (33). Orbach believes the phonon processes should be considered in greater detail than in the resonance mechanism. He does not think it appropriate to merely perceive the electron-phonon interaction as a cuase of transition broadening and a consequent influence on the extent of overlap of spectra. Although he has considered several cases, one of the most pertinent to our study is a two-phonon assisted process where the dominant factors in the process are phonons with enough energy for them to be in resonance with "the energy gap to a nearby excited level".

Resonant Phonon-Assisted Energy Transfer

The resonant energy transfer process requires that transfer take place only between ions for which the sensitizer deexcitation and the activator excitation transition are of equal energy. Recently Orbach and Gurkers (33) have developed theoretical expression for the energy transfer rate to be expected due to various one-phonon and two-phonon processes. The following diagram (Figure 24) indicate the ground state (first two stark levels) and excited states of two sites and various mechanisms of two-phonon processes among those two sites. In addition to the diagram in Figure 24, one has to consider three more processes

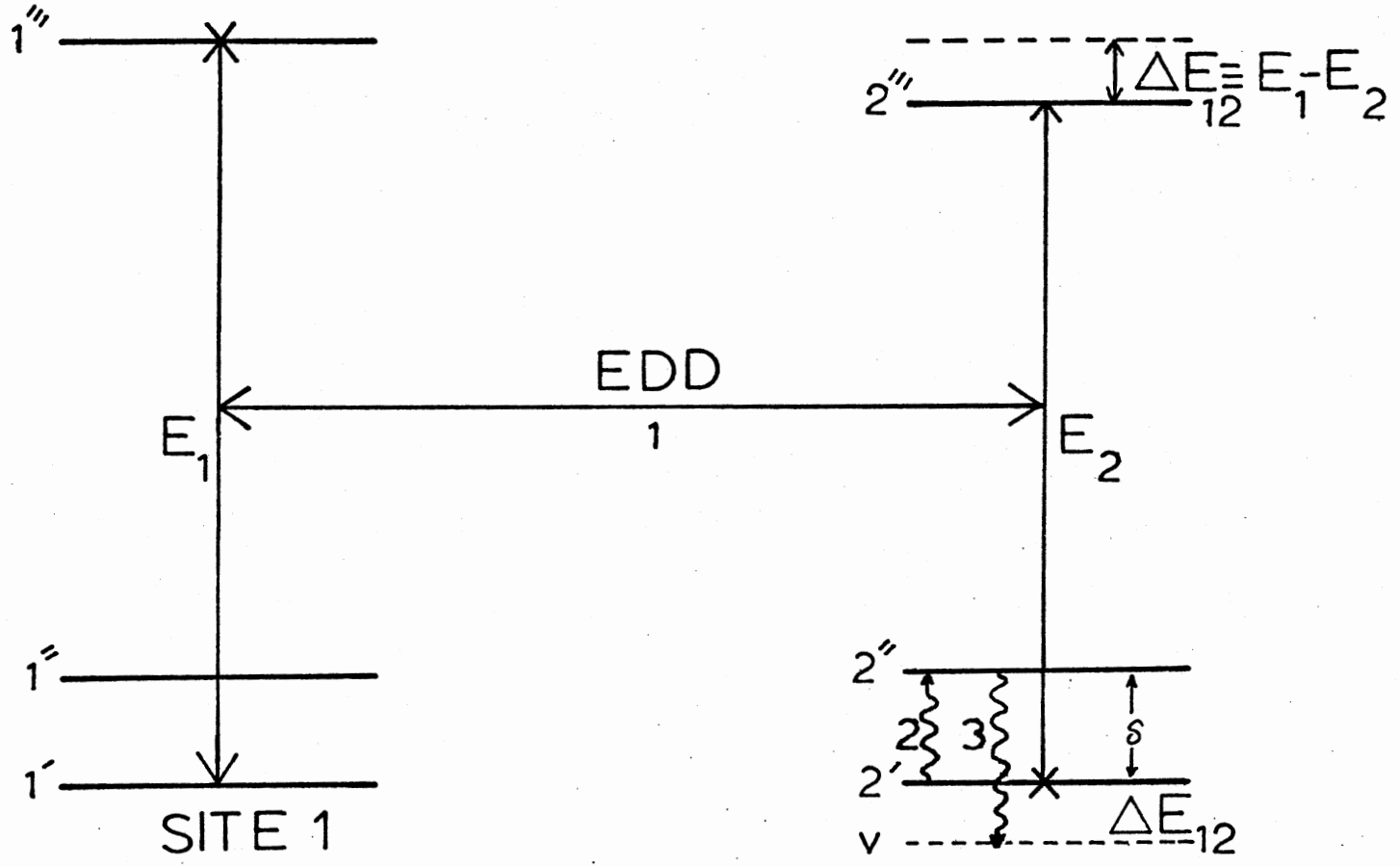

Figure 24. Schematic Diagram Indicating Ground and Excited States of Two Sites, and Mechanisms of Two-Phonon Processes Among These Two Sites

obtained by inverting the sense of all the arrows indicating phonon emission and absorption processes. According to time dependent perturbation theory, the transition rate is

$$W_{2\leftarrow 1} = \frac{2\pi}{\hbar} \sum_{ss',\underset{\sim}{k}\underset{\sim}{k}'} |M_{f\leftarrow i}|^2 \, \delta(\hbar\omega_{s'\underset{\sim}{k}'} - \hbar\omega_{s\underset{\sim}{k}} - \Delta E_{12}) \tag{V-5}$$

where $\omega_{s\underset{\sim}{k}}$ is the phonon frequency with wave vector $\underset{\sim}{k}$ and polarization s, and δ is the Dirac delta function. The M-matrix, contains a number of terms corresponding to various possible intermediate states in the perturbation series, which connect the initial state ($|i\rangle$),

$$|i\rangle = |1^*2, n_{s\underset{\sim}{k}}, n_{s'\underset{\sim}{k}'}\rangle \tag{V-6}$$

to the final state ($|f\rangle$),

$$|f\rangle = |12^*, n_{s\underset{\sim}{k}}-1, n_{s'\underset{\sim}{k}'} + 1\rangle \tag{V-7}$$

The energies of these states are given by

$$\varepsilon_i = E_1, \quad \varepsilon_f = E_2 - \hbar\omega_{s\underset{\sim}{k}} + \hbar\omega_{s'\underset{\sim}{k}'} \tag{V-8}$$

The transfer matrix element is:

$$M_{f\leftarrow 1} = \langle f|H|i\rangle + \sum_{m_1} \frac{\langle f|H|m_1\rangle\langle m_1|H|i\rangle}{E_i - E_{m_1}}$$

$$+ + \sum_{m_1 m_2} \frac{\langle f|H|m_2\rangle\langle m_2|H|m_1\rangle\langle m_1|H|i\rangle}{(E_i - E_{m_1})(E_i - E_{m_2})} \tag{V-9}$$

where H is the interaction Hamiltonian and m_1 and m_2 are intermediate states. The first term in (V-9) is applicable to no phonon transfer

processes, the second term to one and two phonon two-state processes, and so on.

Let us consider the diagram of Figure 24. Designating the electronic ground state and the excited state at site i (i = 1,2) as $|i\rangle$ and $|i^*\rangle$ respectively. Energy Conservation can be obtained in this case by a three stage processes as illustrated in Figure 24. In the beginning Electric Dipole-Dipole (EDD) interaction occurs between site 1 and 2. Then, a phonon of energy $\hbar\omega_{sk}$ is absorbed and the electronic state 2' at site 2 changes into the upper level $|2"\rangle$. Last, a phonon of energy $\hbar\omega_{s'k'}$ is emitted and the electronic state at site 2 changes into the virtual state, v, as shown in Figure 24.

The intermediate state $|m_1\rangle$ and $|m_2\rangle$ and their energies will be

$$|m_1\rangle = |1'2", n_{sk}-1, n_{s'k'}\rangle$$

$$|m_2\rangle = |1"2', n_{sk}-1, n_{s'k'} + 1\rangle$$

$$E_{m_1} = E_1 + \delta - \hbar\omega_{sk}$$

$$E_{m_2} = E_1 - \hbar\omega_{sk} + \hbar\omega_{s'k'} \qquad \text{(V-10)}$$

where δ is the separation between the first and second levels (i.e. 2' and 2"). Defining

$$\langle 2"|H|2'\rangle = AE(1) \text{ and } j = \langle 12^*|H|1^*2\rangle, \qquad \text{(V-11)}$$

the M-matrix for the process of Figure 24 is:

$$M^{(a)}_{f\leftarrow i} = \frac{J}{\Delta E_{12}} \frac{|A|^2}{\delta-\hbar\omega_{sk}+i\Gamma} \langle n_{sk}-1, n_{s'k'}, +1|\varepsilon^2(1)|n_{sk}, n_{s'k'}\rangle \qquad \text{(V-12)}$$

Here the imaginary quantity $i\Gamma$ has been added to the denominator to avoid the divergency at $\hbar\omega_{sk} = \delta$. Γ is the phonon induced half with of the additional excited state induced by the resonant phonon transitions, and is given by

$$\Gamma = \pi \Sigma_{sk} |A\langle n_{sk}+1|\varepsilon|n_{sk}\rangle|^2 \delta(\delta-\hbar\omega_{sk}) \tag{V-13}$$

The contributors of the other two cases to the M-matrix are:

$$M^{(b)}_{f\leftarrow i} = -\frac{J_1|A|^2}{\Delta E_{12}} \frac{\langle n_{sk}-1, n_{s'k'}+1|\varepsilon^2(2)|n_{sk}, n_{s'k'}\rangle}{\delta-\hbar\omega_{sk'}+i\Gamma} \tag{V-14}$$

and

$$M^{(c)}_{f\leftarrow i} = \frac{J_2|A^2|\langle n_{sk}-1|\varepsilon(1)n_{sk}\rangle\langle n_{s'k'}+1|\varepsilon(2)n_{s'k'}\rangle}{(\delta-\hbar\omega_{sk}+i\Gamma)(\delta-\hbar\omega_{s'k'}+i\Gamma)} \tag{V-15}$$

where J_1 and J_2 are the matrix elements for transfer involving the initial excited state and the ground state and for the transfer involving in the process. Equations (V-12), (V-14), (V-15) and using (V-11) ($J = \langle 12^*|H|1^*2\rangle$ result in the following expression for the M-Matrix

$$\begin{aligned} M_{f\leftarrow i} = {} & |A|^2 \langle n_{sk}-1,\ n_{s'k'}+1|\varepsilon^2|n_{sk}, n_{s'k'}\rangle \\ & \cdot \exp[i(k-k')\cdot r_1] \left\{ \frac{J}{\Delta E_{12}(\delta-\hbar\omega_{sk}+i\Gamma)} \right. \\ & \left. - \frac{J_1 \exp[i(k-k')\cdot r]}{\Delta E_{12}(\delta-\hbar\omega_{s'k'}+i\Gamma)} \frac{J_2 \exp[-ik'\cdot r]}{(\delta-\hbar\omega_{sk}+i\Gamma)(\delta-\hbar\omega_{s'k'}+i\Gamma)} \right\} \end{aligned} \tag{V-16}$$

By substituting M-Matrix of Equation (V-16) into Equation (V-1) we can

get the transition rate. For simplifying the calculation, it is assumed that the energy separation δ to be sufficiently large so that the wave length of the resonant phonons is shorter than the distance between the two sites

$$Kr>1 \qquad (\hbar\omega_{sk}=\delta) \tag{V-17}$$

and $|\Delta E_{12}|<<\delta$. (This condition is approximately satisfied in Nd^{3+}). Then the transition rate becomes

$$W_{2\leftarrow 1} = \frac{2\pi}{\hbar} \sum_{ss'kk'} |A^2 \langle n_{sk}-1,\ n_{s'k'}+1|\varepsilon^2|n_{sk}, n_{s'k'}\rangle|^2$$

$$= \left\{ \frac{J_1^2}{(\Delta E_{12})^2} \left[\frac{1}{(\delta-\hbar\omega_{sk})^2+\Gamma_2^2} + \frac{1}{(\delta-\hbar\omega_{s'k'})^2+\Gamma^2} \right] \right.$$

$$\left. + \frac{J_2^2}{[(\delta-\hbar\omega_{sk})^2+\Gamma^2][(\delta-\hbar\omega_{s'k'})^2+\Gamma^2]} \right\} \tag{V-18}$$

One hour assumes that

$$\Gamma << K_B T \tag{V-19}$$

Since the base factors do not vary significantly over the range $h\omega_{sk} \sim\Gamma$. Then the third term in Equation (V-18), which δ symbolize as W_3, is of the form:

$$W_3 = \int_{-\infty}^{\infty} dx \frac{f(x)}{[(\delta-x)^2+\Gamma^2][(\delta-\Delta E_{12})+\Gamma^2]} \tag{V-20}$$

where f(x) varies littler over the range dx $\sim\Gamma$ near the resonances.

Then

$$W_3 \cong [f(\delta)+f(\delta-\Delta E_{12})] \int_{-\infty}^{\infty} \frac{dx}{[(\delta-x)^2+\Gamma^2][(\delta-\Delta E_{12}-x)^2-\Gamma^2]}$$

$$= [f(\delta) + f(\delta-\Delta E_{12})] \frac{2\pi}{\Gamma} \frac{1}{(\Delta E_{12})^2+(2\Gamma)^2} \qquad \text{(V-21)}$$

for $$|\Delta E_{12}| >> \Gamma$$

and $$W_3 \cong f(\delta) \frac{\pi}{2\Gamma^3} \qquad \text{(V-22)}$$

for $$|\Delta E_{12}| << \Gamma$$

By approximating these two limits, we obtain

$$\frac{1}{[(\delta-\hbar\omega_{sk})^2+\Gamma^2][(\delta-\hbar\omega_{s'k'})^2+\Gamma^2]} \cong \frac{2}{(\Delta E_{12})^2+(2\sqrt{2}\Gamma)^2}$$

$$x \left\{ \frac{1}{(\delta-\omega_{sk})^2+\Gamma^2} + \frac{1}{(\delta-\hbar\omega_{s'k'})^2+\Gamma^2} \right\} \qquad \text{(V-23)}$$

where

$$\frac{1}{\pi} \frac{\Gamma}{(\delta-\hbar\omega_{sk})^2+\Gamma} \cong \delta(\delta-\hbar\omega_{sk}) \qquad \text{(V-24)}$$

has been used. Inserting (V-21), (V-22) in (V-16), one finds

$$W_{2\leftarrow 1}^{res} = \frac{2}{\hbar(\Delta E_{12})^2\Gamma} \sum_{ss'kk'} |A^2<n_{sk}-1,\ n_{s'k'}+1|\varepsilon^2|$$

$$\times \quad n_{sk}, n_{s'k'}\rangle|^2 \left\{ J_1^2 + \frac{2(\Delta E_{12})^2 J_2^2}{(\Delta E_{12})^2 + (2\sqrt{2}\,\Gamma)^2} \right\}$$

$$\cdot \quad [\delta(\delta-\hbar\omega_{sk})\delta(\delta+\Delta E_{12}-\hbar\omega_{s'k'})+\delta(\delta-\hbar\omega_{s'k'})\delta(\delta-\Delta E_{12}-\hbar\omega_{s'k'})] \qquad \text{(V-25)}$$

Now it is convenient to define a phonon induced transition rate from the first stark level to the second

$$\omega_v = \frac{2\pi}{\hbar} \sum_{sk} |A\langle n_{sk}-1|\Sigma|n_{sk}\rangle|^2 \, \delta(\delta-\hbar\omega_{sk}) \qquad \text{(V-26)}$$

which is related to Γ (cf. 7), through

$$\omega_v = \frac{2}{\hbar}\,\Gamma\, e^{-\rho\delta} \qquad \text{(V-27)}$$

Equation (V-25) can be rewritten as:

$$W_{2\leftarrow 1}^{res} = \left[\frac{J_1^2 + 2(\Delta E_{12})^2 J_2^2}{(\Delta E_{12})^2 + \delta\Gamma^2} \right] + \left[\frac{n(\delta+\Delta E_{12})+1}{n(\delta)+1} + \frac{n(\delta-E_{12})}{n(\delta)} \right] \frac{w_v}{(\Delta E_{12})^2} \qquad \text{(V-28)}$$

by neglecting the variations of the phonon density of states between δ and $\delta+\Delta E_{12}$ and using of (V-13) and (V-26). Now assuming

$$K_\beta T << \delta \pm \Delta E_{12} \qquad \text{(V-29)}$$

The transition rate finally becomes

$$W_{2\leftarrow 1}^{res} = \left[J_1 + \frac{2(\Delta E_{12})^2 J_2^2}{(\Delta E_{12})^2 + \delta\Gamma^2} \right] \frac{1+e^{\Delta E_{12}/KT}}{(\Delta E_{12})^2} \frac{2\Gamma}{\hbar}\, e^{-\delta/KT} \qquad \text{(V-30)}$$

where J_1 and J_2 are the matrix elements, which represent transfer involving the initial excited state and the ground state and transfer

involving the excited state reached by the phonons. ΔE represents the discrepancies in the energy level of the two ions involved in the process, δ is the resonant phonon energy, and Γ is the width of the spectra line of the additional excited energy level created by the resonant phonon transitions. Temperature dependence is primarily brought in by the $\exp(-\delta/KT)$ factor; according to our data, this would be associated with the $^4I_{9/2}(1\text{-}2)$ energy difference. Kushida (36) gives an expression useful for estimating the squared matrix elements of equation (V-30), and discussed in detail in reference (29).

If Equation (II-120) is used to make analysis of the temperature dependent rate constants, diffusion parameters may be estimated. "This expression contains the temperature dependence of W_{sa}, via alpha, only to the one quarter power, so that if the observed temperature dependence is to be recovered, the diffusion coefficient D must also vary approximately as $\exp(-E_{12}/KT)$". Assuming that transfer from sensitizer to sensitizer occurs by the same means as sensitizer-activator transfer, the expression of Trlifaj (23) may be used to find this temperature dependence, and the diffusion coefficient can be expressed as

$$D = 3.4\, C_s^{4/3}\, R_{ss}^{6}\, W_{ss} \qquad \text{(V-31)}$$

where C_s is the concentration of ions in the sensitizer sites while W_{ss} is the sensitizer-sensitizer interaction strength, and R_{ss} is the nearest distance between two sensitizer ions. The Trlifaj theory is considered appropriate here even though this expression for the diffusion constant is more applicable to a crystal lattice in which sensitizers are distributed uniformly. At this point the theory of diffusion among

random sensitizers is not as well clarified and no other expression for D is established as more accurate.

The rate for sensitizer-sensitizer transfer may be expressed by Equation (V-30) if the site to site energy difference ΔE is changed. All other parameters in this equation may be kept without being altered. Using Equations (II-120), (V-30) and (V-31), we may write the total sensitizer-activator rate of transfer as

$$\omega_s = 71.6\, C_a C_s R_{Nd}^6 (\Gamma/\hbar)(1+e^{\Delta E_{sa}/KT})^{1/4} \left[\frac{J_1^2}{(\Delta E_{ss})^2} + \frac{J_2^2}{4\pi^2}\right]^{3/4} \left[\frac{j_1^2}{\Delta E_{sa}^2} + \frac{2J_2^2}{\Delta E_{sa}+8\Gamma^2}\right]^{1/4} e^{-\delta/KT} \qquad \text{(V-32)}$$

where C_a is the concentration of ions in the activator sites. Here ΔE_{ss} is assumed to be much smaller than Γ and Kt, and all of the Nd ions are assumed to be distributed randomly in the crystal, so R_{ss} and R_{sa} can both be set equal to an average distance R_{Nd}.

Equation (V-32) was used in an investigation of Nd^{3+} in the unmixed garnet hosts (29) YAlG and YGaG as a means for obtaining a quantitative fit to the data measured for energy transfer rate versus temperature. The matrix elements necessary for these cases are obtained from the studies of Kushida (36) and Krupke (37), and spectral observations provide values for δ, ΔE_{sa}, Γ, and sensitizer and activator concentrations. The remaining unknown quantity, ΔE_{ss}, was utilized as an adjustable parameter and for both cases was found to be approximately one-fifth of the inhomogeneous linewidths measured for the transitions. No previous work has developed the required matrix elements for the transitions

found in mixed garnets such as those in this study, but Equation (V-32) can be used to determine the matrix elements provided that we assume the same model should be used to explain the data obtained on mixed as well as unmixed garnet crystals. The energy transfer rate is obtained from fitting the data, and, as for the study mentioned above, δ, ΔE_{sa}, and Γ values and both sensitizer and activator concentrations are determined from spectral observations. Finally, ΔE_{ss} is assumed to be one-fifth of the measured inhomogeneous linewidth. The J values are taken from Equation (V-32). Table IV lists the values obtained by this method and compares them to the values found from the unmixed garnet crystals. Increased matrix elements found for the mixed garnet hosts may be caused by an increased "allowedness" of such forced electric dipole transitions. As an example the results for $Y_3(Al_{0.5}Ga_{0.5})_5O_{12}:Nd^{3+}$ are:

$$J_1^2 = 3.6 \times 10^{-8} \text{ cm}^{-2}$$
$$J_2^2 = 5.1 \times 10^{-8} \text{ cm}^{-2} \qquad \text{(V-33)}$$

Thus Equation (V-30) enables estimation of the sensitizer to activator energy transfer rate values for all parameters are listed in Table V. The temperature dependence for the Γ factor is presumably not as strong as that of the exponentials, for the level which produces this linewidth is broadened by phonon emission even at T = 0.

In addition the coefficient of J_2^2 is in the form of an overlap integral, which varies only weakly with temperature. It is therefore practical to make estimate using an average value for Γ of 4 cm^{-1} for 50% Ga sample, and using the energy difference for $^4I_{9/2}$ (1-2) from Figure 5, δ = 95 cm^{-1}, with ΔE = 8.5 cm^{-1} in $Y_3(Al_{0.5}Ga_{0.5})_5O_{12}$:Nd, we

find the rate to be:

$$W_{sa} = \left[J_1^2 + \frac{2J_2^2(\Delta E)^2}{(\Delta E)^2+8\Gamma^2} \right] (1+e^{\Delta E/KT}) \frac{2\Gamma}{\hbar(\Delta E)^2} e^{-\delta/KT}$$

$$= 1460(1+e^{12.27/T})e^{-136.7/T} \qquad \text{(V-4)}$$

If we consider temperatures greater than or equal to 70 K for $Y_3(Al_{0.5}Ga_{0.5})_5O_{12}:Nd^{3+}$, the fitting transfer rates we find for Nd are in approximate proportion to the $\exp(-E_{12}/KT)$. The problem arose of deviation of fitting parameters from the Orbach rate calculation at the lowest temperatures. One explanation might be that phonons in resonance with the $^4F_{3/2}$(a to b) transition would possibly bring a less obvious temperature dependence with only became revealed at low temperatures, "as would a simple one phonon process connecting the sensitizer and activator sites. Perhaps multistep transfer processes do not occur at the lower temperatures. And if the single step processes were dominant in these lower temperatures, temperature dependence might be different.

An estimation of the diffusion coefficient and parameters related to it may now be made. By using both the method just described for treating the experimental results and Equation (V-34) enter into this calculation; the energy transfer rate can be expressed as (20)

$$\omega_s = 8.5\, C_a\, D^{3/4}\, W_{sa}^{1/4}\, R_{sa}^{3/2} \qquad \text{(V-35)}$$

or

$$D = \left[\frac{\omega_a}{8.5\, C_a (W_{sa} R^6)^{1/4}} \right]^{3/4} = 5.27 \times 10^{-10}\ cm^2\ sec^{-1}$$

with values at $T = 133^{o}K$ and $R = 2.03 \times 10^{-7}$ cm.

The diffusion length is given by (38)

$$l = (6D\tau_s^{o})^{\frac{1}{2}} \qquad \text{(V-36)}$$

and the temperature independent component of the diffusion coefficient is given by

$$D = D_o \exp(-\Delta E/KT) \qquad \text{(V-37)}$$

The other secondary parameters such as t_{step}, the average time between transfer steps and n_{step}, the average number of steps taken:

$$t_{step} = R_{av}^{2}/6D \qquad \text{(V-38)}$$

$$n_{step} = \tau_s/t_{step} \qquad \text{(V-39)}$$

Values for these parameters are listed in Table V. These expressions are used only as approximations, for they apply directly only for a sensitizer arranged in a simple cubic lattice (39).

CHAPTER VI

SUMMARY AND CONCLUSIONS

In this study the researchers have reported energy transfer characteristics among trivalent neodymium ions in mixed garnet host crystals containing several different percentages of gallium.

Laser excited site selection spectroscopy was used to study various garnet crystals having the general formula $Y_3(Al_{1-x}Ga_x)_5O_{12}$ and values for the x parameter of 0, 0.10, 0.22, 0.39, 0.50, and 1.0. Time-resolved spectroscopy was carried out on crystals with x values of 0.22, 0.39, and 0.50. Nd^{3+} was selected as the impurity ion at concentrations of approximately 1% of each garnet's composition.

Each crystal sample is optically excited by a tunable pulsed dye laser. When this instrument is tuned to different wavelengths the fluorescence spectra which are emitted vary. These spectral properties make it apparent that the Nd^{3+} ions occupy sites with unequal neighboring crystal fields and hence vary in their transition energies; their energy band splits into distinct energy levels. The range of Nd sites is attributed to the inhomogeneity at Al and Ga lattice positions which is created in mixed crystals, as well as to the presence of impurities and lattice defects near the Nd^{3+}, although the former is by far the most important.

When the neodymium ions are energized by the laser pulses, they rise to a level approximately 16,800 cm^{-1} above ground level and then

undergo non-radiative decay and fall to the $^4F_{3/2}$ level, approximately 11,450 cm^{-1} above ground level. The ions then undergo radiative transitions and in association with these emit luminescence signals. Characteristics of the radiation such as the line shape and the time evolution facilitate analysis of the inhomogeneous and homogeneous broadening of the levels as well as the rate of energy migration among sensitizer and activator ions in the crystal host. This study aimed at characterizing the properties of the $^4F_{3/2}$ transitions to the $^4I_{9/2}$ ground state manifold.

The site selection for the mixed crystal hosts in this study is observed to vary linearly with the wavelength of the laser pulse. The degree of homogeneous broadening resulting from phonon relaxation processes is so marked that it is rather unexpected to observe the degree of site selection exhibited when one pumps into such a high energy absorption band. One factor may be that the terminal levels of the absorption have previously been found to be hypersensitive to variances in the local crystal fields (40).

Data from the site selection spectroscopy indicated that crystal field splittings varied linearly with the composition parameter x. The variation of the transfer strength with x is shown in Figure 19. Inhomogeneous broadening of the fluorescent lines also is observed when Ga is added. The line shape analysis indicates that the Ga ions are apparently distributed fairly uniformly.

The transfer strengths are obtained by determining the transfer rates for the energy and then accounting for the influence of the sensitizer concentration, the activator concentration and the average Nd^{3+} ion concentration by dividing these factors out. The resultant figures

indicate an increase in the transfer strength as x increases until Al and Ga quantities are equal (e.g., the transfer strength of the crystal with x=o, was 3.0 x 10^2 sec^{-1}, the transfer strength of the crystal with x = 0.5 was 2 x 10^4 sec^{-1} at 14°K. However, once x = 1.00, the data indicate a drop of transfer strength (21). The change in transfer strength could be attributed to either of two parameters. The first is the inhomogeneous broadening of the sensitizer transition and the second is the transition matrix elements. If we examine Figure 19, it can be seen that the ω_s component goes in the opposite direction as would be predicted by the effects of inhomogeneous broadening but is qualitatively consistent with the observed changes in matrix element). And, moreover would be consistent in qualitative terms with the emission of spectra shown in Figure 6.

This finding has application for the understanding of the diffusion of the excitation energy transport in this crystal. The mechanism causing transport in this system is apparently enhanced by the disorder and irregularities of the structure; this overrides the normal influences of disorder that have an inhibition effect on the transport efficiency.

The dominant mechanism effecting the transport in this situation is found to be two-phonon assisted forced electric dipole-dipole interaction. This two-phonon assisted energy transfer was dominated by phonons of energy resonant with the difference in energy between the ground and first excited states of the $^4I_{9/2}$ manifold, a situation also found by Merkle (20) for unmixed garnets.

A small quantity of back transfer, temperature independent, emerged from the analysis of the time-resolved spectroscopy data for

the x = 0.50 crystal. This is yet to be explained. When the results of the spectroscopy for the different crystal samples with the varying x values are fitted, finite values of N_a had to be included in the gases x = 0.00, x = 0.22, x = 0.39, and x = 0.50. However, this was not necessary in the cases of x = 1.000.

The time independent energy transfer rate could also be explained by single step transfer between pairs of sensitizer and activator ions that are consistently at the same fixed distances. However, such an ion distribution is not likely. It would be possible if some Nd^{3+} ions were clustered, but such an arrangement would produce cross-relaxation quenching, and this phenomenon was not observed.

The model utilized for interpreting the results on energy transfer between the rare earth impurity ions in the garnets is based on a multi-step energy migration process in which resonant two-phonon processes assist both the hopping between ions in similar types of sites and trapping or energy transfer to ions in non-equivalent crystal field sites. This two-phonon assistance involves resonant transitions between the ground and first excited states.

The complex nature of the system introduces some complications in interpreting the results. The excitation migrates within a lattice environment with randomly distributed Nd sites further complicated by variations in the numbers of Ga and Al atoms occupying positions in the lattice, and with a consequent random distribution of transition energies superimposed. The numerical techniques used in our analysis produce an approximate solution, but should not be considered an exact method. The assumption was made in our treatment that more weight should be given to the inhomogeneities in the transition energies than

to the inhomogeneities in the ions spatial distribution in the lattice when we determine the energy transfer characteristics. The error introduced appears to be minimal but still should not be removed from consideration. Work should focus on developing a theory which can more exactly treat the energy migration between randomly placed sites. The basic diffusion equations will continue to be handicapped by the assumption of uniformly distributed sites.

REFERENCES

1. Brecher, C., L. A. Riseberg, and M. J. Weber, Appl. Phys. Lett. 30, 475 (1977); Brecher, C. and L. A. Riseberg, Phys. Rev. B 13, 81 (1976).

2. Hsu, C. and R. C. Powell, Phys. Rev. Lett. 35, 734 (1975); Hsu, C. and R. C. Powell, J. Phys. C 9, 2467 (1976); Venikouas, G. E. and R. C. Powell, Phys. Rev. B 17, 3456 (1978); Merkle, L. D. and R. C. Powell, J. Chem. Phys. 67, 371 (1977).

3. Tallant, D. R. and J. C. Wright, J. Chem. Phys. 63, 2074 (1975); Kruz, M. D. and J. C. Wright, J. Luminezlenle 15, 169 (1977).

4. Riseberg and Holton, J. Appl. Phys. 43, 1876 (1972); Riseberg, L. A., R. M. Brown and Holton, Appl. Phys. Lett. 23, 127 (1973).

5. Watts and Holton, J. Appl. Phys. 45, 873 (1974).

6. Szabo, A., Phys. Rev. Lett. 25, 924 (1970).

7. Riseberg and Holton, Optics Comm. 9, 298 (1973).

8. Flach, R., D. S. Hamilton, P. S. Selzer, and W. M. Yen, Phys. Rev. B 15, 1248 (1977); Selzer, P. M., D. S. Hamilton, and W. M. Yen, Phys. Rev. Lett. 38, 858 (1977); Hamilton, D. S., P. M. Selzer and W. M. Yen, Phys. Rev. B 16, 1858 (1977).

9. Selzer, P. M., D. L. Huber, B. B. Barrett, and W. M. Yen, Phys. Rev. B 17, 4979 (1978); Blach, R., D. S. Hamilton, P. S. Selzer, and W. M. Yen, Phys. Rev. Lett. 35, 1034 (1975).

10. Watts, R. K. and H. J. Richter, Phys. Rev. B 6, 1584 (1972).

11. Dexter, D. L., J. Chem. Phys. 21, 836 (1953).

12. Foster, T. Z. Naturforsch A4, 321 (1949).

13. Foster, T., Ann. Physik 2, 55 (1948).

14. Powell, R. C., Physics Rev. B2, 1207 (1970).

15. Chandrasekhar, B., Rev. Mod. Phys. 15, 1 (1943).

16. Spitzer, F., Principles of Random Walk (D. Van Norstrand, Inc., Princeton (1964).

17. Montroll, E. W., J. Soc. Ind. Appl. Math. 4, 241 (1956).

18. Rosenstock, H. B., Phys. Rev. 187, 1166 (1969).

19. Weber, M. J., Phys. Rev. B4, 2932 (1971).

20. Yokota, M. and O. Tanimota, J. Phys. Soc. Japan 22, 779 (1967).

21. Eisenthal, K. B. and S. Siegal, J. Chem. Phys. 41, 652 (1964).

22. Burshtein, A. I., Sov. Phys. JETP 35, 882 (1972).

23. Trlifaj, M., Czech. J. Phys. 8, 510 (1958).

24. Wanderziel, J. P., L. Kopt, and L. Van Uitert, Phys. Rev. B6, 615 (1972).

25. Watt, R. K. and H. J. Richter, Phys. Rev. B6, 1584 (1972).

26. Krasutsky, N. and H. W. Moos, Phys. Rev. B8, 1010 (1973).

27. Gandrud, W. B. and H. W. Moos, J. Chem. Phys. 49, 2170 (1968).

28. Reisfeld, R., Struct. Bonding (Berlin) 13, 53 (1973).

29. Merkle, L. D., Ph.D. Dissertation, Oklahoma State University (1978).

30. Marezio, M., J. P. Remeika and P. D. Denier, Acta Cryst. B 24, 1670 (1968).

31. Wychooff, R. W. G., Crystal Structures, Vol. 3 (J. Wiley and Sons, N.Y., 1965), p. 22.

32. Merkle, L. D. and R. C. Powell, Phys. Rev. (to be published).

33. Holstein, T., S. K. Lyo, and R. Orbach, Phys. Rev. Lett. 36, 891 (1976); Holstein, T., S. K. Lyo, and R. Orbach, Phys. Rev. B (to be published).

34. Huber, D. L., D. S. Hamilton and B. Barnett, Phys. Rev. B 16, 4642 (1977).

35. Ching, W. Y., D. L. Huber and B. Barnett, Phys. Rev. B 17, 5025 (1978).

36. Kushida, T., J. Phys. Soc. Japan 34, 1318 (1973).

37. Krupke, W. F., IEEE, J. Quant. Elec. QE 7, 153 (1971).

38. Powell, R. C. and Z. G. Soos, J. Lumineslenle 11, 1 (1975).

39. Powell, R. C. and Z. G. Soos, J. Lum. 11, 1 (1975).

40. Judd, B. R., Phys. Rev. 127, 750 (1962).

VITA [2]

Masud Zokai

Candidate for the Degree of

Doctor of Philosophy

Thesis: LASER TIME-RESOLVED SITE-SELECTION SPECTROSCOPY OF Nd^{3+} IONS IN MIXED GARNET CRYSTALS

Major Field: Physics

Biographical:

Personal Data: Born in Shahreza, Iran, April 4, 1944, the son of Mr. and Mrs. A. Zokai.

Education: Graduated from Sadie High School, Shahreza, Iran, in 1962; enrolled at Isfahan Teachers Training College, 1962 and having successfully passed its required courses, 1963; enrolled at Isfahan University, 1967; received Bachelor of Science degree from Isfahan University in January 1970; enrolled in graduate program at the Pahlavi University in January, 1970; received Master of Science degree in May, 1972; enrolled at University of Kansas at Lawrence, Kansas, 1974, received Master of Science degree in May, 1976; completed requirements for the Doctor of Philosophy degree in May, 1979, at Oklahoma State University.

Professional Experience: Employed as a teacher in the Iranian Ministry of Education, 1963-1972; graduate teaching assistant, Pahlavi University, 1970-1972, and taught at Pahlavi University High School at the same time; employed by the University of Isfahan as an Instructor, 1972-1974; graduate teaching and research assistant, Oklahoma State University, 1976-1979; teacher of physics at Langston University, 1978-1979.